DEFORMATION OF POLYCRYSTALLINE COBALT

by

C. C. Sanderson

B.A.Sc., University of British Columbia, 1965

A THESIS SUBMITTED IN PARTIAL FULFILMENT OF

THE REQUIREMENTS FOR THE DEGREE OF

DOCTOR OF PHILOSOPHY

in the Department

of

METALLURGY

We accept this thesis as conforming to the standard required from candidates for the degree of DOCTOR OF PHILOSOPHY

THE UNIVERSITY OF BRITISH COLUMBIA

July, 1972

In presenting this thesis in partial fulfilment of the requirements for an advanced degree at the University of British Columbia, I agree that the Library shall make it freely available for reference and study. I further agree that permission for extensive copying of this thesis for scholarly purposes may be granted by the Head of my Department or by his representatives. It is understood that copying or publication of this thesis for financial gain shall not be allowed without my written permission.

Department of Metallurgy

The University of British Columbia
Vancouver 8, Canada

Date August 11, 1972

ABSTRACT

The deformation of polycrystalline cobalt has been investigated over the temperature range where the hcp phase is stable (0 to 0.39 T_m).

The structure of cobalt following various annealing procedures has been detailed. Following heat treatment, cobalt is a two phase aggregate of fcc and hcp phases. A maximum of 50-60% retained fcc occurs in small grained specimens (6 - 10 microns) decreasing to less than 15% retained fcc for 60 micron material. The amount of retained fcc phase also decreases with increasing purity. The variety of substructures arising from the multivariant transformation are discussed.

The yield stress for cobalt exhibits differing temperature dependence above and below 0.25 T_m. Below 0.25 T_m, the 0.2% yield stress is almost temperature independent, whereas above 0.25 T_m the yield stress decreases rapidly. The behaviour below 0.25 T_m is related to the bulk transformation of retained fcc phase while the decreasing stress levels observed above 0.25 T_m are explained in terms of decreasing Peierls stress on the $\{11\bar{2}2\}$ slip planes.

The yield stress increases rapidly as the grain size is reduced. This effect is compared to similar behaviour in other hcp metals that exhibit a limited number of slip systems.

The ductility of cobalt is related to the retained fcc phase by equations of the form $\varepsilon = A(10)^{m\%fcc}$. A larger fraction of retained fcc phase gives rise to increased ductility. The elongation to fracture decreases as test temperature increases, reflecting obeyance of Considére's Criterion.

The observed work hardening rates are high, as are the measured values for flow stress. The values are compared to data obtained for other metals that transform martensitically while undergoing deformation.

Metallographic evidence is presented to substantiate the occurence of non-basal slip in cobalt above 0.25 T_m. Twins having high and low shear values occur at all temperatures where the hcp phase is stable. The intense surface shear resulting from transformation and continuing dislocation production on variously oriented basal planes is discussed.

TABLE OF CONTENTS

PAGE

PAGE

TABLES

FIGURES

PAGE

PAGE

PAGE

PAGE

ACKNOWLEDGEMENTS

The author acknowledges the advice and assistance given by his research director, Dr. N. R. Risebrough. Thanks are also extended to other members of the faculty and the graduate students for helpful discussions. Financial assistance provided by the National Research Council is gratefully acknowledged.

1. Introduction

Cobalt is a high melting point transition metal lying between nickel and iron in the periodic table[1,2]. Upon cooling, cobalt undergoes an allotropic phase transformation from face-centred-cubic (fcc) to hexagonal-close-packed (hcp) at approximately 417°C[3]. This martensitic transformation proceeds to completion only under very special circumstances, such as a single interface transformation in a single crystal [4,5]. Cobalt is ferromagnetic and has a Curie Point of 1115°C[2,6].

The incomplete martensitic transformation from one close-packed phase to another yields many interesting possibilities for investigation. In the present work, an attempt has been made to obtain a detailed understanding of the structure and tensile properties of cobalt polycrystals at temperatures where the hexagonal-close-packed phase is stable. A summary of pertinent information available in the literature is presented in this introduction.

1.1 Cobalt and the Common Hexagonal-Close-Packed Metals

Cobalt is unique among the common hcp metals in many respects (Table I). The observed slip systems and twinning modes for the common hexagonal metals as well as other relevant information are shown in this table. The data are drawn from many sources; the most important being Partridge[7], Chalmers[1], the A.S.M. Handbook[8] and Reed-Hill[9].

The hcp metals may be divided into two categories. Zirconium, titanium and beryllium are high melting point

TABLE I Data Sheet for the Common Hexagonal-Close-Packed Metals

Metal	Cd	Zn	Mg	Co	Zr	Ti	Be
c/a Ratio	1.886	1.856	1.623	1.623	1.592	1.587	1.568
Melting Point °C	321	420	650	1495	1852	1668	1277
Allotropic Transformation and Temp. °C	- -	- -	- -	fcc hcp↓ 417	bcc hcp↓ 862	bcc hcp↓ 882	bcc hcp↓ 1260
Slip Modes							
Basal $\{0001\}\langle 11\bar{2}0\rangle$	*	*	*	*[12,13]	Obs.	Obs.	*
Prism $\{10\bar{1}0\}\langle 11\bar{2}0\rangle$	-	-	Obs.	-	*	*	Obs.
Pyramidal $\{10\bar{1}1\}\langle 11\bar{2}0\rangle$	Obs.	-	Obs.	-	2nd	2nd	Obs.
Corrugated $\{11\bar{2}2\}\langle 11\bar{2}3\rangle$	2nd	2nd	Obs.	Obs.[14]	Obs.	-	Obs.

TABLE I (Con't)

Twinning Modes							
$\{10\bar{1}2\}$	Obs.	Obs.	Obs.	Obs.[4]	Obs.	Obs.	Obs.
$\{10\bar{1}1\}$	-	-	Obs.	Obs.[4]	-	-	-
$\{10\bar{1}n\}$	-	-	$\{10\bar{1}3\}$	-	-	-	-
$\{11\bar{2}1\}$	-	-	-	Obs.[11]	Obs.	Obs.	-
$\{11\bar{2}2\}$	-	-	-	Obs.[14]	Obs.	Obs.	-
$\{11\bar{2}n\}$	-	-	-	$\{11\bar{2}4\}$[14]	$\{11\bar{2}3\}$	$\{11\bar{2}4\}$[15]	-
Estimated Stacking Fault Energy ergs/cm^2	150	300	300	20[19-21]	-	300	180

* -- Predominant slip mode

2nd -- Secondary slip mode

Obs. -- Observed

metals with c/a ratios less than ideal while zinc and cadmium, with high c/a ratios, and magnesium with an almost ideal c/a ratio are low melting point metals. Cobalt straddles both groups with a high melting point and a c/a ratio similar to magnesium.

Attempts have been made to explain the observed deformation modes of the hcp metals based on geometric considerations of their c/a ratios[7,10]. This approach appears to explain the predominant deformation mode in most cases but does not account for the individual diversity of secondary deformation processes.

For c/a ratios equal to or greater than ideal ($\sqrt{8/3}$) the predominant deformation process forecast is slip on the basal plane in a close-packed direction. Indeed, basal slip is the most important deformation mode in the metals zinc, cadmium, magnesium and cobalt. Over a range of c/a ratios less than ideal, first order prism slip becomes the preferred mode. Zirconium, and titanium with c/a ratios of 1.592 and 1.587 respectively, slip predominatly on the $\{10\bar{1}0\}$ $\langle 11\bar{2}0\rangle$ prism system. Beryllium with c/a equal to 1.568 deforms mainly via $\{0001\}$ $\langle 11\bar{2}0\rangle$ basal slip which is not the expected mode.

Although the primary deformation mode appears to be a strong function of the c/a ratio, the secondary deformation processes are more complex and are influenced strongly by variables such as temperature, stacking fault energy and purity.

Although prism slip is the primary slip mode in zirconium and titanium, both the pyramidal and basal slip systems have been observed[7]. Basal slip predominates in high purity beryllium yet prism slip and pyramidal slip also occur. In cobalt the only slip mode commonly observed is basal slip [4,5,11,12,13]. Non basal slip $\{11\bar{2}2\}\langle 11\bar{2}3\rangle$, has been observed by Seeger[14] but this observation has not been duplicated elsewhere. Holt[4] was unable to initiate non basal slip although single crystal specimens were stressed in orientations specifically for this purpose.

Kink boundary formation, especially at high temperatures, is an important deformation mode. In zirconium, Reed-Hill[9] postulates that kink boundaries ease constraint and thus reduce the need for twinning at high temperature. Kink boundary formation has been observed in zinc[16], magnesium[7], cobalt[24], zirconium[9], and titanium[15]. The bend plane is often a simple $\{11\bar{2}0\}$tilt boundary made up of dislocations having the same Burgers vector. Other more complex kink boundaries, or accomodation kinks, are often observed near twins.

All the hexagonal metals twin in the $\{10\bar{1}2\}$plane. This mode of twinning involves the lowest shear and requires only simple shuffles in the plane of shear. The observed shape of deformation twins is influenced by the twinning shear[7,9]. When the twinning shear is small as for $\{10\bar{1}2\}$ the twin becomes lenticular as it grows because the twin interface can deviate considerably from the twinning plane without a large increase in twin interface energy[7]. When the shear

is large the twins formed are narrow and have essentially parallel boundaries.

In zirconium and titanium both $\{11\bar{2}1\}$ and $\{11\bar{2}2\}$ twins have been observed. Twins of this form have a much higher shear value than those in the $\{10\bar{1}2\}$ plane. For titanium, the ratio of shear values are 1.7/2.3/6.4 for $\{10\bar{1}2\}$/ $\{11\bar{2}2\}$/ $\{11\bar{2}1\}$ type twins respectively. Thus the $\{11\bar{2}2\}$ and $\{11\bar{2}1\}$ twins are observed as narrow and straight while $\{10\bar{1}2\}$ twins are commonly very wide and lenticular in shape.

Magnesium with a c/a ratio similar to cobalt, twins on the $\{10\bar{1}1\}$ and $\{10\bar{1}3\}$ planes as well as on the $\{10\bar{1}2\}$ plane. Twinning has also been observed on higher order planes of the form $\{10\bar{1}n\}$. The complexity arising in $\{10\bar{1}3\}$ and higher order twinning has led investigators to propose that a double-twinning mechanism involving retwinning of a primary twin is required to form these twins.

$\{10\bar{1}2\}$ twins have been observed in cobalt by a number of investigators[4,5,11,12]. Davis[11] observed $\{11\bar{2}1\}$ zig-zag twinning in cobalt, similar to those observed in titanium by Rosi[15]. Seeger observed both $\{11\bar{2}2\}$ and $\{11\bar{2}4\}$ twinning in single crystal cobalt[14]; these twin planes have also been observed in titanium. Holt[4] in a comprehensive single crystal study observed $\{10\bar{1}1\}$ twins which have also been observed in magnesium.

The preceding should not be construed as a complete compilation of the slip and twinning modes noted in the literature for the hexagonal metals. The data has been presented to allow a comparison to be made between cobalt and the other common hexagonal metals with respect to their

normal deformation processes. The important observation is that no prominent secondary slip system has been observed for cobalt but a multiplicity of twinning modes exist. For the other common hexagonal metals several slip systems are observed.

The lack of obvious secondary slip systems in cobalt may arise from two sources. First, cobalt is the only common hexagonal metal that has a low stacking fault energy. As noted in Table I, the stacking fault energy on the basal plane in cobalt is at least a factor of five less than for any of the other common hexagonal metals. The stacking fault energy has been measured by several techniques and although there are small differences in the values obtained, it is unanimous that the value is below 30 erg/cm^2 [19,20,21]. The value usually quoted is 20 ergs/cm^2 compared to 150 to 300 ergs/cm^2 for the other common hexagonal metals. The low stacking fault energy in cobalt ensures that the majority of dislocations in the basal plane are extended[22,23,24]. For dislocations to move from the basal plane to other planes by a cross-slip process the partial dislocations must constrict. Therefore, the probability of many dislocations arriving on secondary planes to provide slip on these planes is small. To obtain appreciable dislocations on the secondary planes, they must either nucleate or be grown in, on these planes. This introduces the second problem regarding secondary slip in cobalt.

Upon cooling from high temperature, fcc cobalt transforms martensitically to hcp cobalt. One of the close-packed {111}

planes in the face-centred phase becomes the basal plane in the hexagonal lattice. This is the only plane that remains relatively unchanged during transformation. The disappearance or absorption of dislocations on other {111} planes or any other plane in the face-centred-cubic phase is not understood at present. It has been observed by several authors, that the dislocations observed in cobalt are primarily basal[22,23,24]. Sufficient non-basal dislocations to yield finite amounts of deformation by slip have not been observed in thin films.

1.2 Cobalt Single Crystals

Several investigations of cobalt and cobalt-nickel alloy single crystals are available in the literature. Researchers such as Davis[11,12,13], Holt[4], and a group of workers at the Max Planck Institute have limited their investigations predominantly to the deformation behaviour of cobalt single crystals[5,14,24,25,26]. Christian[27], Alstetter and co-workers[28,29,30,31], have tested crystals to discover the detailed mechanism of the transformation. The work by the latter group will be discussed in the next section where a complete review of the transformation and related topics will be outlined.

Hexagonal cobalt single crystals exhibit tensile curves similar to other hexagonal metals. In cobalt crystals, Stage A and Stage B are observed but a third stage is not.

The critical resolved shear stress of cobalt varies significantly with purity[12,14,24,25], rising from 1400 psi for 99.998% purity[24] to 2800 psi for 99.1% material[14].

This parameter is also temperature dependent rising from 1400 psi at room temperature to 2400 psi at -196°C . Seeger[14] postulated that the high shear stress was due to either retained cubic phase or a very high basal dislocation density.

Hcp cobalt exhibits a long initial region (Stage A) which may extend to several hundred percent strain. The work hardening rate in Stage A (θ_A) is temperature dependent, rising from 2000 psi to 2500 psi as the temperature is reduced from room temperature to -196°C [12,14,5]. θ_A also increases with increasing impurity content.

During tests of hexagonal cobalt crystals, the slip line spacing decreases with increasing deformation up to 20% strain. Throughout the remainder of Stage A, the step height increases while slip line spacing remains constant [14,24,25]. Thieringer determined that the dislocation density in 99.998% cobalt lies between 0.4 and 1.2 X 10^9 per cm^2 with a stacking fault density of 2 to 6 X 10^4 per cm. He observed that the dislocation density increases approximately linearly with stress and strain in Stage A. Boser[5] and Thieringer[24,25] both reported that no increase in non-basal dislocations occured during deformation.

The number of active slip lines and the work hardening rate increase upon entering Stage B. Thieringer [24,25] found that the stress at which Stage B begins is independent of purity and occurs at 2300 psi at room temperature. The onset of Stage B in hexagonal cobalt has been explained by: the operation of a second slip system[12], a strong increase in the frequency of twinning[24,25], the agglomeration of

impurities[5], and the production of excess vacancies[4].

The critically resolved shear stress and work hardening rates are much higher for fcc cobalt crystals than for hcp crystals[4]. Stage I of the face-centered-cubic tensile curve is not detected due to the high test temperatures required to attain the cubic phase while Stage II and Stage III portions of the curve are observed. The shape of the tensile curves are similar to those for other fcc metals.

Holt tested specimens while cycling through the transformation temperature range. The temperature was changed in steps in some cases and continuously in others. These tests showed that the flow stress is not a strong function of the crystal structure but depends only upon the existing defect structure. The work hardening rate, on the other hand, is strongly dependent upon the crystal structure, being much higher in the fcc phase.

A comparison of critically resolved shear stress for a number of crystals is presented in Table II. The stress for cobalt is considerably higher than for metals with similar structure. The hcp modification has a c/a ratio similar to magnesium and deforms predominantly on the basal plane as does magnesium, yet it has a critically resolved shear stress more representative of the metals titanium and zirconium which deform on the prism system. In fact, the critically resolved shear stress for cobalt on the basal plane is larger than the value required to yield prism slip

TABLE II Critically Resolved Shear Stress for Various Metals

METAL		SLIP SYSTEM	C.R.S.S. (psi)	TEST T/M.Pt.	PURITY
Cd	hcp	Basal	82	0.51	99.996
Zn	hcp	Basal	26	0.43	99.999
Mg	hcp	Basal	63	0.33	99.996
Co	hcp	Basal	1400	0.17	99.998
Zr	hcp	Prism	900	0.14	-
Ti	hcp	Prism Basal	1980 16000	0.16 0.16	99.99 -
Be	hcp	Basal	5700	0.19	-
Co	fcc	{111}<110>	2680	0.40	99.998
Al	fcc	{111}<110>	148	0.32	99.93
Ag	fcc	{111}<110>	54	0.24	99.99
Au	fcc	{111}<110>	132	0.23	-
Cu	fcc	{111}<110>	92	0.22	99.999
Ni	fcc	{111}<110>	820	0.17	-
Fe	bcc	{110} <110> {112} {123}	4000	0.17	99.6
Mo	bcc		7000	0.10	-

Data drawn from:

Holt[4]

Ahktar[32]

Deiter[33,34]

Reed-Hill[35]

in zirconium. This data implies that the low stacking fault energy and the martensitic transformation in cobalt produce a unique situation that at present is not well understood.

1.3 The Allotropic Transformation and Structure of Cobalt

The relationship between single and polycrystal cobalt is complicated due to the martensitic transformation that occurs at a low homologous temperature. The literature shows that polycrystal cobalt does not transform completely to the hcp phase upon cooling[36,37]. Thus, polycrystal cobalt, at temperatures below the transformation temperature, contains two allotropic modifications. The following section will outline the avaliable data on the transformation and the resulting structures in cobalt.

1.3.1 History of the Transformation

The original discovery that cobalt existed in two allotropic modifications is credited to Hull[38] in 1921. The early cobalt studies dealt with the determination of lattice parameters and the transformation temperatures. This early work is summarized in Table III.

Until 1942, there was controversy regarding a second high temperature allotropic transformation[39,49]. The detailed high temperature x-ray work by Edwards[55] and others[56,57], showed conclusively that a second transformation did not occur. More recent investigators attribute the high temperature transformation observed to the change from the ferromagnetic to the paramagnetic state, i.e. the Curie Point[6].

TABLE III Martensitic Transformation Studies

DATE	AUTHOR	METHOD	A_s (°C)	M_s (°C)	NOTES
1921	Hull[38]	x-ray			determined allotropy
1925	Umino[39]	specific heat	460	-	
1926	Masumoto[40]	x-ray, thermal expansion, etc.	427-477	360-403	
1927	Sekito[41]	x-ray	447	-	lattice parameters
1927	Schulze[42,45]	many	400-500	down to 100	
1929	Wever[43]	dilatometry	465	-	
1930	Uffelmann[44]	optical expansion	450	330	
1930	Hendricks[46]	x-ray	400±20 1015± 20	-	
1931	Cardwell[47]	photoelectric effect	570 850	-	
1932	Wassermann[48]	x-ray	450	-	
1933	Sykes[49]	x-ray	420 1020	- -	
1935	Seybolt[51]	solubility of oxygen	875	-	
1935	Sykes[50]	thermal analysis	420	-	
1935	Von Steinwehr[52]	heat evolution	380-420	-	
1936	Marick[53]	electrical resistance	492	-	
1937	Meyer[54]	x-ray			lattice parameters
1941	Ellis[57]	x-ray			lattice parameters
1942	Wilson[55]	x-ray			stacking faults
1942	Edwards[55]	x-ray	410-460 500	300 400	powder rod
1948	Troiano[56]	x-ray	431	388	sheet and powder

1.3.2 Mechanisms for the Martensitic Transformation

The mechanism whereby the high temperature fcc lattice transformed into the low temperature hcp phase was originally envisioned by various researchers[58,59] as being accomplished by the passage of Schockley partial dislocations over every second plane in the fcc lattice to yield the hcp lattice. All theories regarding the transformation have assumed this type of dislocation motion, they differ only in proposals as to how the partial dislocations arise and how they operate to transform a bulk of material from one phase to the other.

Christian[59] first advanced a hypothesis involving reflection of partial dislocations at a free surface to give rise to a hcp lattice. This mechanism was thought by later workers to be improbable. The pole mechanism postulated by Seeger[60,61] is a more successful attempt at explanation. He assumes that perfect dislocations of the form a/2 [101] dissociate in the (111) plane. If the dislocation is pinned by a sessile "pole" dislocation with a screw component equal to twice the (111) interplaner spacing the hcp lattice will be generated from the fcc lattice. Following investigators found problems with this mechanism [31,62-71] related to the number of these high energy pole dislocations required to give rise to bulk transformation. This is critical when single crystal whiskers are considered[62].

Bollman[22], in 1961, postulated that the transformation proceded by a nucleation mechanism based on the intersection of stacking faults on various {111} planes. To accomodate

stress when one stacking fault impinged on another, a new stacking fault was nucleated. Due to free energy considerations it grew and the mechanism repeated. The problem with this theory is that it does not allow formation of a single crystal. Transformation on more than one of the {111} planes in the parent crystal, (i.e. multivariant transformation) must be under way before suitable conditions are available to allow further transformation.

Altstetter and coworkers[26-31] studied cobalt single crystals and polycrystals. Their formulation of the transformation appears promising in that the mechanism they propose explains many observations made by others[24,25,36,37,65-71]. Delamotte and Altstetter[31] present a nucleation theory based on work by Venables[72] and other workers[73,74]. They propose that partial dislocation loops are nucleated on every second (111) plane and consider the free energy for formation of a loop of radius r as follows:

$$\Delta F = \underbrace{2\pi r\ (Gb^2/4\pi)\ \ln(2r/r_o)}_{i} - \underbrace{\pi r^2(\tau b)}_{ii} - \underbrace{\pi r^2 c\Delta g_t}_{iii} \quad .....1)$$

G = shear modulus
σ = shear stress
c = twice the layer spacing
Δg_t = energy per cm^3 for transformation
b = Burgers vector

Where:

i) is the elastic energy (dislocation loop line energy) required for dislocation formation with Burgers vector b. For realistic nucleation rates the shear modulus, G, at the interface between phases must have an anomalously low value. This problem has been treated by other workers[75].

ii) is the reduction in free energy due to partial dislocations sweeping over the fcc-hcp interface under the influence of stress τ. τ can arise from both internal constraints as well as from externally applied shear stress.

iii) is the free energy available due to transformation of a volume of material from one phase to the more stable phase. c is equal to twice the layer spacing. g_t is the free energy per cubic centimeter for transforming one phase into the other.

This mechanism operates for the initial fcc to hcp transformation when nuclei of Shockley partial dislocations form from perfect a/2[$\bar{1}$01] type dislocations that have been drawn from sub-boundaries at low stress, or produced by deformation. It may be expressed as:

$$1/2\ a[\bar{1}01] \rightarrow 1/6\ a\ [\bar{1}\bar{1}2] + 1/6\ a\ [\bar{2}11] \qquad .....2)$$

As the temperature is decreased the driving force increases until further stacking faults (loops of partial dislocation) can be nucleated. As certain numbers of a given 1/6 a <121> loop are nucleated on successive planes, the constraints due to transformation will cause a different coplanar variant 1/6 a <121> loop to nucleate. In other words, once an intrinsic stacking fault exists, formation of subsequent partial dislocations will be controlled by the local value of shear stress.

1.3.3 Multivariant Transformation

A multivariant transformation is one that takes place on more than one of the planes available for transformation; in this case, more than one (111) type plane. If transformation proceeds in more than one direction on a given (111) type plane, this is termed coplanar multivariance.

The mechanism outlined above gives rise to coplanar multivariance i.e. operation of different 1/6 a [121] type dislocations in a given {111} plane. The analysis is equally valid for all {111} planes in the high temperature fcc phase and therefore transformation can occur on all {111} planes if sufficient nuclei are present and no external constraints are imposed.

The absence of strong surface shear markings has been pointed out in the literature[76]. Bulk transformation by coplanar multivariance is possible with little average shear strain if the operative shear direction of the transforming {111} plane changes often. Thus, it is not surprising that shear markings were overlooked by some authors. If high external applied stresses are involved during transformation, the nucleation of partial dislocation loops will occur for 1/6 a [112] shear directions that will minimize the effect of the external stress. By this technique, Delamotte[31] observed surface shear close to the theoretical maximum calculated for this transformation[28].

In polycrystal material, the operative partials nucleated are influenced by the constraints arising out of

thermal anisotropy and volume changes due to the transformation. Thus, for polycrystalline material various shear values are observed depending on grain size and other factors.

Multivariant transformations in cobalt polycrystals have been observed by numerous investigators[28,71,76,77]. This phenomenom has also been observed in alloy systems where a similar phase transformation occurs[78,79].

The absence of a multivariant transformation in the production of cobalt single crystals has been explained in various ways. Seeger[60,61] postulated that the {111} plane having the greatest area in the single crystal is the one that operates during the transformation; later investigators found this was not the case. The explanation put forward by Altstetter and Adams[30] and verified by them for single crystals, is that the unidirectional cooling during crystal solidification is the deciding factor. The {111} plane that has the greatest area normal to the cooling direction invariable gives rise to the transformation. They also discovered that upon reheating the single crystal through the transformation two possibile orientations may occur. These are either the original fcc orientation or its twin as has been verified by Adams[30] and observed by Holt[4].

After the initial cooling transformation for a single crystal or a polycrystal, the next annealing cycle has an important effect on the transformation that will then occur upon cooling. If the annealing treatment is carried out below 600°C, the operative habit planes during the heating

transformation are the same habit planes that operate during cooling[71,30]. Thus, a single crystal remains a single crystal and a polycrystal maintains the same degree of multivariance. If a specimen is annealed at higher temperatures, or at 600°C for very long periods of time, each region of crystal that was of one orientation before annealing will exhibit a multivariant transformation upon cooling. Further annealing treatments of this type will further refine the structure within a given fcc grain. The above observations are due to the production and mobility of dislocations as related to temperature and the transformation.

1.3.4 Retained FCC Phase

Except in the special case of single crystals (or very fine particles)[80] cobalt at room temperature is a mixture of fcc and hcp phases. The retention of fcc in particles larger than 1 micron or in bulk specimens arises from the multivariance of the transformation and the small thermodynamic driving force tending to complete the transformation. Other factors that affect the amount of retained fcc are the defect structure, purity and grain size of the specimens involved.

The transformation takes place at a relatively low temperature ($0.39T_m$) where some dislocation rearrangement and annihilation may occur, but major redistribution cannot take place[76]. As the untransformed areas decrease in size they will remain fcc either because of a lack of suitable dislocation sources or because the surrounding transformed

material cannot accommodate further volume changes. During research on powders[55-57], thin films[36,37], whiskers[62-64] and polycrystalline cobalt[81-83], measured values for retained fcc phase vary from zero to over 50%. It has also been observed that any type of deformation forces the transformation towards completion[83-86].

1.3.5 Thermodynamics of the Transformation

The thermodynamics of the transformation have been studied[30] and the enthalpy for the transformation is approximately 100 calories per mole. Adams[30] determined that about 15% of the enthalpy change is associated with defect production. This is sufficient energy to produce stacking faults on every 10th plane, a dislocation density of $10^{11}/cm^2$, or an increase in vacancy concentration of 0.04%. Therefore, as cobalt is transformed, the defect structure may increase perceptibly. As pointed out by Yegolayev[85,86] and Houska[76] the final defect structure depends upon the temperature to which the cobalt specimen is cycled. Defects are produced during each transformation cycle but annihilation also takes place at the high temperature. As the number of cycles increases, either a balance is reached where a large proportion of the defects produced by one cycle is annihilated at the high temperature or recrystallization begins. The results of any given set of cycling experiments depend upon the specimens used and the temperatures involved.

1.3.6 The Hysteresis of the Transformation

Data for the transformation[28], indicates that the hysteresis is smaller for single crystals than for polycrystals[30]. For both types of material the hysteresis increases with cycling through the transformation, but eventually reaches a stable value. Adams[30] determined M_s-A_s to be 13°C for single crystals, and 30°C for polycrystals. Other authors [36,85,86] have found values considerably larger for other forms of cobalt. Parr[63], working with cobalt whiskers, observed a hysteresis of less than 5°C. The hysteresis is very large for small particles and thin films. Petrov[80] found that 500 Angstrom aersol particles of cobalt did not transform to hcp at any temperature in the absence of deformation. However, upon heating, the transformation to fcc occured at about 500°C. Votava[36,37] working with thin films in the electron microscope found that the hysteresis was increased radically by one cycle through the transformation. He postulated that the observed hysteresis of 450°C (M_s equals 100°C, A_s equals 550°C) was due to loss of nuclei for transformation and lack of constraint in the thin films.

1.4 Scope of Present Work

The object of the present study is to provide a detailed profile of the tensile properties of cobalt polycrystals over the temperature range where the hexagonal phase is stable. A major portion of the work is related to

the effect of the incomplete allotropic phase transformation on the deformation behaviour of cobalt.

It is proposed that by monitoring the completeness of the transformation at all stages of deformation, clarification of much anomalous data present in the literature may result. The deformation of cobalt is examined while varying purity, annealing procedures, completness of transformation and test temperature. The experimental program begins with evaluation of the structure of specimens before testing. All further experimental resuls are related to the structures observed in this prepared material.

2. Experimental Procedure

2.1 Materials

The lack of agreement between results gathered from the literature has often been attributed to differences in purity of the cobalt tested[87,88]. The method of cobalt production has also been shown to have important effects on properties[81]. The majority of the data in the literature deals with electrolytic cobalt, either as deposited or in remelted form. In recent years, cobalt powders have also become an important source of material. The properties of the bulk material produced by powder metallurgy differ somewhat from the refined electrolytic materials .

Three levels of purity have been investigated in this study. The nominal purity values are 99.7%, 99.9%, and 99.998% cobalt; a detailed report on the impurities present is presented in Table IV. Cobalt analyses were obtained from Koch Light Laboratories, Colnbrook, England and Sherritt Gordon Mines Limited, Fort Saskatchewan, Alberta.

The major difference between the three grades of cobalt is the nickel content. In all cases, nickel, silicon and iron are the major impurities. Zinc, lead, and other elements that have been shown to have deleterious effects on the tensile properties of cobalt are well below critical levels[82].

All three grades of cobalt were obtained as cold worked rod. The diameter of the "as received" material was as follows:

TABLE IV Spectrographic Analysis of Cobalt Matrix

Element	99.7%+	99.9%+	99.998%+	99.998%*
	%	%	%	P.P.M.
Ni	0.1	0.02	<0.005	N.D.
Si	0.05	N.D.	<0.005	7
Fe	0.005	<0.01	-	3
Al	0.005	-	-	-

i) Elements quoted at levels less than 100 P.P.M. (<0.01%) in all specimens by Sherritt Gordon -- As, Cd, Li, Te, Zn.

ii) Elements detected at levels of 1 P.P.M. or less by Kock Light Laboratores in the 99.998% material -- Ag, Ca, Cu, Mg.

iii) The following elements were specifically sought but not detected (N.D.)

-- By Sheritt Gordon
Ag, B, Ba, Be, Bi, Ca, Cr, Cu, Ge, Hg, Mg, Mn, Mo, Pb, Sb, Sn, Ti, V, Zr.

-- By Kock Light
Al, As, Au, B, Ba, Be, Cd, Cr, Cs, Ga, Ge, Hg, In, Ir, K, Le, Mn, Mo, Na, Nb, Os, Pb, Pt, Rb, Re, Rh, Ru, Sb, Se, Sn, Sr, Ta, Te, Ti, Tl, V, W, Zn, Zr.

+ Analysis by research and development division, Sheritt Gordon Mines Limited, Fort Saskatchewan, Alberta, Canada. Maximum sensitivity quoted as 50 P.P.M.

* Analysis by Kock Light Laboratories, Colnbrook, England. Maximum sensitivity quoted as ±50% of the amount present.

Nominal Purity %	Diameter
99.7	3 mm (0.125")
99.9	6.25 mm (0.250")
99.998	5 mm (0.200")

The very high purity material (99.998%) was supplied by Kock Light; the two lower purity grades (99.7% and 99.9%) were obtained from A. D. MacKay Inc., New York, U. S. A.

2.2 Preparation of Tensile Specimens

2.2.1 Machining

The important dimensions of the tensile specimens which were produced on a small lathe are shown in Figure 1. From the 5 mm and 6.25 mm material, double buttonhead specimens were machined to minimize problems related to gripping constraints during tensile tests. For the 3 mm material, a double buttonhead type of specimen would have given an unworkably small specimen diameter. The 3 mm material was therefore machined into single buttonhead specimens. In all cases the gauge length was maintained at ten times the reduced specimen diameter. All specimens were machined 0.1 mm (0.004") oversize to allow for subsequent electropolishing.

Tensile testing grips for the Instron were machined from tool steel (Atlas Keewatin) and heat treated to a hardness of 54-56 R_C. The pull rods and sleeves for the split grips were made from 316 stainless steel.

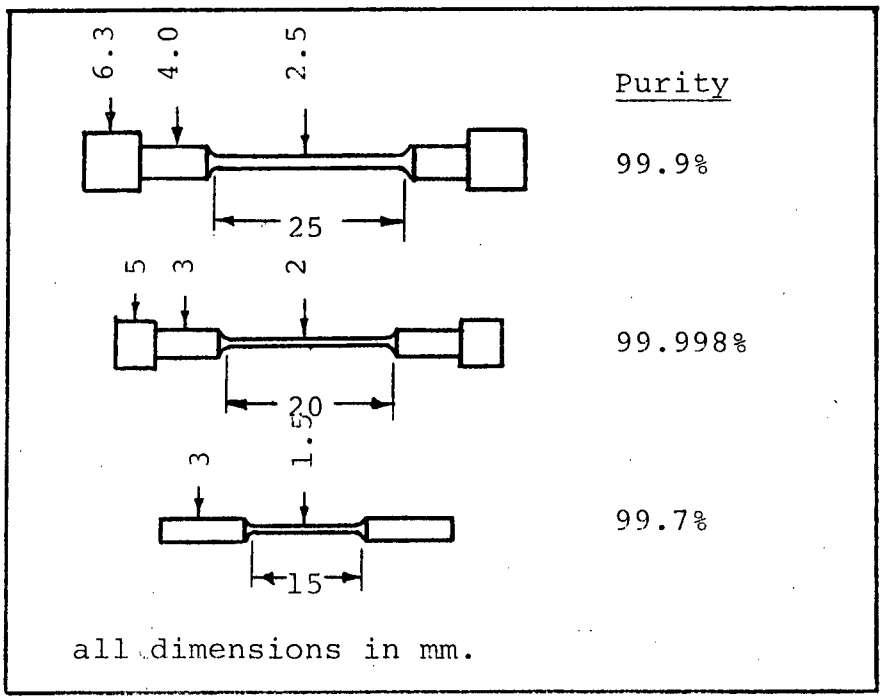

Fig. 1 Tensile specimens and important dimensions

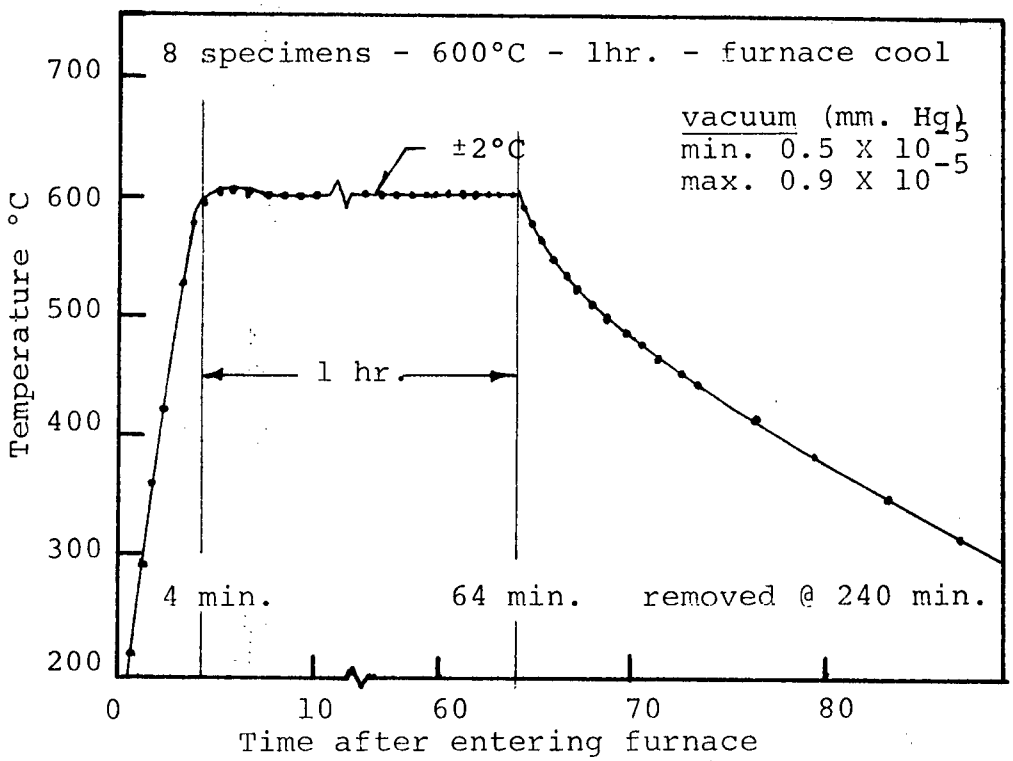

Fig. 2 Typical record of vacuum annealing treatment

2.2.2 Annealing Procedures

A typical heat treatment profile is shown in Figure 2. Treatments were carried out at temperatures up to 1000°C with temperature monitered via a chromel-alumel thermocouple placed directly among the specimens undergoing heat treatment. Heat up rates were rapid, four minutes to reach 600°C from ambient temperature, increasing to a maximum of eight to ten minutes to attain 1000°C from ambient. The rate of furnace cooling through the transformation temperature range was between four and six degrees centigrade per minute. Vacuum was maintained between 0.4 and 1.0 X 10^{-5} mm of Hg throughout the annealing procedures.

The specimens retained an excellent surface through the heat treatments and surface markings due to the martensitic transformation could only be ascertained by replica techniques.

2.2.3 X-Ray Analysis

Quantitative x-ray analysis was adopted for determining the proportions of the two allotropic modifications of cobalt present in all specimens. The analysis was carried out after heat treatment and following deformation procedures.

The method adopted was first put in quantitative form by Sage and Guillard[90], in 1949, and has been utilized by many authors[65-71,82,84,85]. The method does not require a standard which simplifies analysis.

Information regarding the presence of the two phases is obtained by comparing the diffracted intensity of the $(10\bar{1}1)$

line in the hcp phase to that of the (200) line in the fcc phase. When the multiplicity factor and other variables are taken into account, the proportion of fcc phase present may be determined from the formula:

$$x = \frac{2I_{fcc}}{2I_{fcc} + I_{hcp}} \qquad .....3)$$

x = proportion of metastable fcc phase

I_{fcc} = Intensity of the (200) fcc line

I_{hcp} = Intensity of the $(10\bar{1}1)$ hcp line

The derivation of this formula and the required analysis is presented in Appendix 1.

All x-ray work was carried out with a Phillips PW 1011/60 diffractometer utilizing manganese filtered iron radiation. The rate at which the diffractometer was rotated varied from 1/4 to 2 degrees 2θ per minute.

Using iron radiation, the $(10\bar{1}1)$ hcp intensity peak occurs at approximately 60.3 degrees 2θ, and the (200) fcc peak approximately 66.7 degrees 2θ[84]. To allow intensity calculations directly from the x-ray chart, a slow rate of diffractometer rotation was used (one quarter degree per minute) to provide a clear intensity traverse from 59 to 69 degrees 2θ. The areas under the respective peaks were then measured and substituted into formula 3. This method was tedious and due to inherent scatter in this type of measurement a statistically more reliable method was undertaken for the majority of the x-ray analysis.

The method may be outlined as follows:

The x-ray equipment allowed integration over a given period of time, or for a predetermined number of pulses. The two intensity peaks in question could be completely traversed within 4 degree ranges, 59 to 63 degrees for the $(10\bar{1}1)$ hcp peak and 65 to 69 degrees for the fcc peak. The background x-ray count to be subtracted from the total integrated intensities obtained by counting all pulses over the 4 degrees 2θ above, was determined by scanning 2 degrees 2θ on both sides of the peak in question. The respective angles 2θ are given below and a typical x-ray chart is shown in Figure 3.

Degrees 2θ	Description
57-59	1/2 of background for hcp peak (B.G. #1)
59-63	Total hcp peak $(10\bar{1}1)$
63-65	1/2 of background for hcp and fcc peaks (B.G. #2)
65-69	Total fcc peak (200)
69-71	1/2 of background for fcc peak (B.G. #3)

Therefore:

Intensity of hcp peak (I_{hcp}) = Total hcp - (B.G. #1 + B.G. #2)

Intensity of fcc peak (I_{fcc}) = Total fcc - (B.G. #2 + B.G. #3).

In practice, it was found that the differences between B.G. #1, B.G. #2 and B.G. #3 were very small and scanning B.G. #1, and B.G. #3 was not justified because the measurements did not improve the accuracy of the analysis. For this reason, the net integrated intensity of the two peaks was determined by subtracting twice the "B.G. #2" intensity from each peak.

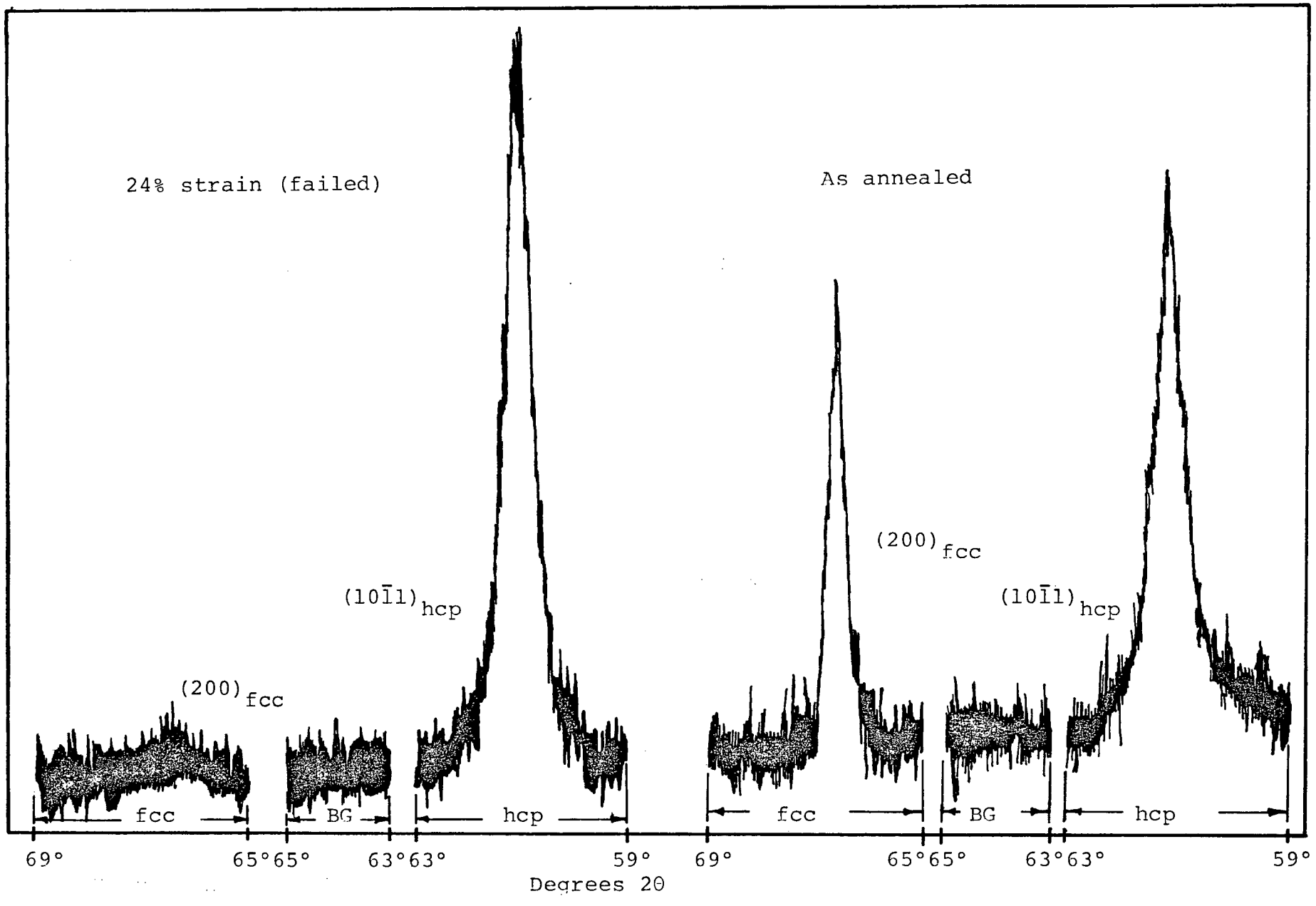

Fig. 3 Raw x-ray data for 99.7% cobalt

A minimum of five intensity integrations were carried out on each specimen. Each integration was taken from a different area on the specimen and the results from the five scanning procedures were then added and substituted in equation 3.

The data obtained using this method was reproducible, but the scatter in results was always large. This problem with quantitative x-ray analysis is discussed by Giamei[91] who attempted to reduce the scatter by scanning a number of peaks and solving the data via computer techniques. The technique is not applicable where a large number of specimens are to be analyzed because of the equipment time involved.

The large number of specimens analyzed and the number of scanning procedures carried out ensure that any trends observed are in fact real and not a consequence of the analysis[91].

When data regarding the proportion of the two phases present is quoted, the value given will be the average value for all specimens that have the same purity and have undergone the same treatment.

There are several facts that should be noted when considering x-ray data. Diffraction is essentially a surface measurment, with the majority of the diffracted x-rays coming from the outer 25 microns of material. When the grain size is of this order, the x-ray results are due almost exclusively to the surface grains. The surface grains exist under different constraint than the interior grains and this becomes important when the martensitic transformation

in cobalt is considered. If the surface grains are less constrained, the transformation will proceed further towards completion in these grains; thus the x-ray results will give a high value for the completeness of the transformation. This analysis leads to the conclusion that the measured amount of transformation is a maximum, and the interior of the specimen may contain more metastable face-centered phase than the x-ray data reveals.

Recognizing the above considerations, the x-ray data is more accurate where a small grain size is involved because the diffraction will take place from interior grains as well as surface grains. In any case, the analysis adopted ensures that the measured amount of transformation can be considered a maximum value.

2.3 Tensile and Hardness Tests

All tensile tests were carried out on a floor model Instron machine using cross-head speeds between 0.2 in./min. and 2×10^{-3} in./min. The majority of tests were carried out at 2×10^{-2} in./min. corresponding to a strain rate of 2×10^{-2} per min. for the largest specimens and 3.3×10^{-2} per min. for the smallest.

Testing media for the temperature range investigated were as follows:

Media	Temperature Range
liquid nitrogen	-196°C
petroleum ether	-140°C to -100°C
ethanol	-100°C to 0°C
water	0°C to 100°C
silicone oil	100°C to 250°C
salt bath (draw temper 275)	250°C to 400°C

The temperature of the testing baths was measured with a copper-constantan thermocouple immersed close to the specimen. The test temperature was maintained within $\pm$ 1°C while testing was underway.

Tensile data are presented in the F.P.S. system. True stress and true strain data were calculated on the basis of instantaneous area and length. These values were calculated assuming uniform deformation throughout the gauge length.

At low temperatures, the baths could be changed and testing resumed in less than a minute while at high temperatures the physical handling difficulties and temperature control problems extended the time required before continuing a test to 5 to 8 minutes. During the time that the temperature baths were being changed the tensile specimens were maintained in tension by a small cyclic load.

All hardness tests were carried out on a Vickers Hardness Tester with the 10 Kg. applied load. The D.P.H. data was produced to allow comparisons to be made with data available in the literature.

2.4 Metallography

The metallography of cobalt is difficult because of the complex structures arising due to the incomplete martensitic transformation in the material[92,93]. The grain size, internal structure, and deformation mechanisms were examined optically and via replica techniques.

2.4.1 Optical Metallography

The incomplete martensitic transformation in cobalt can be forced towards completion by deformation. This strain induced transformation was measured at distances greater than 50 microns from a scratch. For this reason, at least 100 microns were removed from all machined or ground surfaces by electropolishing before any metallography was attempted.

A number of the circular tensile specimens were ground flat and then electropolished to obtain a large enough flat area for grain size determinations. The circular cross section of the tensile specimens was a barrier to good metallography.

The most successful electropolishing solution was found to be 15% perchloric acid in acetic acid. The specimens were suspended in a water cooled stainless steel beaker in which the polishing solution was stirred continuously. Polishing was carried out at 20 volts, with the specimen rotating in the stirred solution. The specimen was slowly inverted every 30 seconds to avoid taper. These precautions produced specimens with $\pm$ 0.01 mm. maximum

taper along the gauge length. This procedure yields a surface with an apparent mirror finish. The surface shows little evidence of preferential attack at grain boundaries or other high energy sites.

The metallographic features of the specimens were determined by utilizing a second anodic etch. The etchant used was 5% concentrated hydrochloric acid in distilled water. The specimen was placed in the etching bath and given a very short pulse of current at less than one volt and then examined. The resulting structure is very sensitive to the size of the pulse of current. Overetching occurs very easily and extreme caution must be exercised if a reproducible surface is desired.

As an adjunct to the x-ray analysis of the proportion of the two phases present, a polarized light technique was employed. Several problems arose when metallography under polarized light was attempted. A polished or ground surface was of no use because of the stress induced transformation and an electropolished surface did not give a definitive result due to the presence of a thin oxide layer. Observation could only be made following the second etching procedure and this caused problems relating to the scattering of light from grain boundaries and surface fine structure. The periodic nature of the transformation shears give rise to a fine structure which can etch to yield an anisotropic effect although small lamellar volumes of the fcc phase may still exist. For these reasons interpreation of polarized light photomicrographs was attempted cautiously.

Polarized light metallography proved to be most successful with large grained material. When the proportion of isotropic material (fcc) measured by this technique was compared to the results of the x-ray analysis, acceptable agreement was found.

2.4.2 Electron Microscope Replicas

Replicas were produced by soaking cellulose acetate sheet in acetone and then pressing the sheet to the surface to be analyzed. The acetate sheet was removed from the specimen and shadowed with chromium and coated with carbon. The acetate was dissolved away in acetone, leaving the replica to be mounted in 150 mesh copper grids. All replicas were examined in a Hitachi HUllA electron microscope at 50 KV.

The replica procedure was carried out on specimens tested between -196°C and 250°C. To ensure protection of the surface at all times while testing, thick silicone grease was spread over the specimen surface. The grease could be dissolved away in trichlorethane when a replica was desired. The upper temperature limit (250°C) for the replica procedure was dictated by the breakdown of the protective grease, which allowed oxide to form on the cobalt surface. Replicas were produced from annealed structures as well as from deformed specimens. The procedure was also carried out on the fracture surfaces of a number of specimens.

3.1 The Structure of Polycrystalline Cobalt

This section outlines the methods used to determine the structure of the specimens on which all tensile procedures were carried out. The data produced during this work are combined with information taken from the literature in order to examine the complex structures observed. It is then possible to predict the structures that will exist in cobalt polycrystals after a given set of annealing procedures.

3.1.1 As Received Material

From the cold worked cobalt rod, random samples from each purity lot were prepared for testing. Quantitative x-ray analysis showed that the material was almost 100% hcp phase. Integrating the measured peaks and substituting in equation 3 gave a fcc content of less than 5%.

$$\%fcc = \frac{2I_{fcc}}{2I_{fcc} + I_{hcp}} \cdot (100) \qquad ....3)$$

Tensile tests were carried out at room temperature with specimens from each purity grade. In all cases the ductility was found to be less than 3%. In the high purity material, (99.998%) the specimens fractured at yield.

3.1.1.1 Preferred Orientation

The texture in cold worked cobalt has been investigated by several authors[66,82,89,94]. Wilcox[89] investigated electrodeposited cobalt sheet and sponge material. Beckers[82], et al worked with bars and rods of commercial grade cobalt. Wilcox observed that electrodeposited cobalt has an as deposited $\{10\bar{1}0\}$ texture which is difficult to annihilate. After annealing above the transformation temperature and introducing 20% cold work he observed a $\{0001\}$ $<11\bar{2}0>$ rolling texture with the basal planes rotated 20 to 25 degrees in the rolling direction from the rolling plane normal. Beckers observed a similar result for hot rolled slabs. For extruded rods of cobalt, a preferred orientation with a high density of $\{0001\}$ planes perpendicular to the extrusion axis is obtained[82]. The preferred orientation in severly worked material was found to disappear when annealing treatments were carried out above 500°C[82].

3.1.1.2 Stacking Fault Energy and Fault Analysis

The low stacking fault energy of cobalt and the introduction of many stacking faults both by deformation and by transformation have led many investigators to study the faulting densities in cobalt. Various experimental methods have been chosen with most work performed via x-ray techniques[76,85,86,95,96]. Measurements of nuclear magnetic resonance (NMR)[97] frequencies and direct observation in the electron microscope have also been carried out[24,36,98].

A stacking fault is an error in the original sequence of layers in a crystal lattice. Faults arise during growth of crystals and also from deformation. The distinction between the two types of faults should be made clear.

The ideal hcp structure can be described as an ABABABAB sequence of close-packed planes. A fault is an error in this regular sequence with the restriction that adjacent layers must be different. Thus, the growth of an hcp crystal by the addition of close packed planes is governed by the fact that every second layer is identical except when a fault occurs. The fault layer is unlike the preceding two layers. For a deformation fault, it is presumed that a perfect stacking sequence exists before deformation takes place.

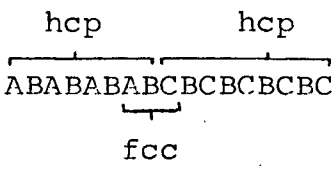

Growth Fault

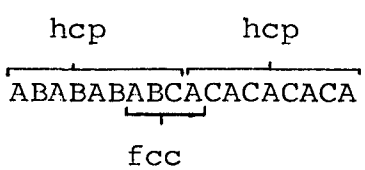

Deformation Fault

Either type of fault can be formed by the growth of two out-of-phase hcp lattices together. The deformation fault can also be formed by partial slip which converts A planes into C planes, and B planes into A planes. The two fault types may be differentiated because a growth fault contains three planes of fcc stacking and a deformation fault four layers. The analysis of x-ray data to yield differentiation between growth and deformation stacking faults has been carried out by Ananthraman and Christian[99].

Analysis via NMR has been published by Toth and coworkers[97]. The results of these analyses may be summarized as follows:

i) In both the annealed and the deformed state the fault density is high with faults observed in both the fcc and the hcp phases. A highly deformed specimen may have a total fault density as high as one faulted plane in every ten. In annealed material this value may drop to one plane in three hundred.

ii) All observed stacking faults are of the intrinsic type. More complex extrinsic faults are also possible but they have not been observed[97,98].

iii) Both growth and deformation faults are present. The density of growth faults is not strongly affected by annealing procedures but is substantially decreased by deformation and is increased by cycling through the transformation. Deformation faults, as their name implies, increase with the amount of deformation introduced. The density of these faults is reduced sharply by annealing procedures, even at temperatures below the transformation temperature.

3.1.2 Recovery, Recrystallization and Grain Growth

The annealing spectrum of cobalt has been investigated by several authors[81,100-103]. Some studies detailed the important parameters affecting the annealing behaviour such as prior treatment, purity, type of specimen, etc, while others did not. Thus, the data in many cases differ significantly.

The lack of agreement arising from differences in purity has been outlined by Morral[87] and Winterhager[88].

The most often quoted property is diamond pyramid hardness (DPH), and for this reason a record of DPH versus annealing procedures was obtained during this study to allow comparisons to be made. The diamond pyramid hardness (DPH) for the as-received material was as follows:

Purity	DPH
99.7% Co	285
99.9% Co	279
99.998% Co	260

Figure 4 gives the data gathered for the three purity levels investigated and comparable data drawn from the literature. In all cases, data are shown for room temperature hardness after a one hour anneal at the indicated temperature.

The general conclusions drawn from this data may be reported as follows:

i) The room temperature hardness is not affected by annealing below 220°C ($0.28T_m$), even for high purity material. As the impurity level increases the temperature at which any major dislocation rearrangement occurs increases. Thus, in the temperature range 220°C to 350°C polygonization and recovery occur depending upon purity.

ii) Over the temperature range that includes the region where the martensitic transformation takes place, recovery and recrystallization occur. It would

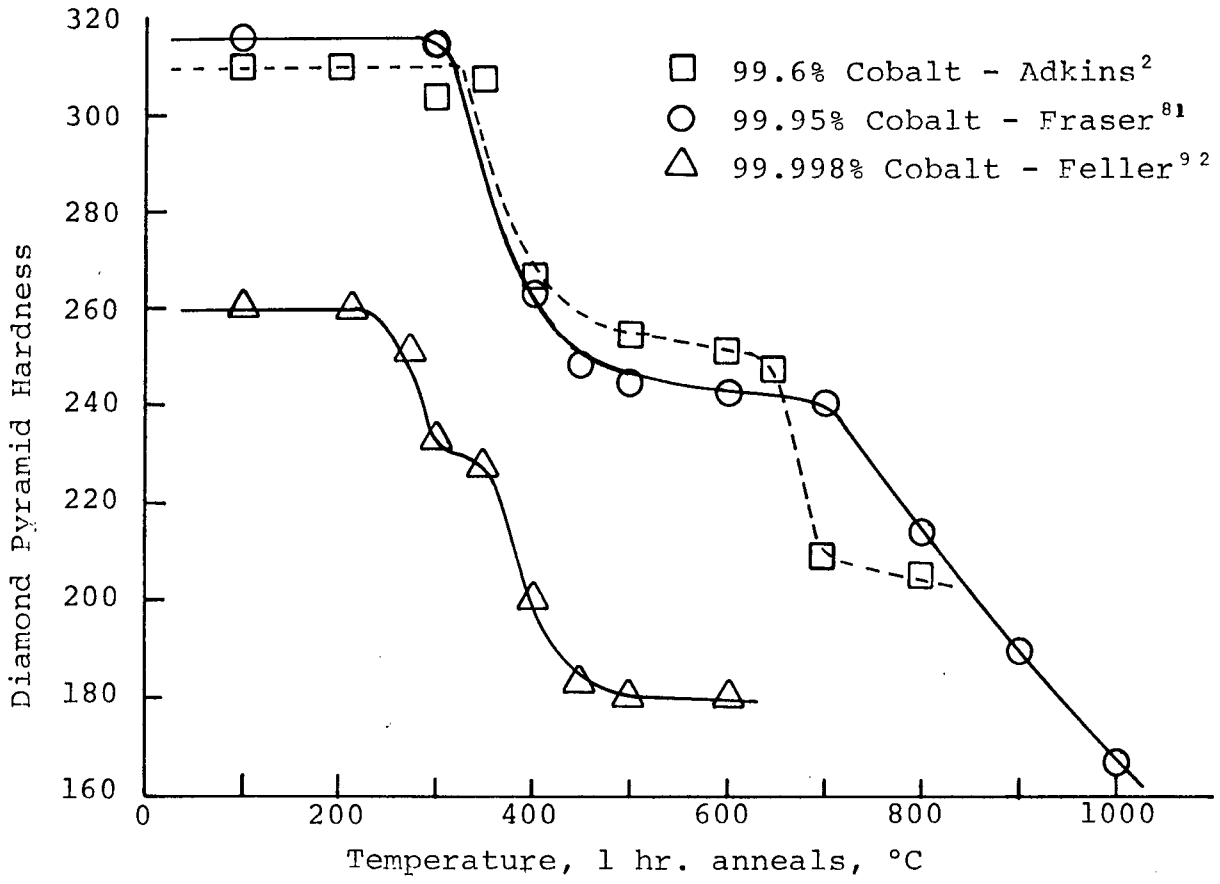

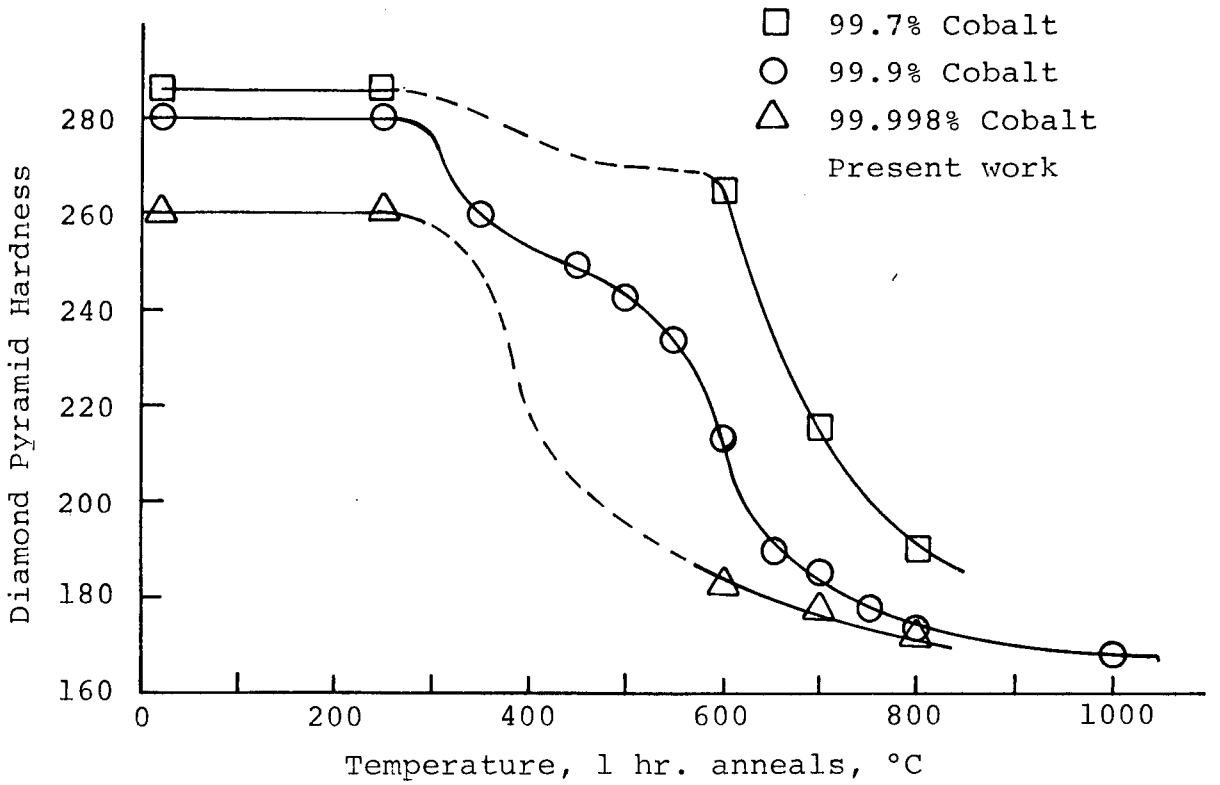

Fig. 4 Diamond Pyramid Hardness data for cobalt.

appear that recyrstallization at a temperature where hcp cobalt is stable, may be possible for very pure material.

iii) Grain growth predominates at temperatures above 600°C.

3.1.2.1 Recovery

Although the recovery of hardness values has been quoted as low as 220°C by Feller-Kneipmier[101] no change in the bulk flow stress at room temperature has been observed for annealing treatments below 350°C ($0.35T_m$). The work by Sharp[102] showed that following deformation at -196°C some recovery of electrical resistivity occured in cobalt at $0.06T_m$ and $0.13T_m$, but found no recovery of flow stress for short anneals at $0.38T_m$. They observed some flow stress recovery with long term anneals at 0.38 and $0.39T_m$.

A set of tests similar to that by Sharp[102] et al were carried out in the present study to substantiate their results for the cobalt used in the present investigation.

No reduction in bulk flow stress was obtained for treatments below $0.35T_m$. Annealing for several days at $0.37T_m$ allowed recovery of only 2% of the flow stress in the purest material.

3.1.2.2 Recrystallization and Grain Growth

The recrystallization temperature range for most metals lies between $0.4T_m$ and $0.5T_m$[1], a temperature range from 430°C to 610°C for cobalt. The annealing treatment required for

recrystallization is modified by the initial grain size, cold work present, and the purity of the specimens considered. Increasing purity tends to lower the recrystallization temperature as does increasing amounts of cold work and smaller grain sizes.

Bibring and Sebileau[65-71] worked with 99.5% cobalt and postulated that recrystallization occured at temperatures below the transformation temperature. They presented no metallographic evidence and with the low purity material they employed this result is doubtful. In a more recent study, Beckers[82] determined that recovery started after one hour at 450°C and recrystallization was visible after one half hour at 500°C for 99.7% cobalt. In the present work, no change was observed in the surface structure of specimens for annealing procedures below 450°C. At 500°C, recrystallization was visible after short time anneals.

The rate at which grain growth proceeds is influenced by the purity of the cobalt treated. As the purity increases, the number of obstacles retarding grain coalescence and reduction of high angle boundaries decreases, thus grain growth proceeds more quickly. This result is shown clearly in Figure 5 where the data from the present study are plotted. Several data points drawn from the literature have been included for comparison.

The method used for determining grain size was straight forward but tedious. Metallographic specimens were photographed and the number of grains present were counted directly.

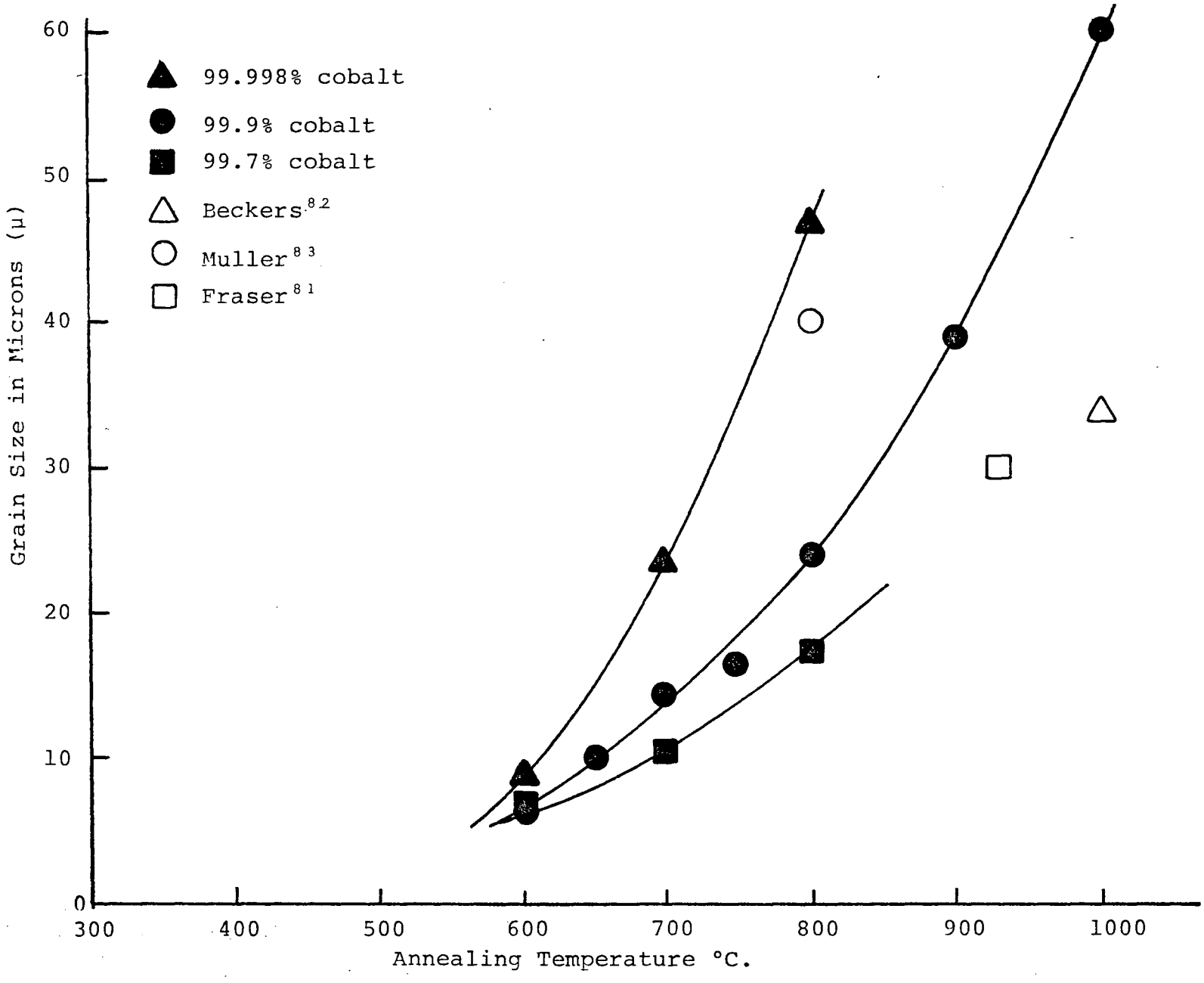

Fig. 5 Variation in grain size for 1 hour anneals at indicated temperatures.

The magnification used for analysis was varied to obtain as many grains as possible in the field of view while retaining reasonable grain definition. The smaller grain sizes were also checked by a grain count taken from replicas examined in the electron microscope.

When grain sizes in polycrystalline cobalt are cited, it should be noted that the values given refer to the high temperature fcc phase. Difficulty arises in measuring the fcc grain size because of the distribution of hcp martensitic plates in the fcc grains.

The relationship between the grain size and the fineness of the hcp structure is complex. All specimens are partially fcc after annealing regardless of the grain size, but the grain size affects the amount of retained fcc phase in two distinct ways. First, as the fcc grain size increases above a certain small value the amount of retained fcc decreases rapidly. For large grain sizes, the amount of retained fcc remains constant at approximately 10%. Secondly, as the grain size increases the multivariance of the transformation changes, that is, the manner in which the retained fcc is distributed throughout a grain changes. This result occurs because the distance over which each martensite plate may propogate before being obstructed changes with grain size. This distance can be further divided as to "in a direction parallel to" and "in a direction perpedicular to" the martensitic plates as they grow.

The main point to be drawn from what has been said above is that the measured grain size is not an indication of the size of regions of crystal lattice having the same crystal structure. The measured value should be considered a measure of the coarsness of the fcc structure existing before transformation takes place.

On the following pages (Figure 6 - 9) the annealed structures of the cobalt used in this study are presented.

The grain structure is not an equilibrium structure; the boundaries present are often straight and change direction at right or acute angles. A large amount of internal structure is visible which causes difficulty in determining individual grains.

An analysis of this internal structure is presented following discussion of the completeness of the transformation.

3.1.3 Completeness of Transformation

X-ray procedures were performed on various areas of individual specimens. The scatter in data from one area of a specimen to another was found to be within $\pm 5\%$ with occasional erratic results. The erratic results were always low and attributed to improper handling. The scatter in results from one specimen to another was found to be greater than that within a given specimen.

It became apparent that not only the variations in as received material but also the specimen preparation procedures involving machining, could influence radically the amount of retained fcc phase. (Table V).

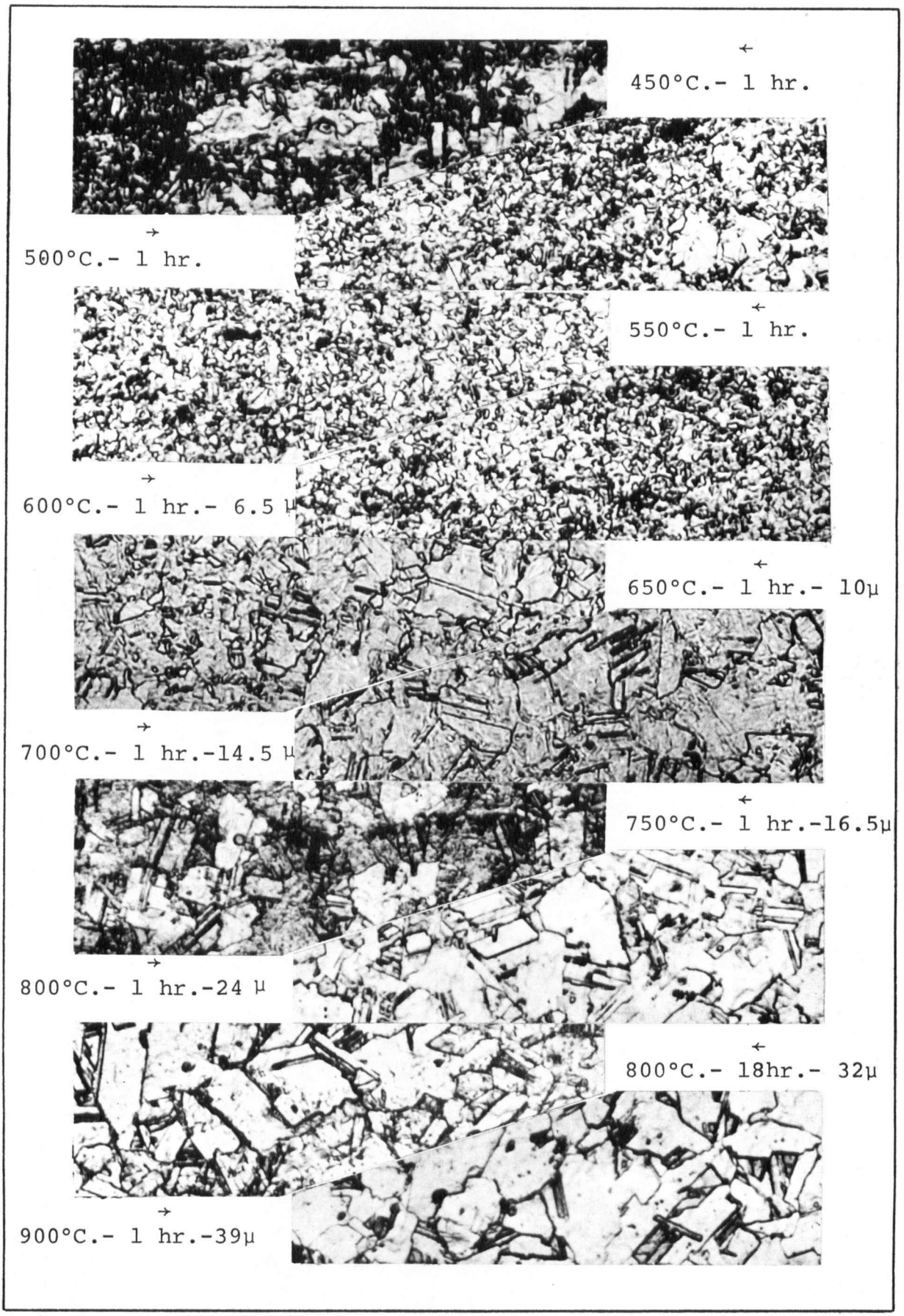

Fig. 6 Annealing spectrum in 99.9% cobalt. 340X

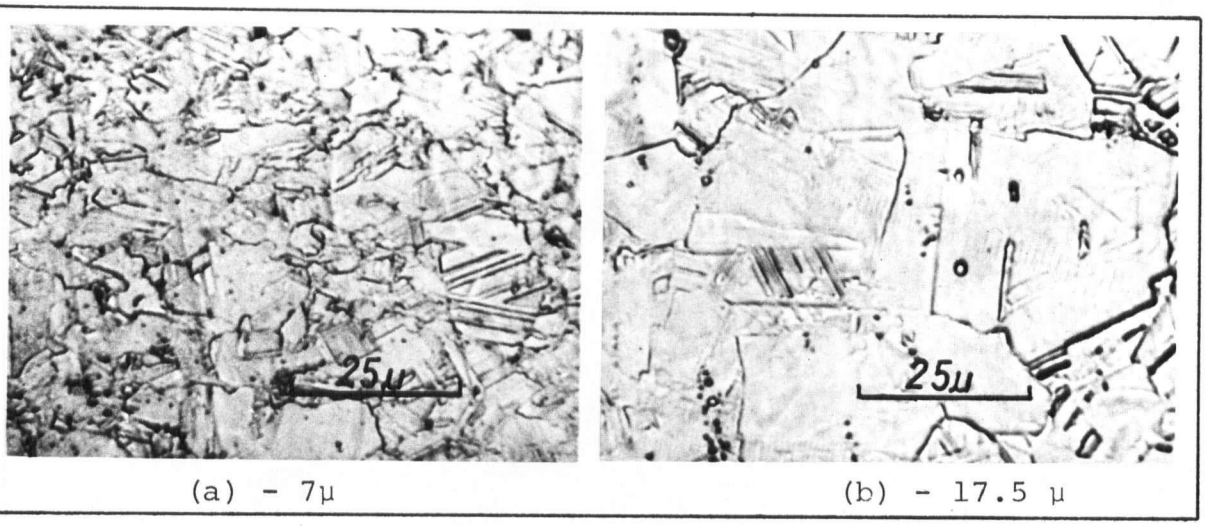

(a) - 7μ (b) - 17.5 μ

Fig. 7 99.7% cobalt, annealed at 600°C (a) and 800°C (b) 1 hr.

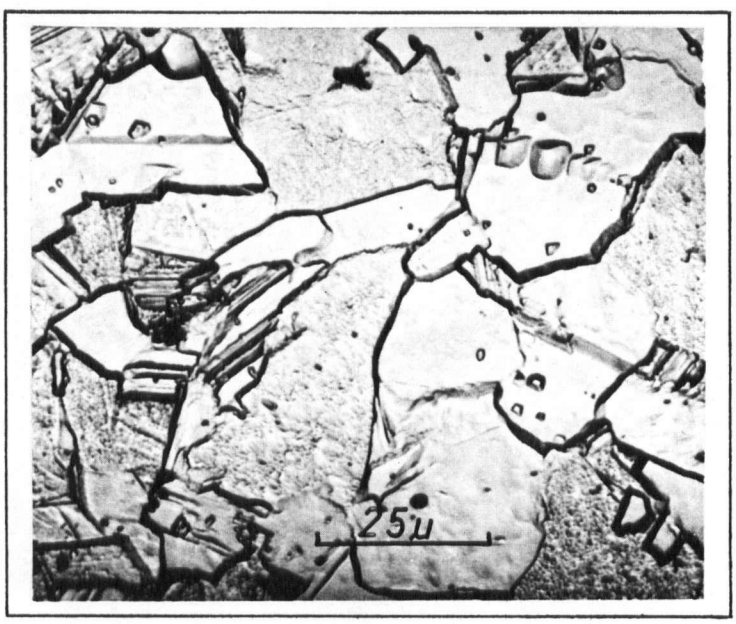

Fig. 8 99.9% cobalt, annealed at 900°C for 1 hr. 39μ.

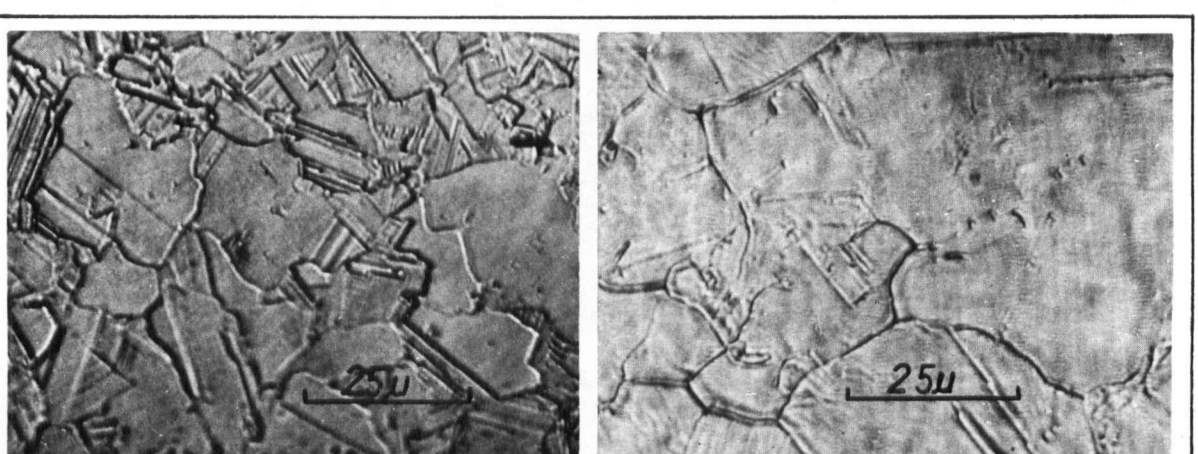

(a) - 9μ (b) - 47μ

Fig. 9 99.998% cobalt, annealed at 600°C (a) and 800°C (b) 1 hr.

TABLE V Summary of Retained FCC Data

Anneal	Purity					
	99.7%	99.9% A	99.9% B	99.9% C	99.9% Total	99.998%
450°C - 1 Hr		49.5			49.5	
500°C - 1 Hr		59.5		55.1	56.8	
550°C - 1 Hr		50.7		43.1	46.0	
600°C - 1 Hr	59.4	49.6	41.1		42.7	40.8
650°C - 1 Hr		38.7		30.4	33.5	
700°C - 1 Hr	46.5	45.3	37.2		41.1	31.7
750°C - 1 Hr		31.8			31.8	
800°C - 1 Hr	41.8	41.6	25.3		34.0	30.9
800°C - 1 Hr				27.3	27.3	
900°C - 1 Hr				17.0	17.0	
1000°C - 1 Hr				14.1	14.1	

A, B, C, represent different lots of "as received" material

The differences between various batches of material could not be rectified "after the fact" but the influence of specimen preparation was removed by electropolishing a minimum of 100 microns from the surface of all specimens before any heat treatment. In this way, anomalous results were avoided.

The results of the x-ray analysis on annealed specimens are given in Figure 10. The scatter in the results is large, especially when it is considered that each point

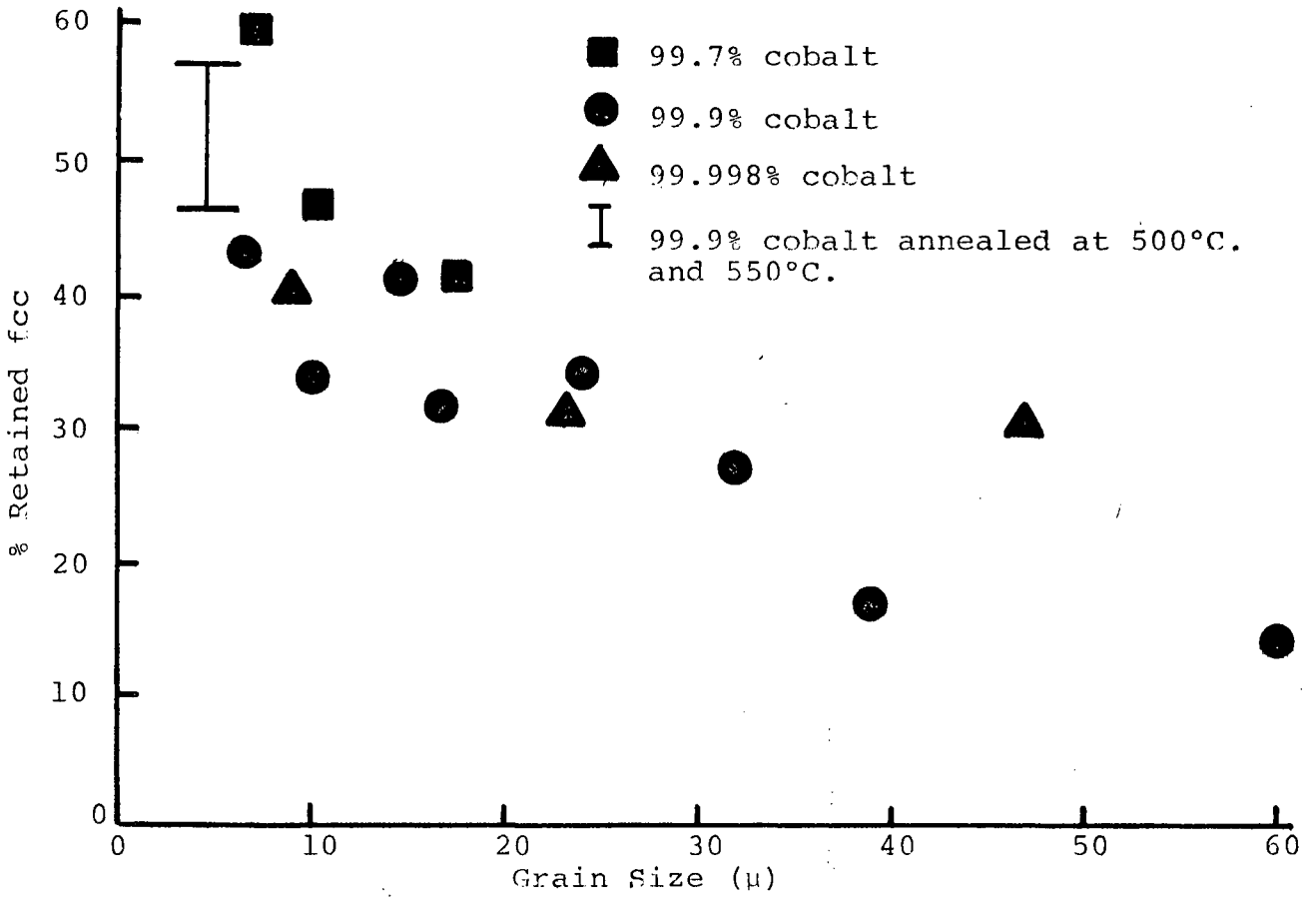

Fig. 10(a) % retained fcc vs grain size

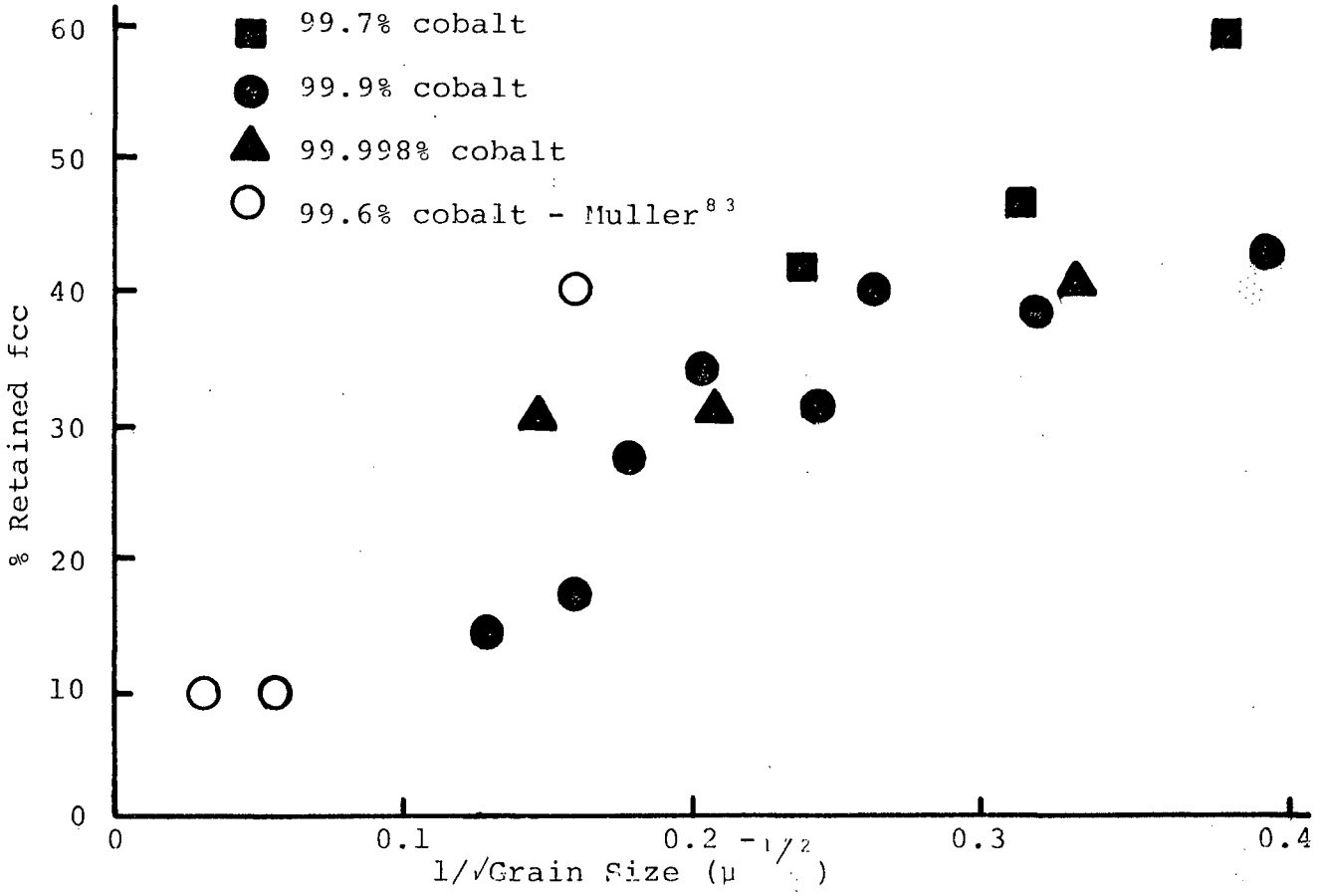

Fig. 10(b) % retained fcc vs 1/√Grain Size
Fig. 10 Progress of the transformation as a function of grain size

represents between 10 and 40 specimens (50 - 200 x-ray analyses). Nevertheless, they are typical of results published elsewhere[82].

The important quantitative results are clear. The amount of retained fcc is an important function of grain size, decreasing very quickly as the grain size increases. Also, as the purity is increased, the transformation proceeds further towards completion.

These results may be explained in terms of defect structure. A small grain size results from a low temperature anneal. The mobility and annihilation of lattice defects that may take place at this low temperature is more limited than for annealing treatments yielding large grained material. Many nuclei for the transformation are available but regions through which the nuclei may operate free of strong obstacles such as grain boundaries or other martensitic plates are small. Thus, we have a situation where many nuclei are present but the growth of the nuclei is strictly limited. For large grain sizes the defect structure is less dense; fewer nuclei are available to transform the lattice from fcc to hcp. If a nuclei begins to grow in the large grained material, it may propogate through a larger region of crystal before interference from other multivariant plates or grain boundaries constrain further growth. It is clear from the x-ray data that this latter situation gives rise to a more complete transformation.

The increasing difficulty in completing the transformation as the impurity content increases is due to substitutional atoms toughening the lattice for dislocation movement. The locking of stacking faults in this manner, making it difficult for them to move and transform the lattice, has been observed by Altstetter et al[28-31].

The present observations agree with data taken from the literature. Beckers[82] observed maximum retained fcc (50-60%) by annealing at 500-600°C and observed a drop to approximately 30% fcc for 800°C anneals. Grain sizes were not quoted but they may be assumed to be in the same general range as in the present study. Fraser[81], also found the maximum retained face-centred phase to occur in this annealing range. Müller[83] annealed sheet cobalt of various purities, between 800 and 1300°C and determined that from 300 micron to 30,000 micron grain size, the retained fcc phase amounted to approximately 10%. For his finest grain size of 35 microns, he measured approximately 40% retained fcc. Other data from the literature is available but it is based on powder specimens[84,55-57].

As mentioned earlier, polarized light was investigated as a secondary tool for determining the distribution of the two phases in cobalt. A photomicrograph is reproduced for a large grained specimen in Figure 11. The material is 99.998% cobalt with an average grain size of approximately 47 microns. Figure 11 shows the complexity of the transformation within a grain in a very striking manner. The central grain has been strongly constrained during the transformation. It was originally a twinned fcc grain and

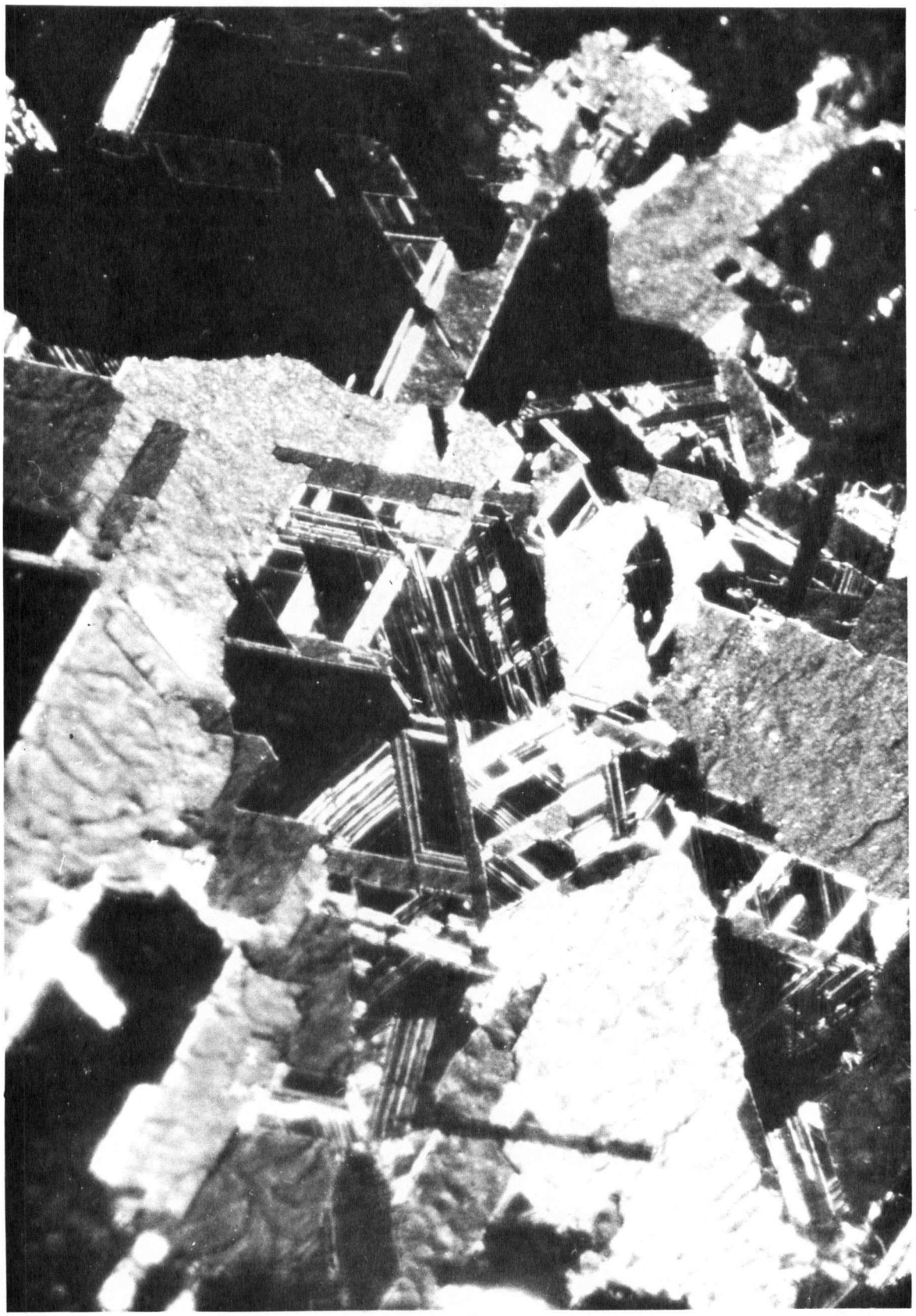

Fig. 11 99.998% Cobalt under polarized light. 900X

the multivariant transformation shows more than 4 planes on which the transformation has proceeded. The dark areas in this grain remain dark throughout the rotation of the polarizer and are retained fcc areas. X-ray analysis of this specimen yields 31% retained fcc phase at room temperature which approximates the value taken from the polarized light photomicrograph.

3.1.4 Discussion and Summary

The following discussion outlines the structures that will occur in polycrystal cobalt following standard annealing procedures.

The microstructures observed may be arbitrarily classified on the basis of annealing temperature. The three types of treatment discussed are:

a) annealing just above the transformation temperature (approximately 450°C)

b) annealing in the range where maximum fcc phase is retained (500 - 600°C).

c) annealing above 600°C where grain growth predominates.

The structures produced in cobalt are related to an annealing treatment as outlined in Figure 12. In all cases, the starting material is severely cold worked and of physical dimensions large compared to the fcc grain size.

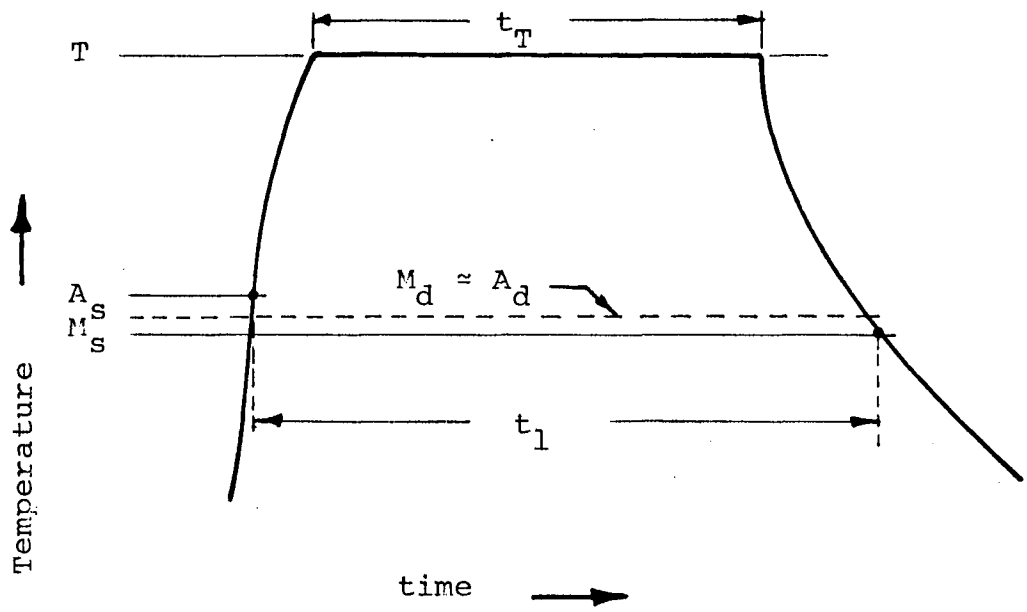

T = annealing temperature

t_T = time at annealing temperature

t_l = time in fcc phase

A_s = the temperature at which the fcc phase begins to form on heating

M_s = the temperature at which the hcp phase begins to form on cooling

M_d = the highest temperature at which the hcp phase can be produced by deformation

A_d = the lowest temperature at which fcc phase can be produced by deformation

$M_d \simeq A_d \simeq 417°C$ [3]

Fig. 12 Annealing Parameters

a) Annealing just above the transformation temperature (A_s)

Upon heating through the transformation, the specimen undergoes recovery and polygonization. Simultaneously, the structure transforms completely to the high temperature fcc phase. The transformation is nucleated at stacking faults in the hcp phase or at retained regions of fcc[27,78]. From many nuclei, fcc grains with a dense defect structure are formed. The transformation upon heating is accompanied by an increase in volume. The theoretical maximum increase possible is 3.6 X 10^{-3}[28-31]. (See Figure 13).

The fault density in the room temperature product depends upon "t". If t, is very small, less than one minute, the number of deformation faults will be reduced and the number of growth faults will be higher than originally present. If t, is large, the number of deformation faults will approach zero, but the growth fault density will remain high. If t, is greater than several minutes recrystallization begins at grain boundaries. A part of the driving force appears to be a supersaturation of vacancies giving rise to recrystallization nuclei[101]. A one hour anneal at 450°C produces a partially recrystallized structure (Figure 6). Long time anneals at this temperature do not yield a fully recrystallized structure.

Upon cooling, the volumes of crystal lattice where recrystallization has not occured, transform to the hcp phase on the same lattice planes that operated during the

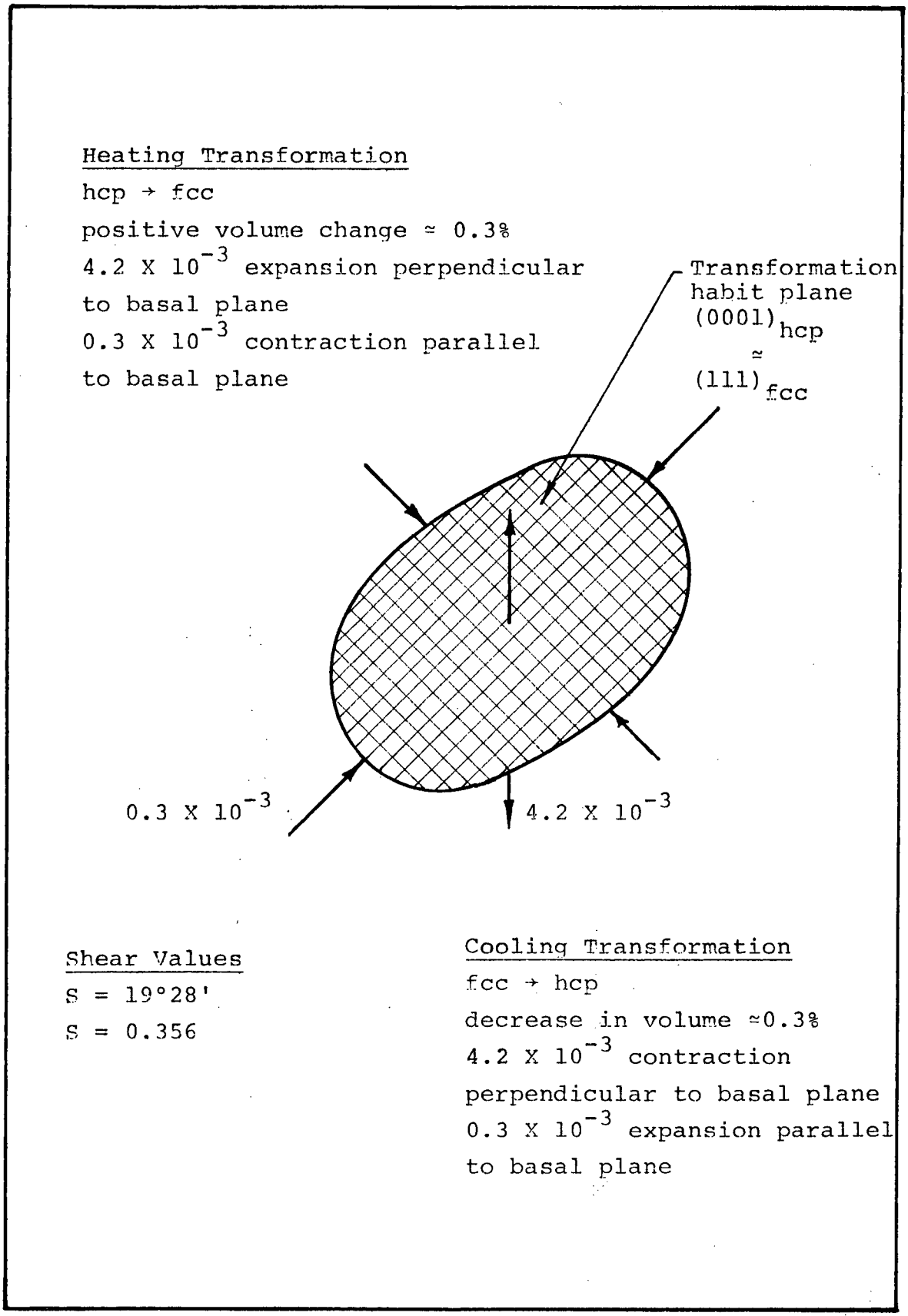

Fig. 13 Volume changes during the martensitic transformation in cobalt.

heating cycle[4,27,71]. The transformation proceeds in this manner because high densities of dislocations are not available on planes other than the (111) variant corresponding to (0001) hcp above the transformation temperature.

In the areas that have undergone recrystallization, dislocation densities are similar on all {111} planes. The planes that will operate to form the hcp phase upon cooling will be determined by the constraints imposed on these new fcc grains. The constraints arise from the decrease in volume accompanying the transformation, and the thermal anisotropy of the hcp lattice.

The amount of retained fcc resulting from this partially recrystallized structure at room temperature varies over a wide range, but is invariable high (30% - 65%).

b) Annealing in the range 500 - 600°C

A treatment of this nature gives rise to complete recrystallization. A small amount of grain growth may occur at the higher temperature. The growth fault density will be high in the room temperature product while the deformation fault density will be low.

The size of grains in any individual specimen varies over a wide range and cannot be considered an equilibrium structure. Many straight and acute angle boundaries are present as well as a variety of substructure. The visible substructure varies according to the etching procedures[93]. Figures 9(a) and 14 show the structure obtained by attack

Fig. 14 Etching of grain boundaries and martensite plates. 99.7% cobalt. 920X

Fig. 15(a) 99.9% cobalt. 4000X

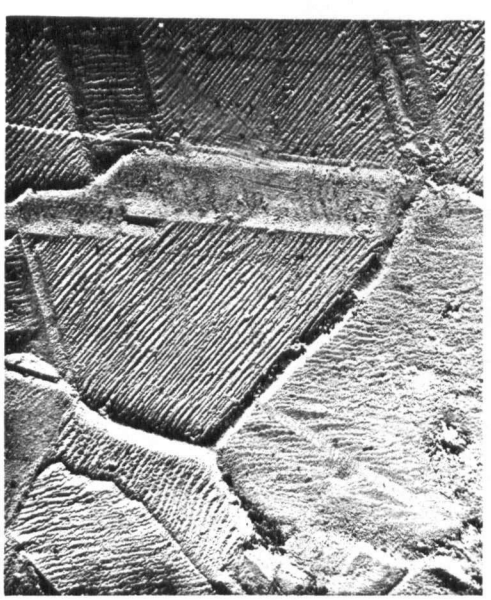

Fig. 15(b) 99.9% cobalt. 10,000X

Fig. 15(c) 99.9% cobalt. 10,000X

on both the grain boundaries and martensite plate boundaries. It should be noted that plate intergrowth or overgrowth in different directions at different depths into the grains is evident. As outlined by Feller[92], preferential etching of certain lattice planes may occur in cobalt. This phenomena is shown in Figure 15. The etching procedure clearly delineates regions of lattice of differing orientation.

The average grain size obtained in this annealing range is less than 10 microns for all purity levels investigated. Two typical views for 99.9% Co are shown in Figure 16. Surface tilting due to transformation is often severe in this fine grained material as shown in Figure 17. This surface was electropolished before heat treatment but no further etching was performed. The shear markings due to the martensitic transformation are obvious.

Optical metallography is discouraging for cobalt and thus replica work is presented to confirm the detailed appearance of the surface in small grained specimens. A range of structures is observed on a single surface of a grain. The most common features are as follows:

i) A few grains have the appearance of a single crystal upon viewing a single plane through the grain. These grains likely contain some multivarient plate growth at constrained grain boundary regions: (Figure 16 (a)).

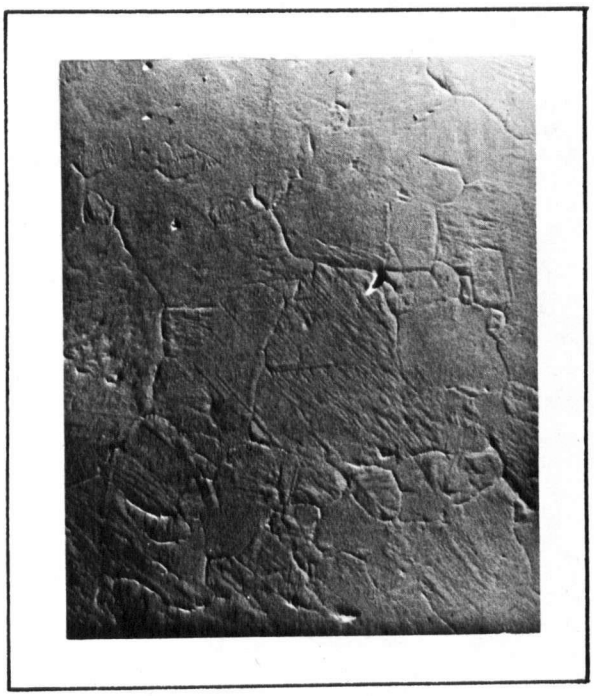

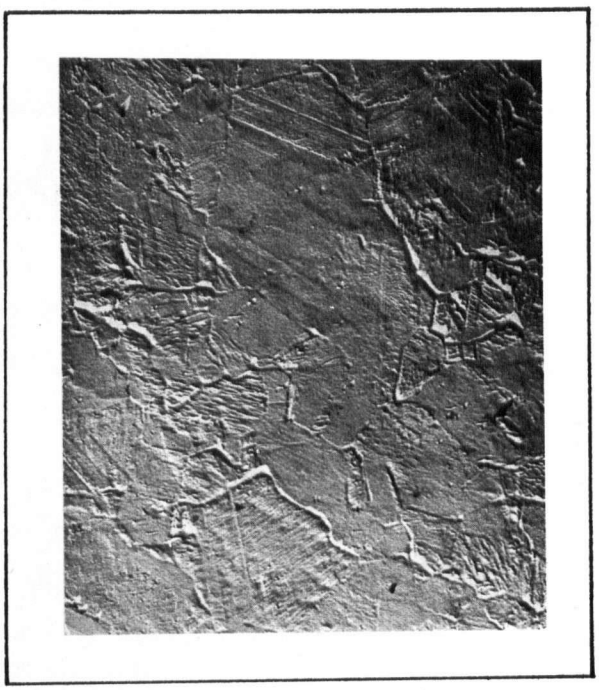

Fig. 16 99.9% cobalt, 6.5 micron grain size, 4000X

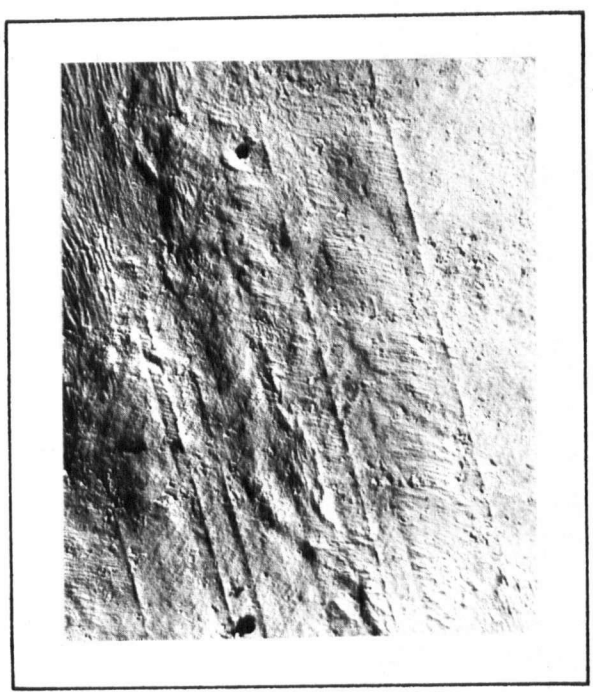

Fig. 17 Shear markings following heat treatment. 6500X

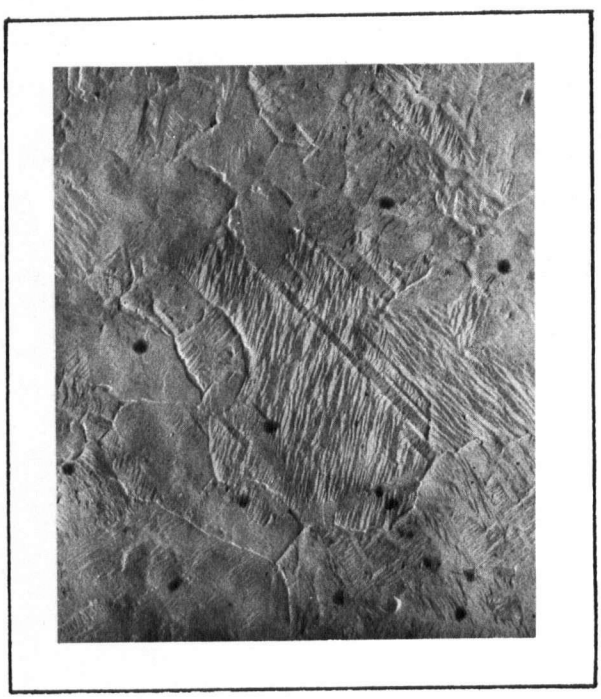

Fig. 18 Annealing twin boundaries in 99.9% cobalt. 5000X

ii) Many grains exhibit different orientation in areas delineated by annealing twin boundaries in the fcc phase; (Figures 15 and 18).

iii) Some grains appear to have random areas of different orientation throughout. This type of substructure is shown clearly under polarized light (Figure 11).

iv) A banded structure is detected in some grains; (Figure 19). These bands are interpreted as hcp regions differing only in operational shear direction in a given (111) type varient during transformation. A similar result has been noted for a martensitic transformation in the copper-germanium system[79] and postulated for cobalt in discussions by Nelson[28]. The bands resolved via replica techniques are 0.1 to 1.0 microns thick and completely traverse a grain. Bands of this thickness require operation of similar partial dislocations on 150 to 1500 close-packed planes. The fact that this banded structure is not always observed is explained by the fineness with which the transformation may operate with respect to shear directions. If the shear direction changes every few close-packed planes, shear markings are too fine to discern by replica techniques. Bands are observed only when the constraints on a volume of crystal yield a strong preference for a given shear direction. This analysis explains why for some years there was a dispute over the martensitic nature of the transformation in cobalt. Without the aid of the electron microscope, the shear is difficult to discern.

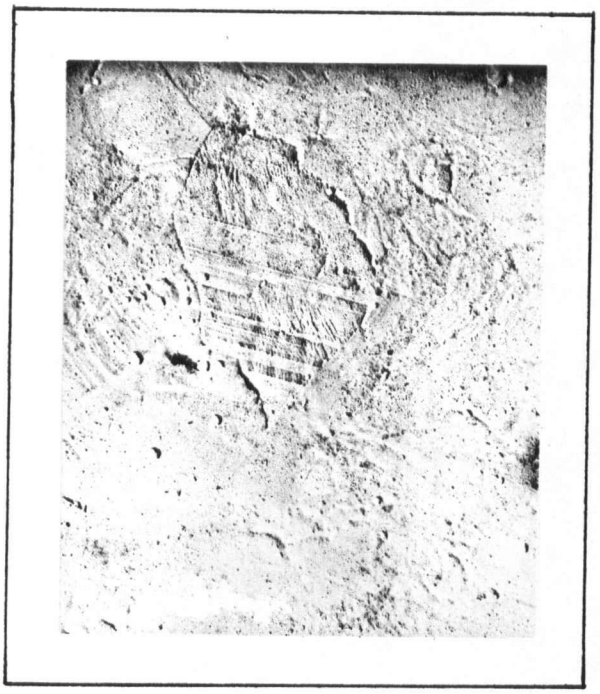

Fig. 19(a) 4000X

Fig. 19(b) 10,000X

Figs. 19(a) - 19(c) Banded structure arising from coplaner multivariance in cobalt.

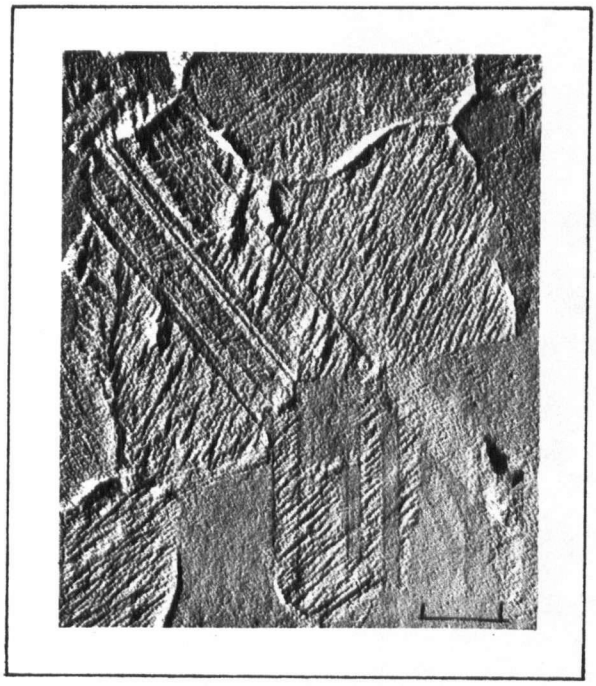

Fig. 19(c) 10,000X

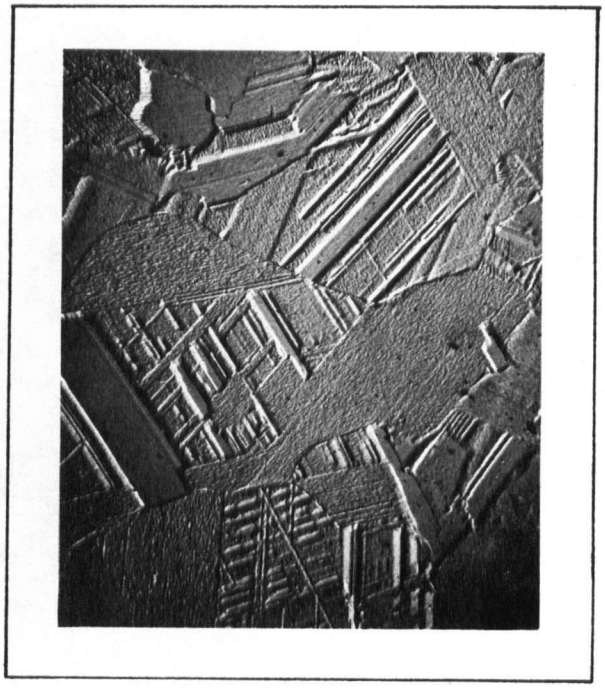

Fig. 20 99.998% cobalt, 47 micron grain size, 2000X

For annealing treatments with T between 500 and 600°C, the retained fcc phase is a maximum. At room temperature, all specimens are 40 - 60% fcc. The retained phase does not occur as individual fcc grains, but as regions of fcc lattice distributed within individual grains.

c) Annealing above 600°C

An annealing cycle above 600°C gives rise to grain growth. For 99.998% cobalt, grain growth is proceeding rapidly at 600°C while for 99.7% cobalt, grain growth is barely underway. As the fcc grain size increases, the grain substructure observed at room temperature becomes less complex. The banded structure noted in fine grained material is not observed for grain sizes over approximately 15 microns. Large volumes of crystal transform on a single (111) varient in large grains. Multivariance occurs but the plates of different orientation are coarser than for fine grained material: (Figure 20).

As the grain size increases the amount of retained fcc decreases. For an fcc grain size of 50 microns, approximately 30% of the lattice remains fcc. For grain sizes over 300 microns, this value drops to 10% retained fcc. For the limiting case of a single crystal the transformation proceeds to completion.

The structure of the cobalt specimens produced for further testing may be summarized as follows:

i) All specimens were recrystallized cobalt, furnace cooled to room temperature at approximately 6°C per minute. Their purity ranged from 99.7% to 99.998%.

ii) The grain size for the material varied from less than 5 to over 50 microns, while the retained fcc decreased from over 50% to less than 30%.

iii) All polycrystal grains were a mixture of fcc and hcp phases. Most crystals had hcp regions of different orientation with very strict orientation relationships. That is, all hcp regions were stacks of close-packed planes that intersect at angles between {111} planes in the parent fcc grain.

iv) The structure was not an equilibrium one. The thermodynamic driving force attempting to complete the martensitic transformation was available, but it was so small that the constraints arising from thermal anisotropy and the volume change involved in the transformation retained material in the fcc phase.

v) The substructure within grains was varied. The shear produced by transformation delineated annealing twin boundaries in the parent fcc grains. The growth of martensitic plates on more than one (111) type planes, termed multivariance, was always present. Repeated transformation in a <112> direction in a given (111) plane produced a banded structure in fine grained material.

3.2 Tensile Behaviour of Cobalt Polycrystals

3.2.1 Tensile Results

3.2.1.1 True Stress - True Strain Curves

True stress - true strain curves for cobalt at selected test temperatures are shown in Figures 21-23. The behaviour as a function of grain size is shown in Figure 24. Several important observations may be drawn from this data;

i) the measured stress levels appear high for a pure metal. The ultimate tensile strength at room temperature exceeds 150 X 10^3 psi for fine grained material.

ii) the temperature dependence of the flow stress is large. As shown in Figures 21-23 the flow stress at yield increases by greater than a factor of 2 for a temperature change from 400°C to -196°C. The ultimate strength decreases by a factor of 5 over the same temperature range (Figure 21).

iii) the yield stress decreases by a factor of 2 as the grain size is increased from 6.5 microns to 60 microns (Figure 24).

iv) the tensile curves exhibit an inflection in the initial portion of the curve. This anomaly is shown clearly in Figure 22 for 99.9% cobalt.

The strength of cobalt is compared to other common hcp metals in Figure 25(a). The tensile behaviour for hcp metals having c/a ratios higher (Zn), similar (Mg), and lower (Ti) than cobalt are included. The data is presented

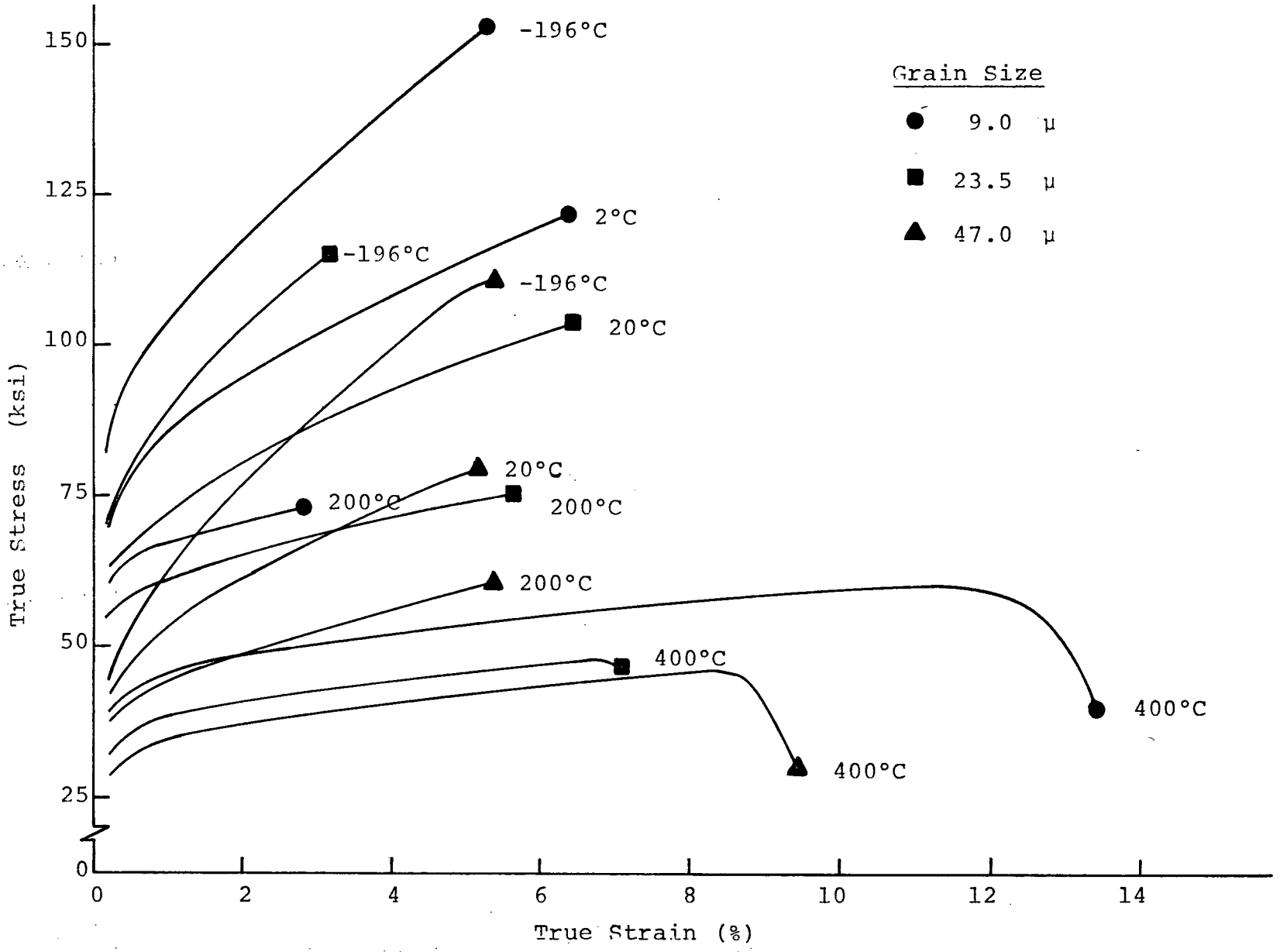

Fig. 21 True stress - true strain curves at selected temperatures, 99.998% cobalt.

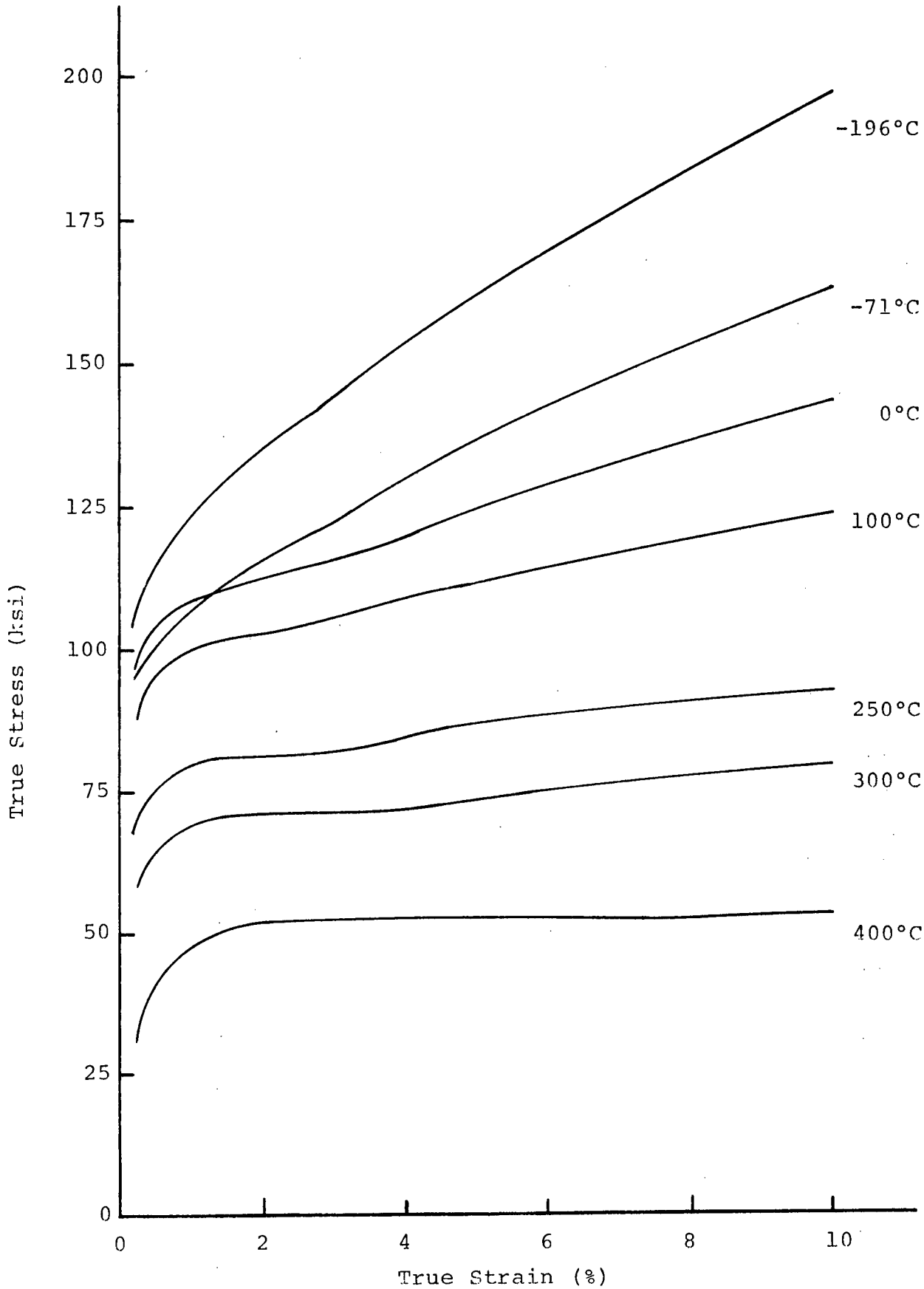

Fig. 22 Initial portion of true stress - true strain curves, 99.9% cobalt, 6.5 micron grain size

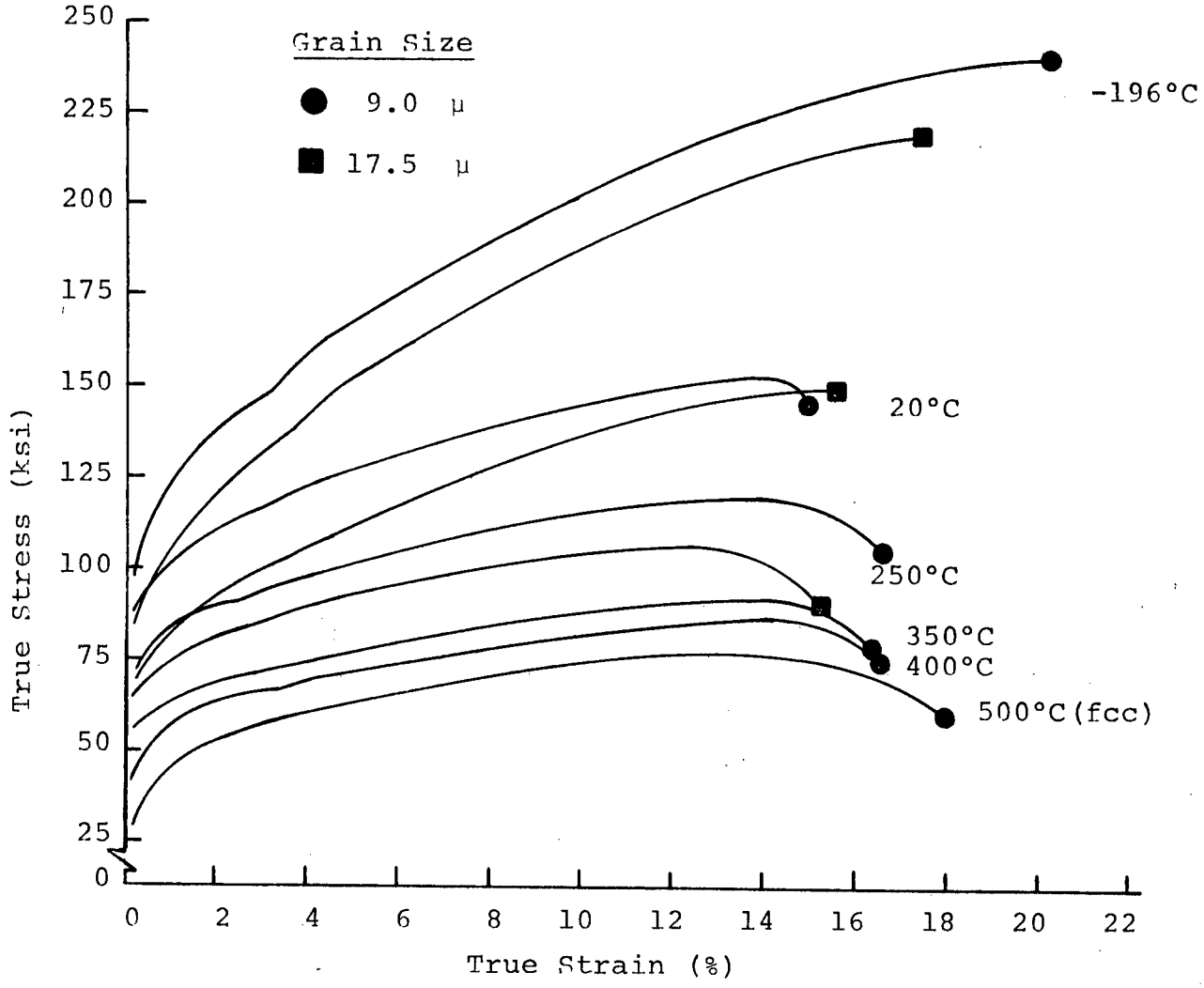

Fig. 23 True stress - strain curves at selected temperatures, 99.7% cobalt.

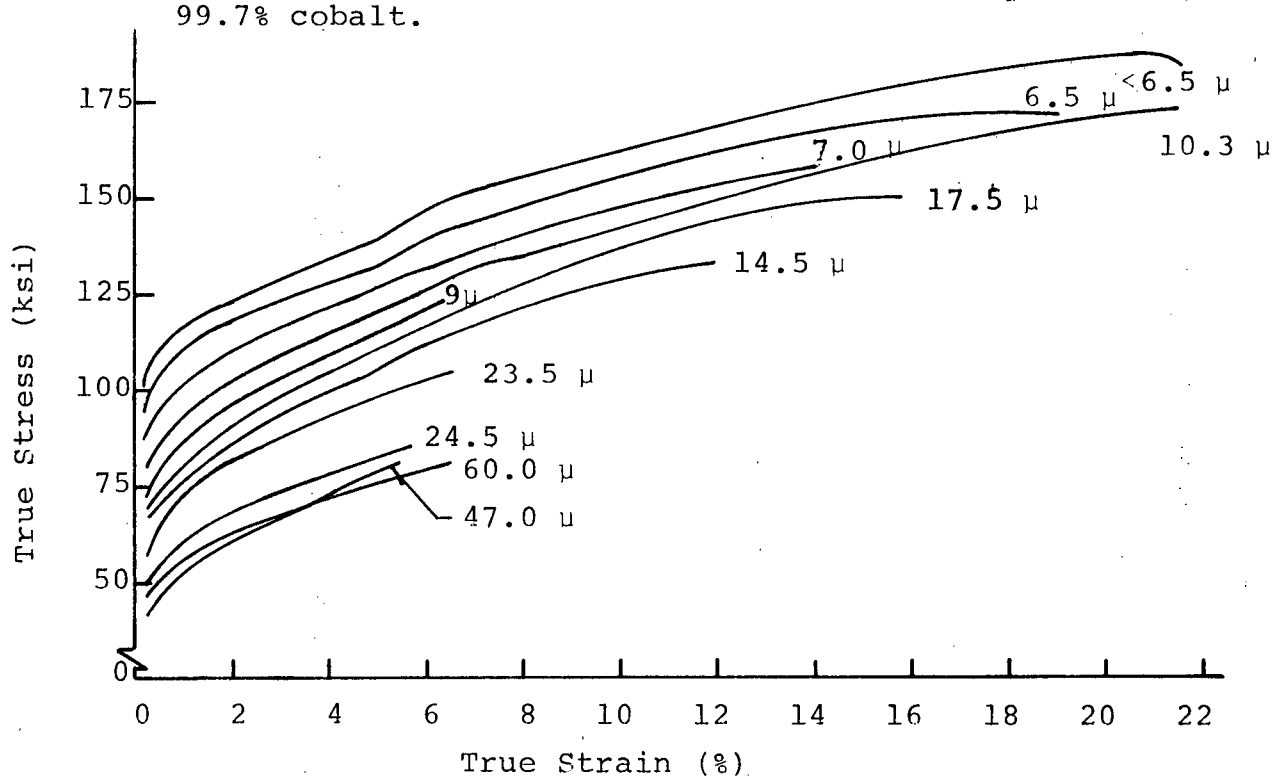

Fig. 24 True stress - true strain curves at 20°C. cobalt.

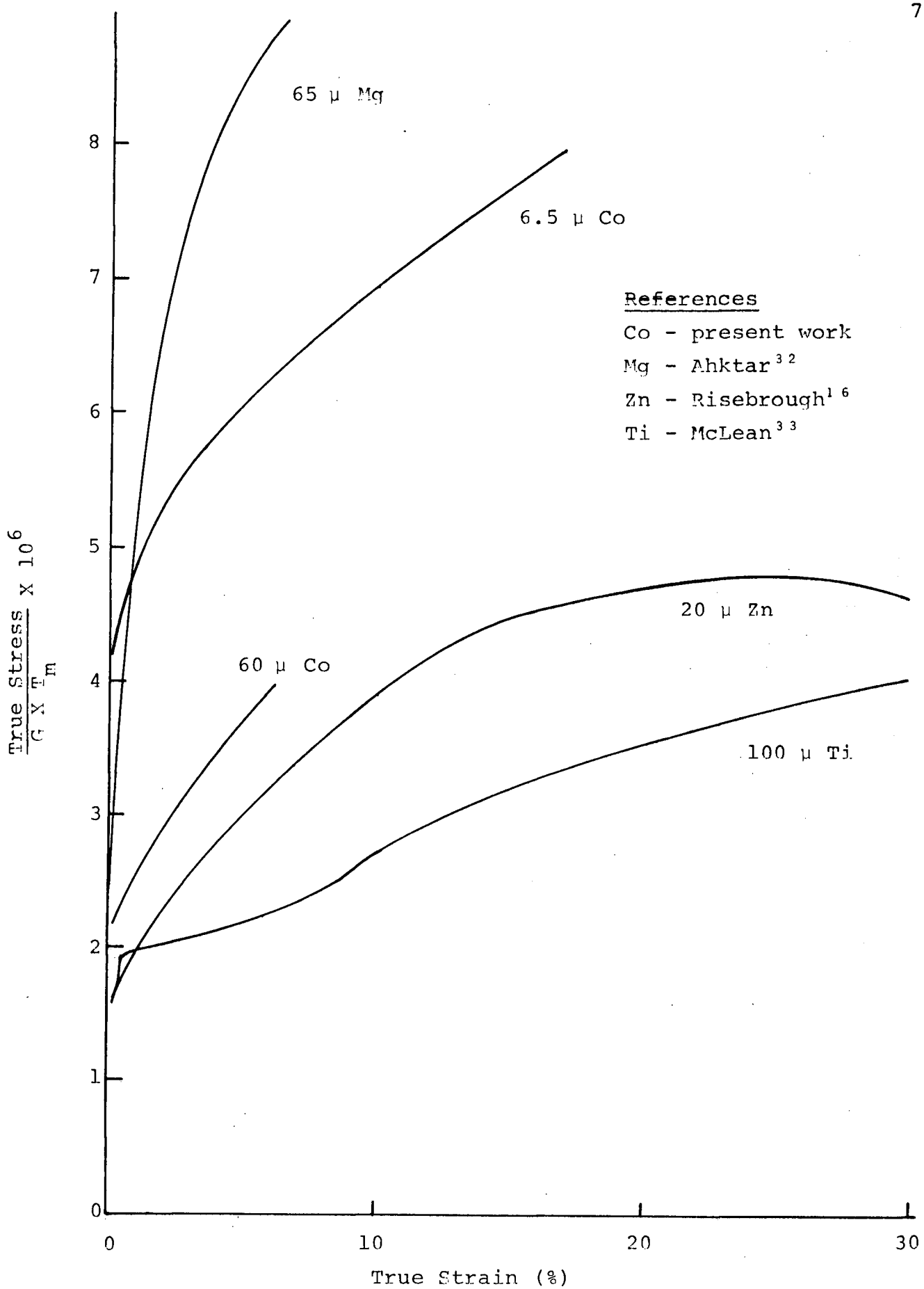

Fig. 25(a) Nominal stress - strain curves for Co, Mg, Zn, and Ti.

for room temperature properties normalized to reduce the affects of shear modulus and melting point. The fact that cobalt undergoes a martensitic transformation during deformation whereas the other metals listed do not, makes comparisons on the basis of crystal structure tenuous.

In Table II the critically resolved shear stress for a variety of metals is listed. It would appear that the common hcp metals may be divided into two groups on the basis of flow stress. One group (Cd, Zn, Mg) which demonstrates a low critically resolved shear stress, similar to the majority of fcc metals, and a second group comprised of Co, Zr, Ti, and Be which exhibit much higher values of resolved shear stress. The importance that must be attached to the presence of grain boundaries in the hcp metals is revealed clearly when the single crystal data in Table II is compared to the polycrystal data shown in Figure 25(a).

Single crystals of Ti are much stronger than single crystals of the other metals shown in Figure 25(a) yet in polycrystalline form Ti cannot be considered a strong hcp metal when compared to Zn, Co, or Mg. This apparent contradiction occurs because Ti may overcome more easily than the other metals, the requirement that coherency be retained at grain boundaries. At room temperature, titanium slips on the basal, prism and pyramidal systems. Although both Mg and Zn deform at very low stresses as single crystals, the constraint imposed by the introduction

of grain boundaries radically increases the stress levels required to continue deformation. In Zn, coherency at grain boundaries is maintained by dislocation motion on the corrugated slip planes in addition to the basal planes. The normalized stress level required to maintain coherency at grain boundaries appears to be higher for Zn than Ti. For Mg, the operation of sufficient slip systems to satisfy Von Mise's Criterion requires very high stress levels as reflected by the steep curve associated with this metal. Co with the same c/a ratio as Mg is unique in that it is a mixture of two close packed phases, fcc and hcp. The results for cobalt fall between those for Zn and Mg.

The data outlined above shows that the observed behaviour of hcp single crystals may not be generalized to include polycrystals. The limited numbers of operative slip systems in hcp metals require that each metal must be investigated individually. In Figure 25(b) curves for Co and a group of fcc metals are shown. Two observations may be made. Cobalt is considerably stronger than Ag, Cu, or Al on a normalized basis. Secondly, the affect of grain refinement is clearly larger for cobalt.

For small grained cobalt an anomaly in the true stress-true strain curves occurs at low strain values, Figures 22-24. The anomaly is not as pronounced for 99.998% cobalt. Although published curves are available, no mention has been made of this effect in cobalt[81-83]. This is not surprising, as the anomaly is not large and becomes clear only after calculating true stress values for many values of strain and plotting to a large scale.

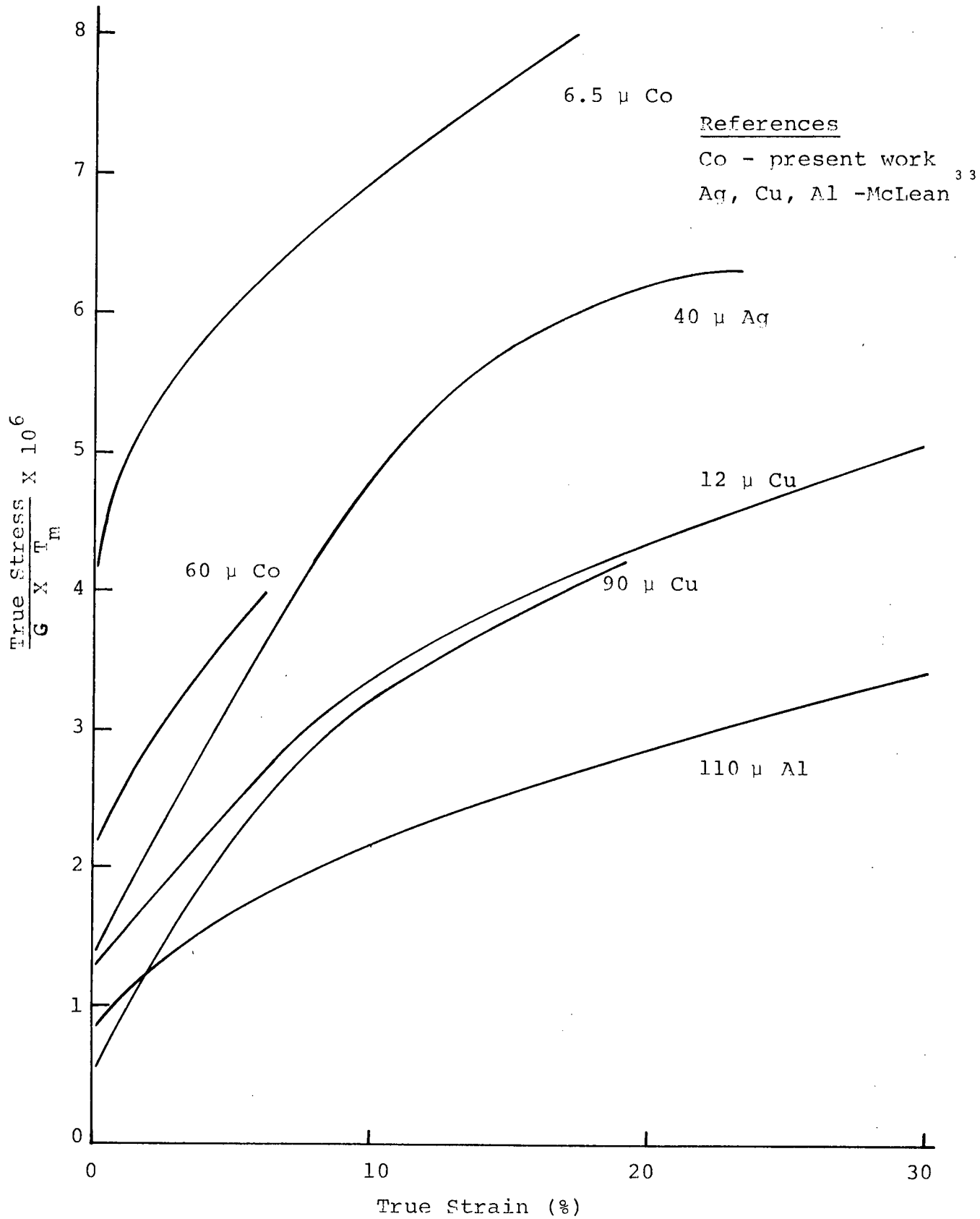

Fig. 25(b) Nominal stress - strain curves for Co, Ag, Cu, and Al.

The anomaly is not obvious for all specimens, but is most pronounced for specimens having a fine grain size. A small grain size is equivalent to a large initial fraction of retained fcc, in other words a large volume of material available for martensitic transformation.

Published true stress - true strain curves for materials known to transform martensitically during deformation are presented in Figure 26. Included are data for 303 stainless steel[105], Hadfield's Manganese Steel[105], equi-atomic Ni-Ti[106], and cobalt.

The retained high temperature phase in 18-8 stainless steel and Hadfield's Manganese steel is fcc. Some hcp martensite is generated by plastic deformation in the 18-8 stainless. This hcp martensite is believed to be a transition phase and most of the end product martensite produced is bcc[105]. This stress induced martensite gives rise to the low initial work hardening rate in the 18-8 stainless steel at liquid nitrogen temperatures[105]. A similar explanation is proposed for the anomalous behaviour in the equi-atomic Ni-Ti shown. The large anomaly observed for 18-8 stainless and equi-atomic Ni-Ti are not evident for Hadfield's Manganese Steel. Although all four materials transform to martensite while undergoing deformation, it is probable that no initial low strain hardening occurs in Hadfield's steel because no significant quantity of low energy martensite is formed. Of all martensitic transformations, the transformation from fcc to hcp is the lowest energy form, requiring only a simple shear which need not be accompanied

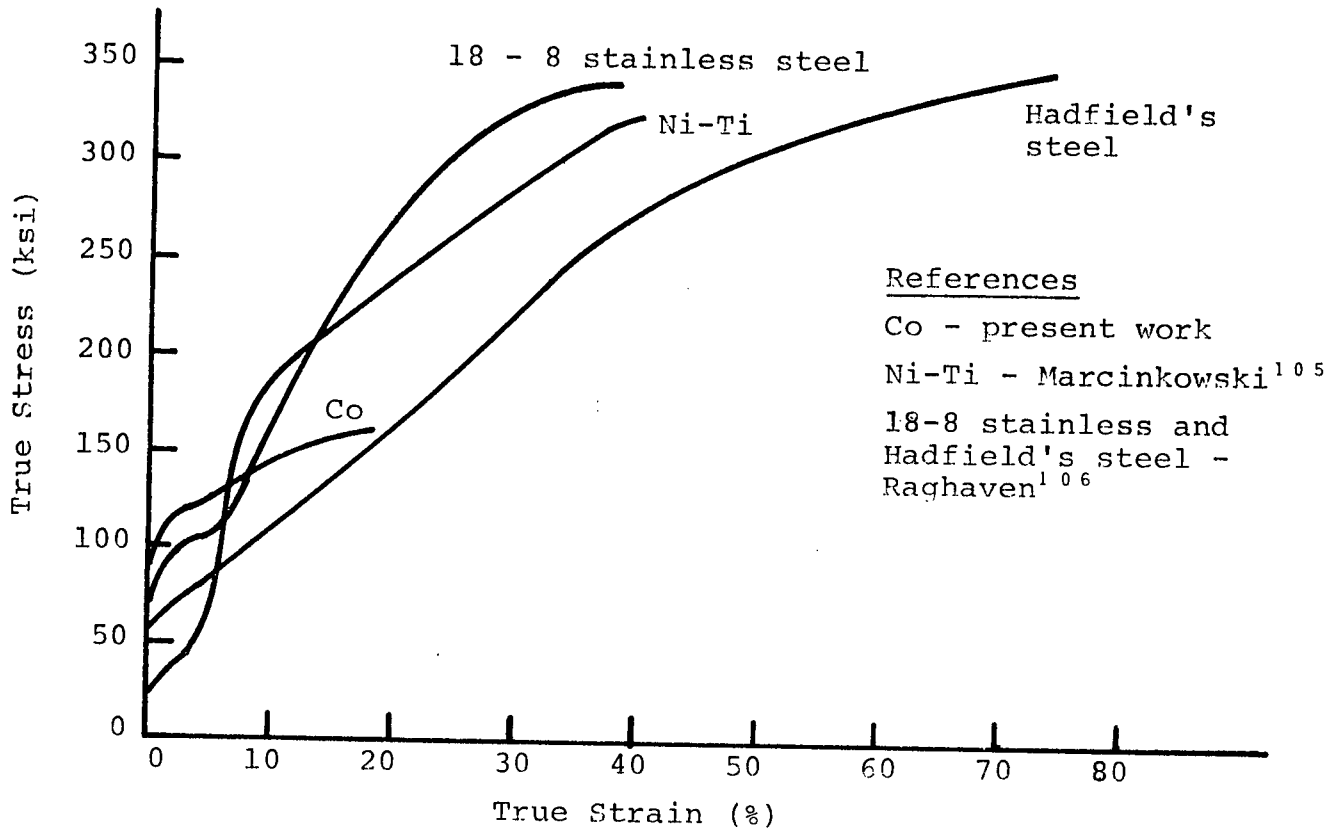

Fig. 26 True stress - true strain curves for materials undergoing strain induced martensitic transformation.

by further deformation to form the second phase (Table VI). Thus, while 18-8 stainless steel forms a low energy form of hcp martensite and Ni-Ti does likewise, the Hadfield's steel probably forms a more complex martensite directly.

Cobalt, like the 18-8 stainless steel and the Ni-Ti forms a simple hexagonal structure from the fcc phase. The anomalies are larger for the 18-8 stainless steel and Ni-Ti because these materials are initially 100% retained face-centered phase while cobalt is a mixture of both phases.

TABLE VI Martensite Transformations in Non-Ferrous Materials

Material and Composition	Structural Change	Additional Deformation
In-Tl (∿20 at. % Tl)	fcc -- fct	T, S
Au-Cu (∿50 at. % Cu)	fcc -- ortho.	T, P
Au-Mn (∿50 at. % Mn)	bcc -- bct	T
Au-Cd (∿50 at. % Cd)	bcc -- bct	T, M, S
Au-Cd (∿47.5 at. % Cd)	bcc -- ortho.	T, M, S
U-Mo (5-10 at. % Mo)	bcc -- ortho.	T, F
Cu-Zn (∿40 wt. % Zn)	bcc -- ortho.	T, E
" "	bcc -- fcc	T, C, E
Cu-Al (∿12 wt. % Al)	bcc -- ortho.	T, E, P
" "	bcc -- fcc	F, E
" "	bcc -- tet.	F, E, P
Li	bcc -- hcp	T, E, ?
Ti, Zr	bcc -- hcp	T, D, ?
Ti-Mn (∿5wt. % Mn)	bcc -- hcp	T, ?
U-Cr (∿1 at. % Cr)	tet. -- ortho.	D, ?
Hg	rhomb. -- bct	?
Co	fcc -- hcp	X

Notation:

T Twinning

X No additional deformation required

? Unknown or information uncertain

C Transformation in thin foil

D Common deformation modes

E Thin foil observations made

M Parent structure ordered

P Product structure ordered

S Single interface transformation observed

3.2.1.2 Yield Stress and Ultimate Tensile Stress

To determine and isolate the effect of purity on the yield strength of cobalt, a large number of tests were carried out on material of 99.7% and 99.998% purity with similar grain sizes. Some variation in the initial amount of retained face-centered phase was unavoidable.

From Figure 5, it was observed that 99.7% cobalt annealed one hour at 700°C has a grain size of approximately 10 microns, as does 99.998% cobalt annealed one hour at 600°C. The initial amount of retained fcc phase is 46.5% for the low purity material and 40.8% for the high purity material.

As shown in Figure 27, the effect of increasing purity on the 0.2% offset yield stress in cobalt is not large. Increasing purity from 99.7% to 99.998% decreases the yield stress by approximately 4000 psi for material with a 10 micron grain size. The difference in strength between the two grades of material remains constant throughout the temperature range from -196°C to +400°C. From the data presented in Figure 27, it is clear that the yield strength of polycrystal cobalt is not a strong function of impurity content at the levels investigated.

Although purity does not affect the yield strength in a strong fashion directly, the impurity differences cause large variations in yield strength for identical annealing treatments. In other words, the yield strength is a strong function of grain size. Tensile data for cobalt

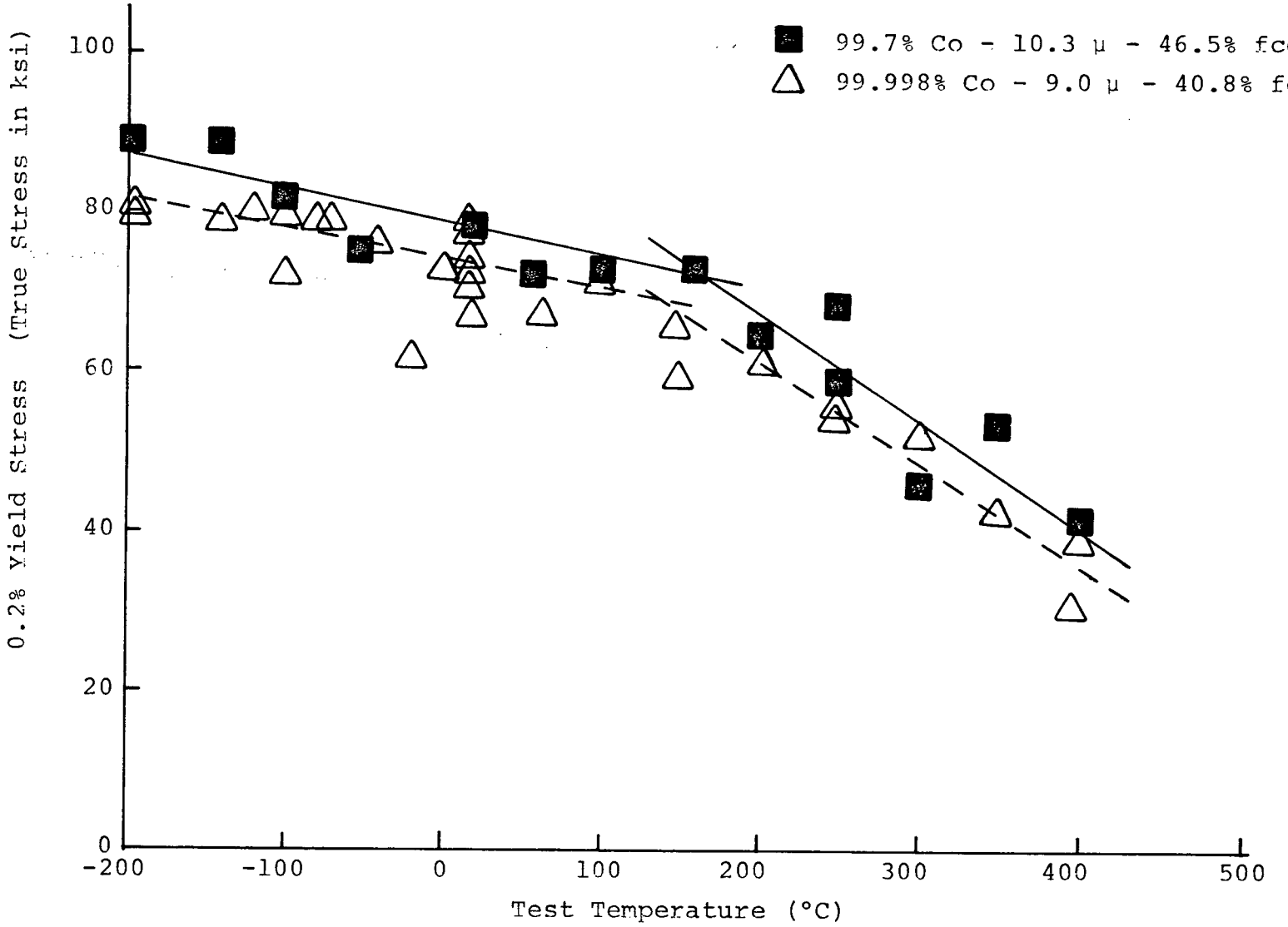

Fig. 27 Yield stress versus test temperature for two purity grades of cobalt

has commonly been tabulated with reference to annealing temperature[81,82,88]. The discrepancies in this data would be reduced if the tensile parameters were normalized to account for grain size. For example, 99.7% cobalt and 99.998% cobalt having undergone identical (one hour) annealing treatments at 800°C, differ in yield strength by approximately 30,000 psi. (See Figure 28).

The variation in stress with test temperature is shown in Figures 28 and 29. For all materials, the temperature dependence of the yield stress has two distinct regions. At low temperatures, the yield stress decreases very slowly with increasing temperature. At higher temperatures, the yield stress drops rapidly with temperature; the effect is not as pronounced for large grained material. (Figure 28).

Due to the scatter in results between individual test specimens, especially regarding the yield stress, it was difficult to accurately define the two regions of temperature dependence. In an attempt to alleviate this problem a further group of specimens were tested.

Single specimens were step pulled over the complete temperature range from -196°C to 400°C. Some specimens were initially yielded at low temperatures and others at high temperatures. The specimens were then retested every 20 or 30 °C for small increments of strain. An intersect method was used to subtract out the work hardening that had taken place up to the given step-pull being analyzed to arrive at the yield stress for the temperature in question.

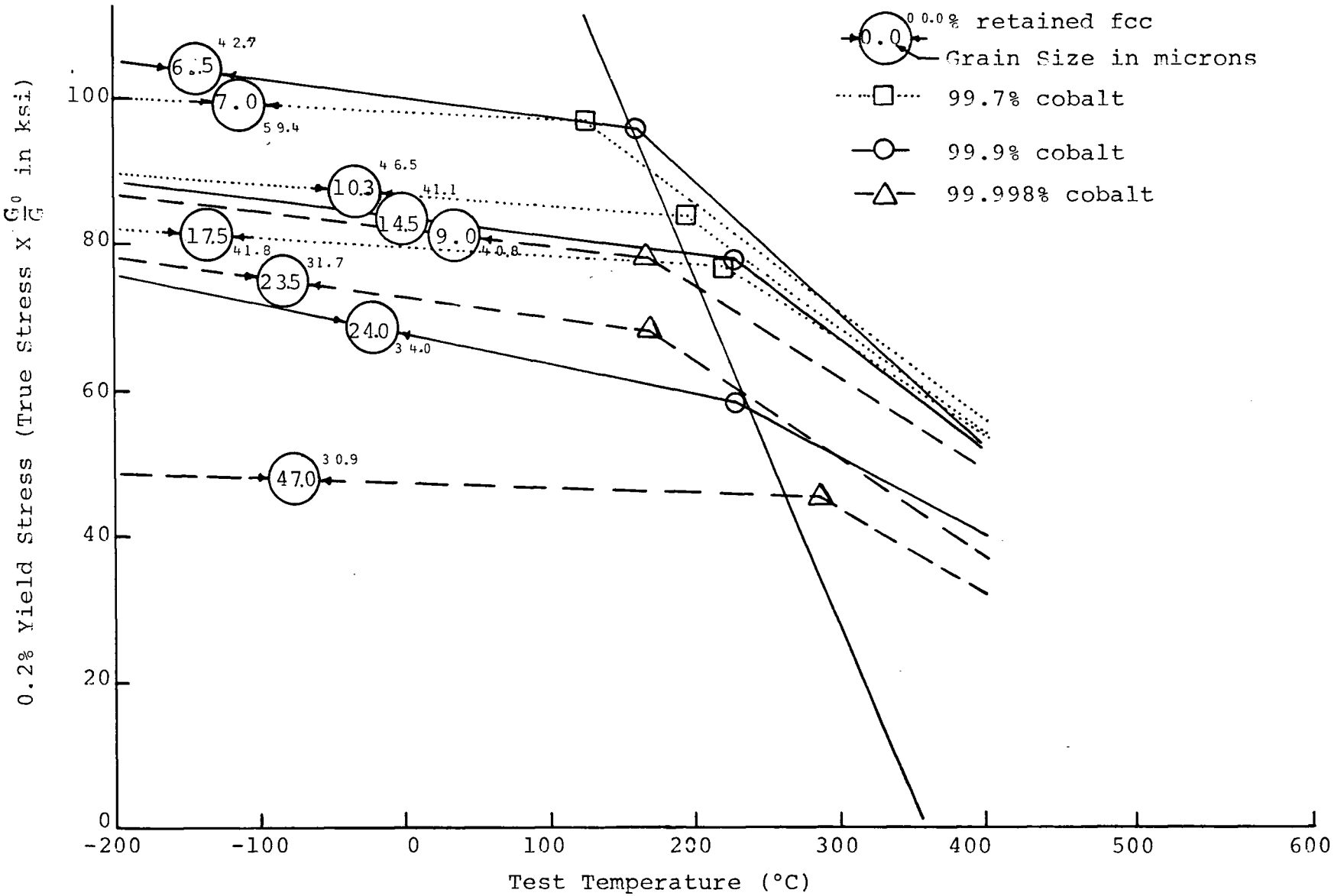

Fig. 28 Yield Stress data for polycrystal cobalt.

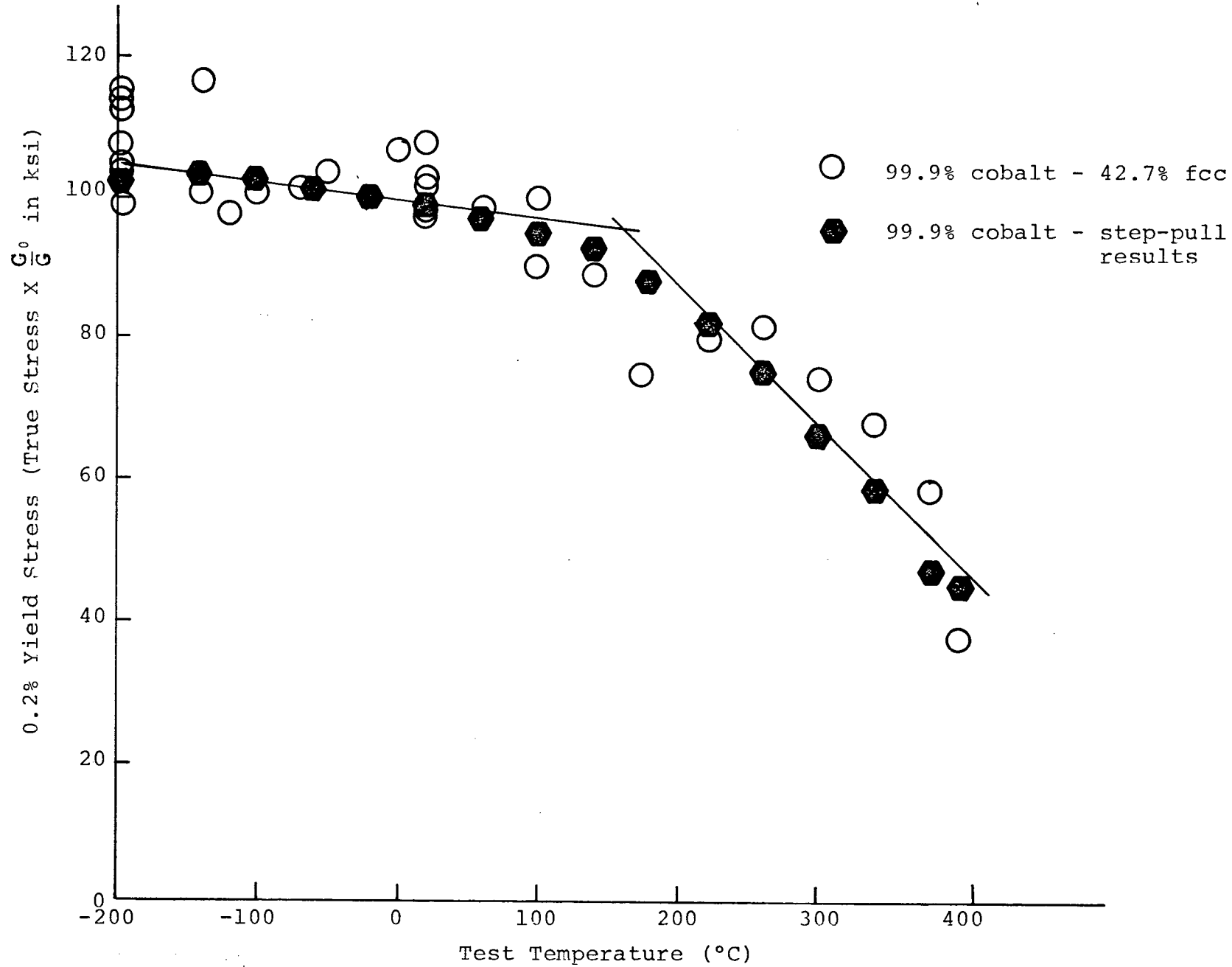

Fig. 29 Comparison of yield stress data obtained by individual tests and interupted single specimen testing. 99.9% cobalt, 6.5 micron grain size

The data provided by this type of test must be evaluated carefully. In addition to physical measurement problems, there are other areas for concern. The stress relaxation that is attendant to the martensitic transformation of cobalt can cause anomalies upon reyielding specimens of cobalt[107-109]. At higher temperatures, dynamic recovery may occur while testing and recovery procedes during the lapses while the temperature of the testing environment is being adjusted. A large correction must be applied to the raw tensile data to adjust for the variation of work hardening rate with strain and temperature. The calculations carried out for tests of this type are outlined in Appendix 2.

Figure 29 is a plot of step-pull test data for 99.9% cobalt annealed one hour at 600°C. The data gathered from many individual tests is included for comparison. The agreement between the two sets of data is encouraging. Further tests were carried out over various temperature ranges with a variety of specimens. In all cases, acceptable agreement with the results determined by many tests were found.

Figure 28 presents the variation in yield stress with test temperature for all material tested. The pertinent information to be drawn from this graph is reproduced in Table VII. Two important observations may be made. The temperature dependence of yield stress has two distinct regions and yield stress is a strong function of grain size.

TABLE VII Polycrystal Cobalt - 0.2% Yield Stress Data

Grain Size (μ)	Purity (%)	0.2% Yield Stress (True Stress X G_o/G / True Stress) -196°C	20°C	250°C	400°C	Temp. for Slope Change °C	T/T_m	Slope at High Temp. / Slope at Low Temp.
6.5	99.9	104.0/101.2	98.0/88.3	78.0/62.5	50.0/38.9	160	0.25	7.2
7.0	99.7	99.5/ 96.8	97.0/87.4	72.0/61.7	53.0/41.2	128	0.22	14.8
9.0	99.998	86.5/ 84.2	81.5/73.4	68.0/54.5	48.5/37.7	167	0.25	8.0
10.3	99.7	89.0/ 86.6	86.0/77.4	75.0/60.0	53.0/41.2	195	0.27	9.0
14.5	99.9	88.0/ 85.6	82.5/74.3	73.0/58.5	50.0/38.9	225	0.28	6.0
17.5	99.7	81.5/ 79.3	79.0/71.1	72.5/58.1	53.0/41.2	220	0.28	8.9
23.5	99.998	78.0/ 75.9	71.5/64.4	56.0/44.9	36.0/28.0	170	0.25	7.2
24.0	99.9	75.0/ 72.7	66.0/58.4	55.0/44.1	39.0/30.3	225	0.28	2.3
47.0	99.998	48.5/ 47.2	47.0/42.3	45.0/35.5	33.0/25.0	288	0.32	11.5
<6.5	99.9	95.5/ 92.9*	100.4/90.4*	81.4/65.2*	62.0/48.2*	-	-	-
60.0	99.9	-	49.2/44.3*	-	-	-	-	-

* Single Tensile Test

The yield stress behaviour of cobalt as a function of temperature is unlike that for most common metals[33]. In copper, zinc, and molybdenum for example, the yield stress drops steeply with increasing temperatures at low temperatures and becomes relatively temperature independent at higher temperatures. Similar behaviour is observed in polycrystal magnesium[32] and single crystal cobalt[4].

For 65 micron magnesium, the yield stress decreases slowly with temperature up to 0.21 T_m (-80°C) and then drops quickly until 0.43 T_m (125°C) is reached. Beyond 0.43 T_m the yield stress continues to decrease at a lower rate once again. (Figure 30). To allow comparisons between polycrystal cobalt and polycrystal magnesium, the data for both metals are plotted with the ordinant normalized for shear modulus and the homologous temperature plotted as abcissa. From this graph, it is clear that the general shape of the curves are similar. Also, the temperature at which both metals change behaviour, and the temperature dependence of stress are comparable.

A comparison between the yield behaviour of polycrystal and single crystal cobalt is presented in Figure 31. The resolved shear stress (τ) in a polycrystal is somewhat less than 1/2 the measured value for tensile yield if the Schmid factor is considered. For this reason, the polycrystal data are plotted as $\frac{\sigma_{0.2\%}/2}{G}$ to allow comparison with the single

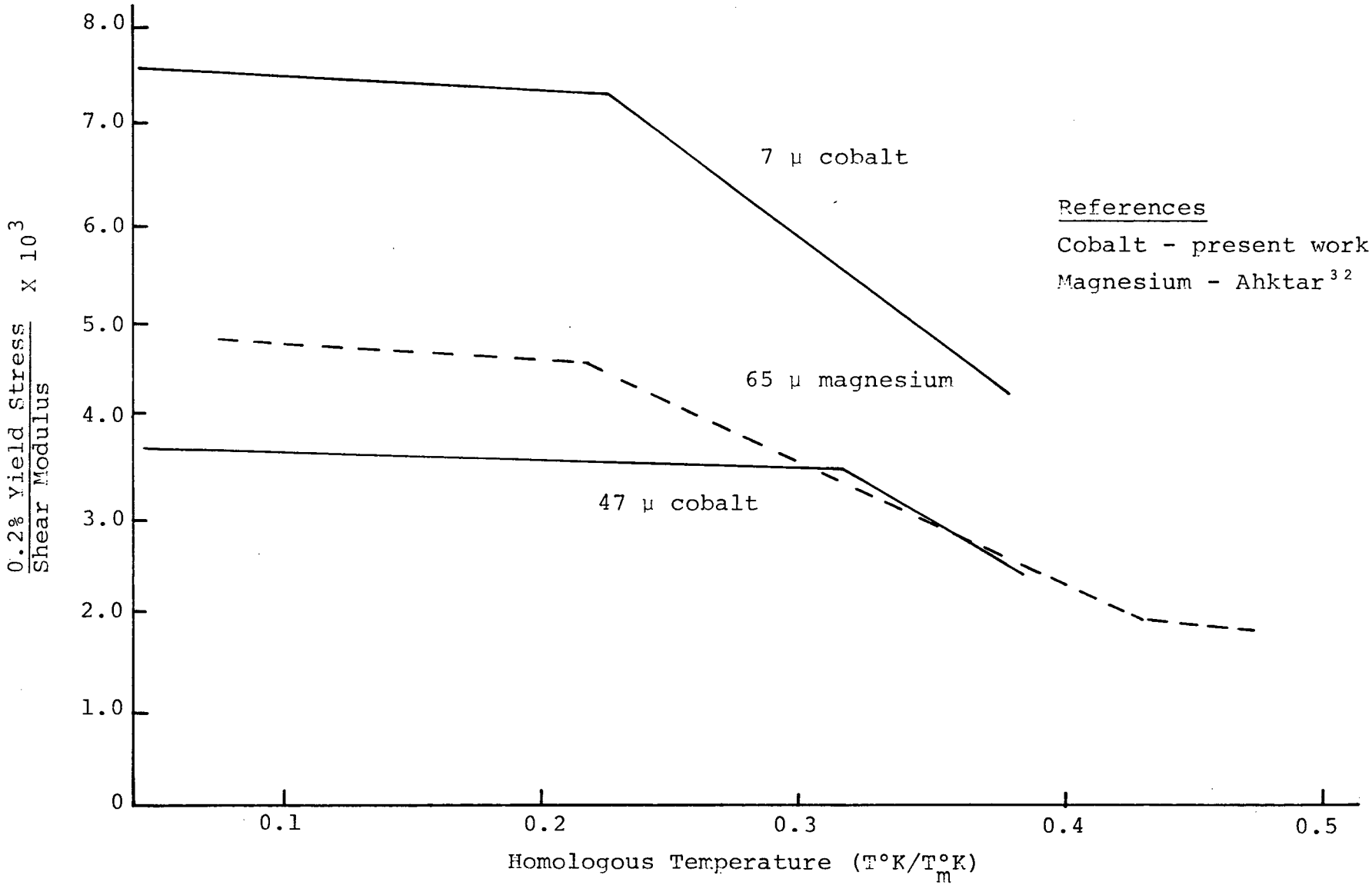

Fig. 30 Yield stress versus test temperature for cobalt and magnesium.

crystal data. Although this correction was made, it is still necessary to plot the single crystal data on a scale a factor of 10 larger than polycrystal results for the trends to be visibly examined. The abcissa is shown both as a fraction of the melting point, and as a fraction of the transformation temperature. The latter scale is included to provide a measure of the metastability of the fcc phase present in the cobalt polycrystals. The data for fcc cobalt single crystals is also presented to show the sharp differences in behaviour between the two phases as single crystals.

Several conclusions may be drawn from Figure 31. The polycrystalline behaviour is similar to that observed in single crystals. Although absolute values for the curves vary, the fact that both types of material exhibit two distinct types of temperature dependence is informative. A second important observation is that the critical temperature at which the yield stress changes behaviour, increases with increasing grain size in a manner that yields upon extrapolation a value close to that obtained for single crystals for very large grained polycrystals. The line representing this trend in Figure 28 is also shown in Figure 31. This line, determined from polycrystal data, predicts a change in yield behaviour at $0.36T_m$ for cobalt that yields at 2 to 3,000 psi. Hcp single crystals of cobalt, in fact yield at this stress level and do change yield behaviour at approximately $0.35\ T_m$.

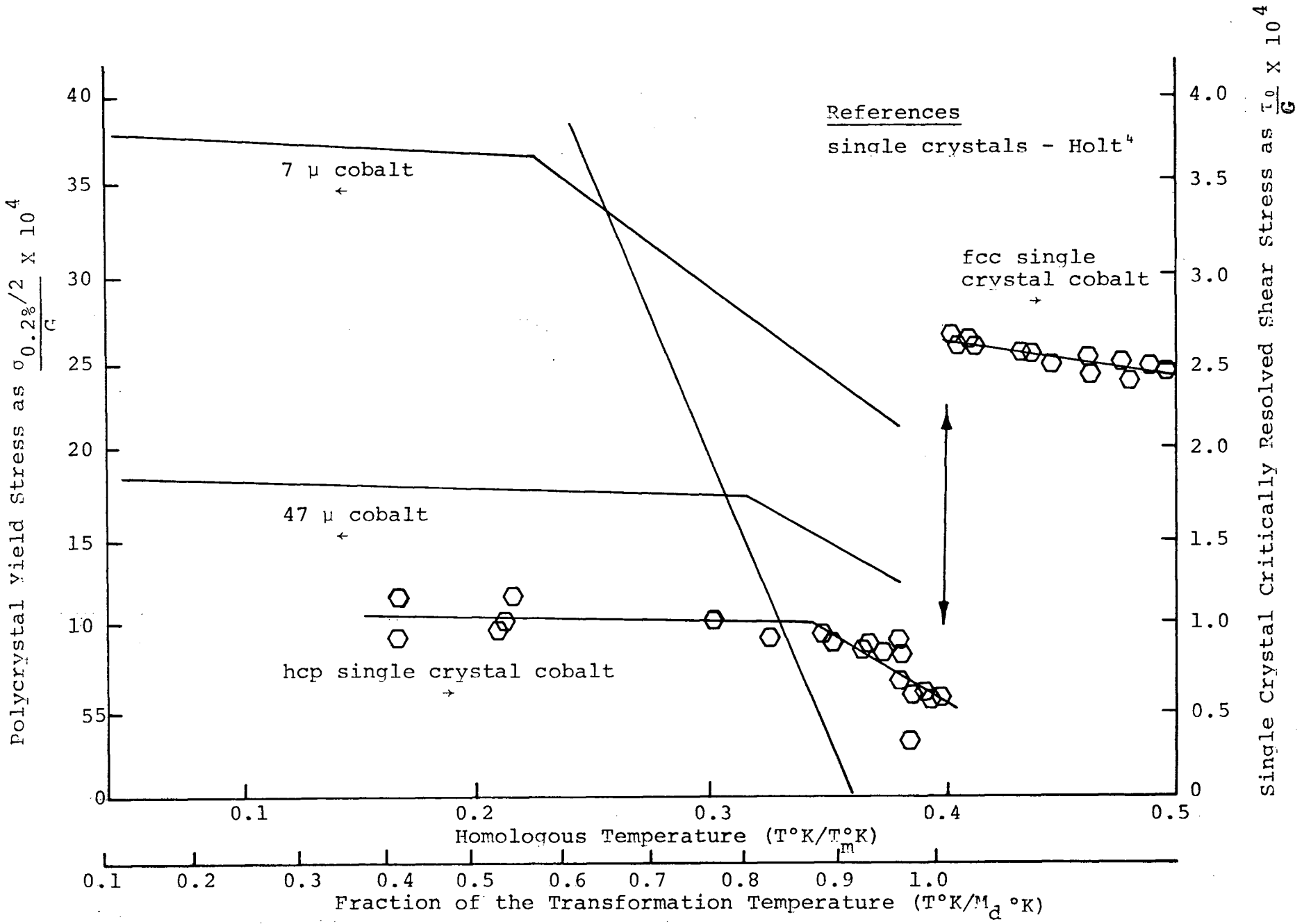

Fig. 31 Yield stress versus temperature for cobalt single crystals and polycrystals

At this juncture two important facts are clear. The yield stress of cobalt appears to be controlled by two processes. One process, which is almost athermal at low temperatures, and a second process which is strongly temperature dependent at higher temperatures. Secondly, the change from one process to the other occurs at higher temperatures as the grain size increases.

A discussion of the processes that may be determining the temperature dependence will be deferred until further aspects of tensile behaviour of cobalt have been presented.

The two regions of temperature dependence noted for cobalt at yield, disappear as strain increases. The temperature dependence of the flow stress at yield and failure is shown in Figure 32. The data is presented for a small grained (6.5 micron) group of specimens of 99.9% purity. Figure 33 shows a typical set of data points from which Table VIII and IX were constructed. Similar curves to that shown in Figure 33 were obtained for all material tested.

In attempting to compare the flow stress behaviour with that of magnesium a problem arises. The limited ductility of pure magnesium, (less than 2% for 65 micron material[32]), does not allow for comparison of the flow stress at the high values of strain that can occur in cobalt. The two materials do exhibit parallel behaviour over the range of strain where comparisons can be made.

The disappearance of the essentially athermal behaviour of flow stress at low temperatures as strain increases may imply that the mechanism controlling the initial deformation

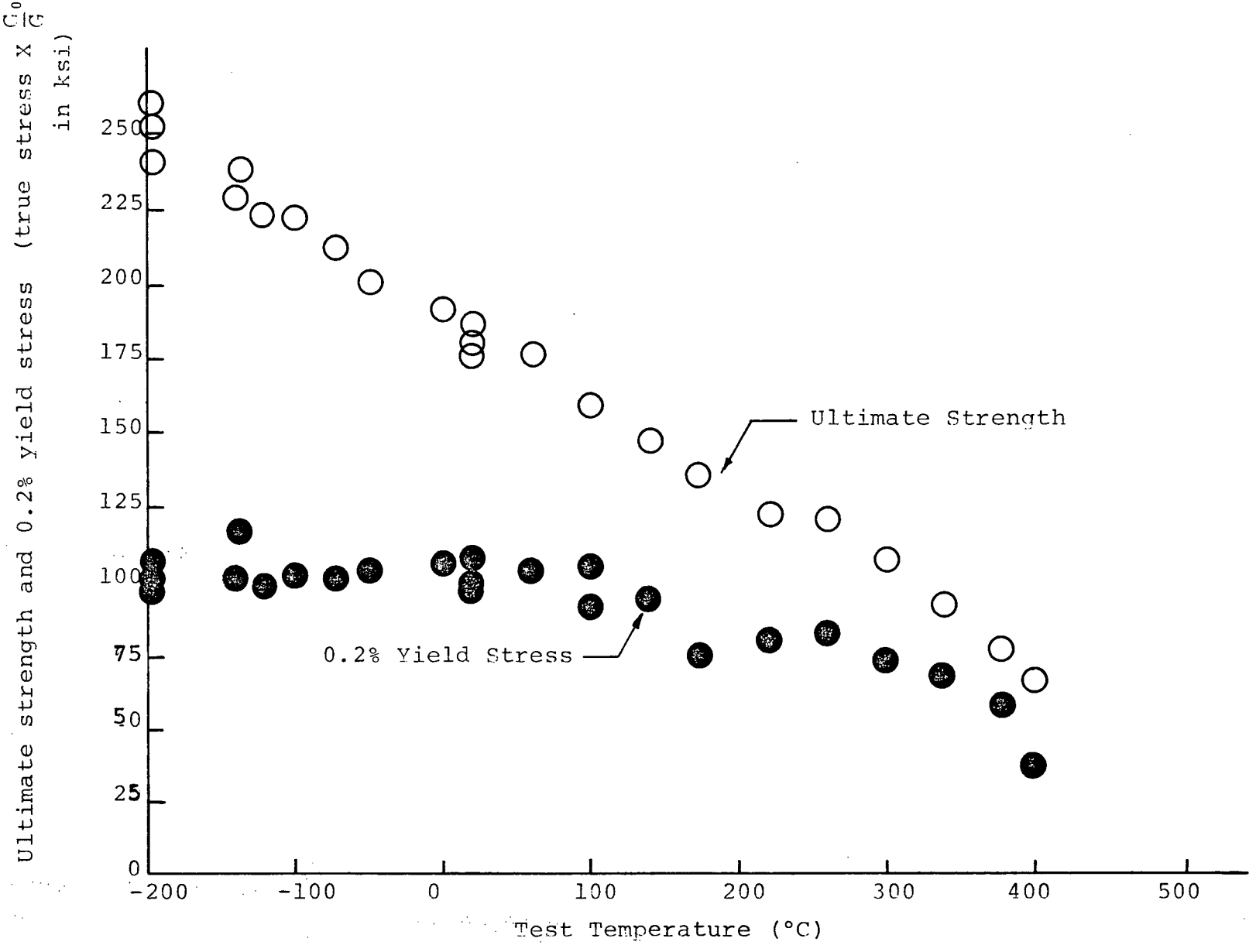

Fig. 32 Yield stress and ultimate strength data for 99.9% cobalt, 6.5 micron grain size.

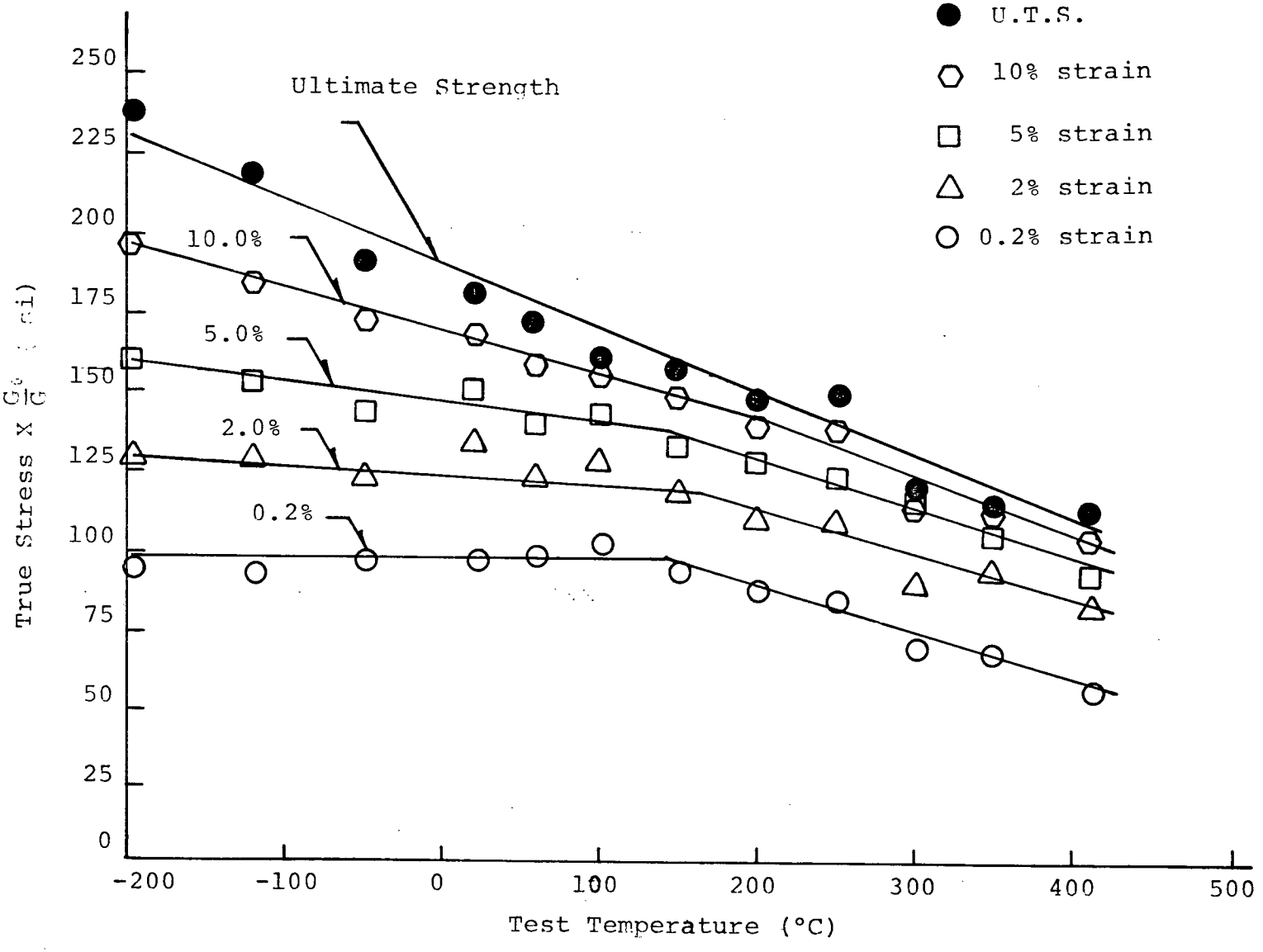

Fig. 33 Typical data for determining the temperature dependence of flow stress. 99.7% cobalt, 7.0 micron grain size.

in cobalt at low temperatures, does not control the stress levels at large values of strain.

The temperature dependence of the flow stress is given in Table VIII as a fraction of the shear modulus for a change in temperature of 100°C. It is clear that for all materials tested, the temperature dependence of yield at low temperature is about an order of magnitude less than at high temperature. The amount of strain required to eliminate this two stage characteristic decreases as the grain size becomes larger. For example, in 99.7% cobalt, two regions of temperature dependence are observed at greater than 10% strain for 7 micron material, yet for 17.5 micron material of the same purity, no difference is observed at 5% strain. (Table VIII).

The absolute effect of purity on the flow stress is small at all values of strain. In Figure 29, the difference was presented at yield. This difference in stress level remains small at all values of strain. Thus, the fact that the impurity level does not affect yield in a strong manner may now be expanded to include the complete stress-strain curve.

As outlined earlier, the ultimate strength of cobalt is very high for a pure metal. This fact was shown in a general way previously in Figure 25. From Table IX it may be seen that polycrystal cobalt fails at stress levels approaching G/50 at -196°C and G/70 at room temperature. The highest stress level sustained by pure polycrystal magnesium is approximately G/100[32]. Other pure metals fail at considerably lower levels[33].

TABLE VIII Temperature Dependence of Flow Stress ($\frac{\Delta\sigma}{G}$ for 100°C temperature change)

Purity		99.7%			99.9%			99.998%		Strain
Grain Sizes	7.0	10.3	17.5	6.5	14.5	24.0	9.0	23.5	47.0	(%)
	7.6	12.1	10.6	19.7	19.7	36.3	12.1	15.2	7.6	0.2
Low temp. slope where required	25.8	34.0	38.0	59.0	68.0	58.0	50.0	58.0	39.0	2.0
	50.0	62.0	-	107.0	118.0	-	-	-	-	5.0
$\Delta\sigma/G$	106.0	-	-	-	-	-	-	-	-	10.0
	-	-	-	-	-	-	-	-	-	U.T.S.
Temp. of change T/T_m	0.22	0.27	0.27	0.25	0.28	0.26	0.25	0.25	0.32	
	0.26	0.28	0.28	0.28	0.29	0.28	0.26	-	-	
	112.0	109.0	94.0	153.0	118.0	82.0	97.0	109.0	88.0	0.2
High temp. slope. or single slope where required $\Delta\sigma/G$	116.0	103.0	100.0	153.0	140.0	120.0	128.0	102.0	90.0	2.0
	117.0	115.0	111.0	155.0	145.0	131.0	152.0	140.0	92.0	5.0
	140.0	143.0	120.0	157.0	149.0	143.0	-	-	-	10.0
	144.0	168.0	175.0	250.0	220.0	190.0	-	-	-	U.T.S.

TABLE IX Ultimate Strength Data for Cobalt Polycrystals

Grain Size (μ)	Purity (%)	Ultimate tensile stress (true stress X G_o/G) / (True Stress) in ksi. -196°C	20°C	250°C	400°C
6.5	99.9	247/241	184/165	115/ 92	66/ 51
7.0	99.7	211/205	176/158	136/109	111/ 86
9.0	99.998	158/154	125/112	90/ 72	65/ 50
10.3	99.7	222/216	183/164	138/111	110/ 85
14.5	99.9	216/210	163/146	103/ 83	64/ 49
17.5	99.7	226/220	183/164	135/108	105/ 81
23.5	99.998	142/138	125/112	78/ 62	57/ 44
24.0	99.9	192/147	145/130	94/ 75	60/ 47
47.0	99.998	116/113	95/ 85	70/ 56	55/ 43

Note: 99.998% cobalt exhibits much less ductility than the lower purity grades.

The strong variation in yield strength with changing grain size is shown very clearly in Figure 31. The yield stress for 47 micron material is less than one half that for material having a grain size of 7 microns.

Grain boundaries affect the strain hardening and strength of metals via two routes. Grain boundaries act as barriers to slip, and secondly to maintain coherency between grains during deformation of a polycrystalline aggregate, complex modes of deformation must take place within individual grains. During the initial stages of deformation, dislocations pile up at grain boundaries. As pile ups form they increase the back stress on dislocation sources inhibiting further dislocation production. At the head of the pile up, stresses increase until dislocation movement is initiated across the boundary in another grain. The measured strain hardening from this avenue will depend upon the ease of initiating slip in adjoining grains. In the case of fcc or bcc metals, where ample slip modes have been observed, the effect is not large. In the hcp metals a larger effect is observed due to the limited slip systems available.

In the outline above, pile ups of dislocations at grain boundaries were postulated. It is not necessary to assume regular arrays of dislocations in this manner. An exact distribution of the dislocations is not important; the important point is that there is a strong stress field around the end of a slip band. When the stress field

initiates slip in an adjoining grain, the back stress on the initial sources is reduced and the hardening due to the back stresses increases less rapidly. The effectiveness of grain boundaries as dislocation barriers is most important during the initial portion of the stress-strain curve while the dislocation pile ups are forming. Thus, the effect of grain boundaries on the tensile parameters is more marked in the initial portion of the tensile curve.

For a number of metals, grain size and yield stress may be related through an equation of the form:

$$\sigma_o = \sigma_i + KD^{-1/2} \qquad .....4)$$

σ_o = yield stress
σ_i = friction stress opposing motion of dislocations

K = measure of the intensity of dislocation pile ups at barriers
D = grain diameter

The derivation of this relationship is given in most standard texts[34]. The slope of a plot of σ_o versus $D^{-1/2}$ determines K. K is assumed to be almost independent of temperature, varying with the square root of the shear modulus. σ_i is the stress required to force a dislocation against the resistances arising from impurities, sub-grain boundaries, the Peierls-Nabarro force, etc. Therefore it is temperature and composition dependent, but independent of the externally applied stress.

A plot of the yield strength versus $1/\sqrt{D}$ for cobalt is shown in Figure 34. Data for zinc alloys[110] and copper[33] are also shown for comparison. Two values for 98.6% cobalt

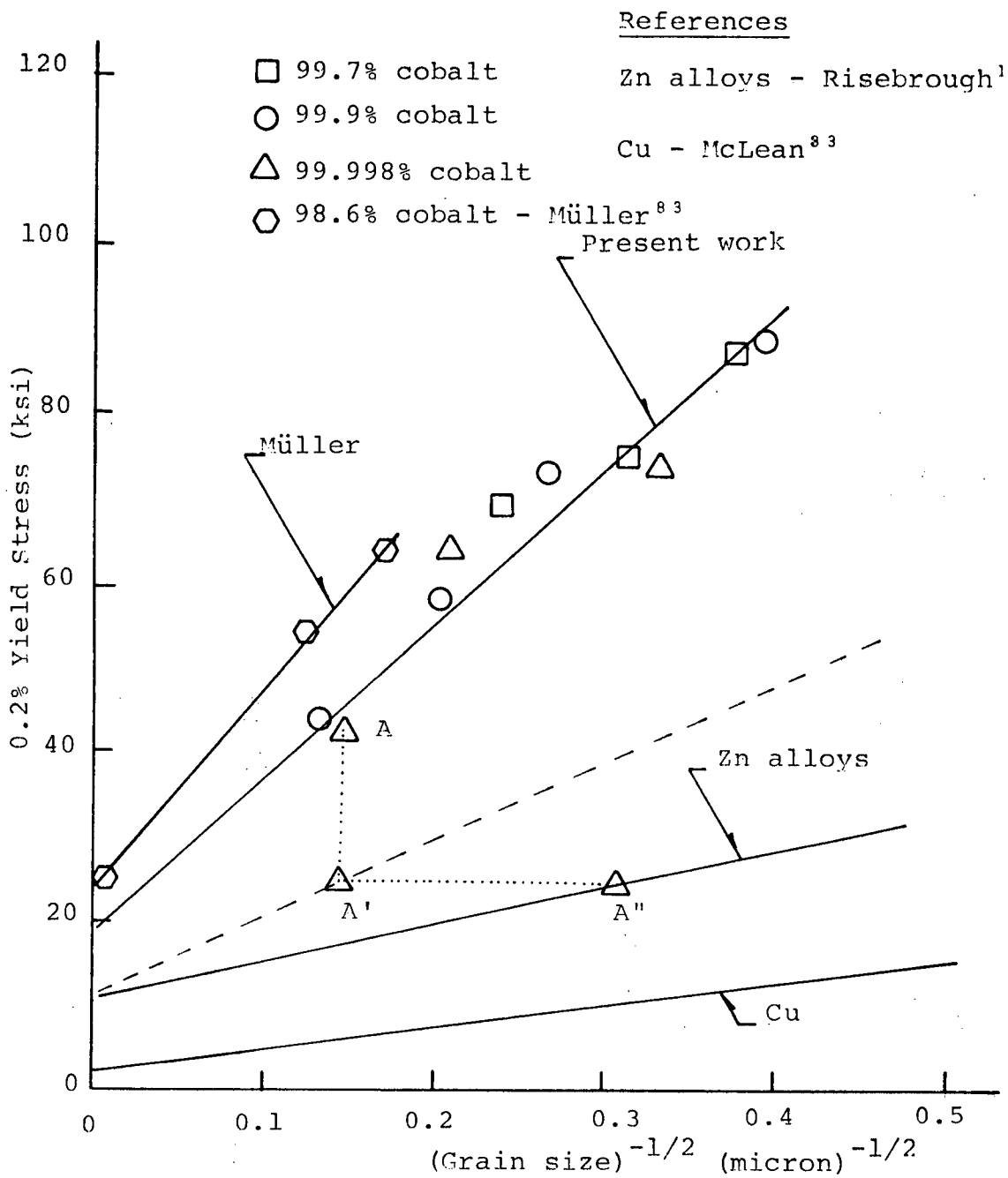

Fig. 34 Yield stress versus reciprocal square root of grain size.

drawn from the recent work by Müller[83] are included as they deal with large grained cobalt of low purity. The values for σ_i and K, for this variety of material are reproduced in Table X. σ_i and K are quite large for cobalt when compared to values for other metals.

A large value for σ_i, is not unexpected. The heterogeneity of the cobalt lattice after cooling through the transformation is well documented. The large amount of lattice debris present has been outlined by Yegoleyev[85,86] and others[36,76]. Even in single crystal cobalt, the dislocation density is found to be much higher than in well annealed crystals of other metals[25].

The extremely high values for K require explanation. It is not reasonable to expect the barriers in cobalt to be 10 times as difficult to overcome as those in copper, or a factor of 5 stronger than those in zinc.

An expression providing the important parameters included in K may be written as follows:

$$K \propto (Gb\sigma_c)^{1/2} \qquad \text{.....5)}$$

G = shear modulus
b = Burger's vector
σ_c = critical stress at the head of a pile up required to initiate slip in a neighbouring grain.

Clearly, if metals with very different shear moduli are to be compared, the data should be normalized for shear modulus. The ratio $(G_{Zn}/G_{Co})^{1/2}$ is about 0.66. If we normalize the K value for cobalt by this factor we find that K for cobalt at room temperature is 120,000 psi/$\mu^{1/2}$

TABLE X Parameters From an Equation of the Form: $\sigma_{yield} = \sigma_i + KD^{-1/2}$

Test Temperature °C	T/T_m	σ_i psi	K psi/$\mu^{1/2}$	Comments
-196	0.04	22,000	212,000	Cobalt - 99.7 - 99.998%
20	0.17	19,500	182,000	Cobalt - 99.7 - 99.998%
20	0.17	24,000	230,000	Cobalt - 98.6%
100	0.21	18,500	182,000	Cobalt - 99.7 - 99.998%
250	0.30	16,000	126,000	Cobalt - 99.7 - 99.998%
400	0.39	13,500	81,000	Cobalt - 99.7 - 99.998%
-100	0.25	11,000	44,000	Zinc Alloys[110] - Zn, Cr, Ti, ZnO, Ni
20	0.22	3,000	26,000	Copper[33]

compared to 44,000 psi/$\mu^{1/2}$ for zinc alloys. The difference in Burgers vector between the two materials should not yield important differences. If σ_c is a strong function of temperature in cobalt, K values must be compared at similar homologous temperatures. From Figure 35, it may be seen that K for cobalt does vary with temperature. Between -196°C and 100°C the variation is not large, but K drops considerably above this temperature. If K values at 250°C (0.3 T_m) are compared to values for the zinc alloys at (0.25 T_m) we find that the K value for cobalt is 1.8 times that for zinc alloys. In Figure 34 a dotted line has been inserted to represent a curve for cobalt normalized for G and homologous temperatures to allow comparison to the curve for zinc alloys. The coincidence of σ_i values for the two curves should be judged fortuitous as σ_i for dilute zinc-aluminum alloys[111] is approximately 0, whereas the zinc alloys that give rise to the line plotted in Figure 34 exhibit a strong contribution to σ_i from precipitate hardening.

The only parameter which has not been analysed is D. If the grain size D has been measured incorrectly, the measured values of K are also in error. The D values used to assemble Figures 34 and 35 are the values associated with the fcc grain size. In section 3.1 it was shown that the fcc grain size is only a measure of the coarsness of the high temperature phase. The regions of crystal lattice that may be considered individual grains depends upon the multivariance of the transformation. The boundaries between

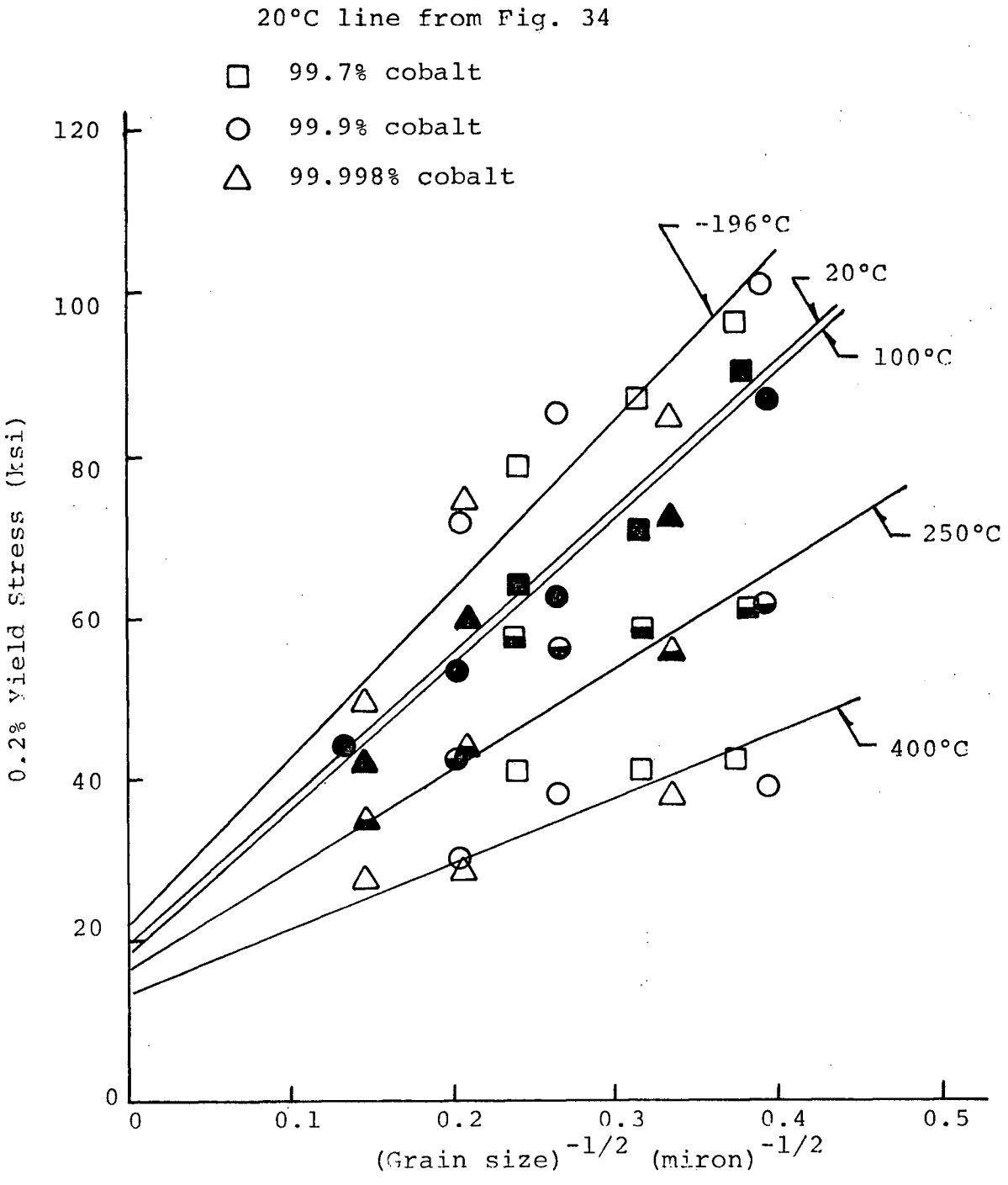

Fig. 35 Yield stress versus reciprocal square root of grain size.

multivariant areas are not true grain boundaries, but they are clearly stronger barriers than subgrain boundaries. Although, it is physically impossible to ascertain the size of the various transformed regions (except in thin films in the electron microscope) these various regions of lattice must be smaller than the fcc grain size. In view of the above observations, the slopes determined in Figure 34 and 35 should be lower than as shown because the distance between boundaries that act as dislocation barriers in cobalt is smaller than the diameter of the fcc grains.

If it is assumed that a normalized K for cobalt is similar to that for zinc, a point on the normalized cobalt curve in Figure 34 may be projected back onto the curve for zinc at constant stress to yield a measure of D for the misoriented regions of cobalt lattice. For example: Move data point A, representing 47 micron cobalt of 99.998% purity to position A' to represent normalizing for G and homologous temperature. Then move to A" which is assumed to reflect the error in measurement of D. The "Grain" size determined in this manner is approximately 10 microns. Upon comparing this value with Figure 11, a photomicrograph, of 47 micron, 99.998% cobalt under polarized light, the result is not unreasonable. Although an accurate "average" size for regions of lattice having similar orientation is impossible, it is clear that the "average" is not over 15 microns nor less than 5 microns.

Although the complex microstructure in cobalt makes an accurate evaluation of K difficult, it is clear that K is large as in other metals that lack a multiplicity of slip systems at room temperature.

The measured variation in K, and σ_i, with temperature is interesting. (Table X). Clearly both parameters differ little between -196°C and 100°C, K drops only 15%, yet between 250°C and 400°C, a temperature change only one half as large, K decreases 35%. Similarly σ_i decreases more rapidly at higher temperatures. These observations parallel the earlier observations regarding tensile behaviour above and below 0.25 T_m.

σ_i is a measure of the force necessary to drive a dislocation against the resistance of impurities, precipitate particles, subgrain boundaries, and the Peierls-Nabarro force. Of all these terms, the Peierls force is strongly temperature dependent whereas the others are not. Thus a sharp change in σ_i with temperature may reflect the change in the Peierls force.

The Peierls force, or the force required to drive a dislocation over a slip plane is small on close packed slip planes. Thus, it is not large in the fcc metals. In the bcc metals, where the slip plane is not close packed, the Peierls force is large. In hcp metals, the Peierls force required to drive dislocations over the basal plane is generally considered to be small, but to obtain "corrugated slip" on the $\{11\bar{2}2\}$ planes may require a very high Peierls force. Thus, one possibility for the sharp drop in σ_i above

0.25 T_m in cobalt is that the Peierls stress for dislocation motion on the $\{11\bar{2}2\}\ <11\bar{2}3>$ slip system becomes rate controlling. The fact that σ_i does not drop as quickly at low temperatures may reflect the fact that some other mechanism operates, reducing the need for corrugated slip. The motion of transformation dislocations on various {111} planes in the fcc portions of the lattice would be one example of an athermal process which could reduce the necessity for movement of dislocations on the corrugated slip plane.

The two factors that may yield the temperature dependence of K are $G^{1/2}$ and $\sigma_c{}^{1/2}$. Between -196°C and 100°C, $G^{1/2}$ decreases about 5%, thus two thirds of the drop in K between -196°C and 100°C must be due to a reduction in the critical stress (σ_c) required to initiate slip in a neighbouring grain. To propose that $\sigma_c{}^{1/2}$ decreases 10% as temperature increases from 0.04 T_m to over 0.2 T_m is reasonable. On the other hand, the change in K between 250°C and 400°C is 35% and only 2% of the variation may be attributed to a change in $G^{1/2}$; thus, $\sigma_c{}^{1/2}$ must decrease by over 30%. This is equivalent to saying that the critical stress at the head of a pile up required to initiate slip in a neighbouring grain, decreases by over 50% between 0.30 T_m and 0.38 T_m. Clearly some strongly temperature dependent dislocation process is operative at these temperatures.

Presentation of the yield stress as a function of the reciprocal square root of grain size and the ensuing discussion has uncovered several important features regarding yield in polycrystal cobalt. The yield strength in cobalt is affected in a strong manner by the grain boundaries present. As barriers to dislocation motion, the grain boundaries in cobalt provide a strengthening effect similar to that found in other hcp metals that do not exhibit a multiplicity of slip systems at room temperature. The stress levels measured in cobalt are much higher than for zinc, cadmium, or magnesium because of differences in shear modulus and melting temperature. The frictional stress, σ_i, in cobalt is very high. In fact, after normalizing for G and homologous temperature, pure cobalt exhibits σ_i values obtained for zinc alloys containing a high density of precipitate particles.

The variation in σ_i and K above and below 0.25 T_m implies that some temperature dependent dislocation mechanism becomes important only above 0.25 T_m. At low temperatures σ_i is large but does not vary strongly with temperature. At high temperature, σ_i drops quickly with temperature. Similar observations apply to K.

One proposal consistent with the observed results is the relationship between Peierls stress on the $\{11\bar{2}2\}$ corrugated plane in hcp cobalt and the stress induced martensitic transformation that occurs in cobalt. A discussion of this relationship must be deferred until the data regarding the martensitic transformation has been presented.

3.2.1.3 Ductility and Fracture

The ductility of cobalt (% elongation) is not well defined in the literature with measured values from almost nil to as high as 25% being quoted[83]. The low ductilities measured in work carried out prior to 1940 were undoubtedly due to impurities in the cobalt. If the concentrations of sulphur, zinc, or lead exceed very low levels, (20, 100, and 20 parts per million respectively) cobalt behaves in a brittle manner[82]. Although the basic impurity effects have been uncovered in recent years, low ductility readings are still in evidence for very pure polycrystal cobalt[83].

Sulphur, zinc, and lead are well below the levels where they cause brittle behaviour in all grades of cobalt used for the present study. Although hundreds of specimens were tested to failure, no clear picture regarding the ductility of cobalt emerged. The values for the three grades of cobalt investigated are presented in Table XI. The scatter in results was always large and mean values are shown in the table. A large scatter is also prevalent in other studies where raw data has been published.

The ductility of 99.7% cobalt is high for all grain sizes tested, averaging 19.2% strain for the 55 specimens pulled to failure. The differences in ductility for the various grain sizes are too small to be able to propose, with authority, any trend, although there is a trend towards lower ductility as the test temperature is increased.

TABLE XI Summary of True Strain Data For Polycrystal Cobalt

Purity	Annealing Temp. (1 Hr.)	Grain Size (μ)	Strain (%) at Failure				
			Average	-196°C	+20°C	250°C	400°C
99.7%	600 - 800°C	7 - 17.5	19.2	21.6	19.7	17.3	15.4
99.9%	500°C	<6.5	23.9	25.0*	20.5	29.9*	24.8*
	550°C	<6.5	22.9	11.8*	22.2*	33.2*	23.6*
	600°C	6.5	20.8	24.7	21.8	18.9	16.9
	650°C	10.0	21.7	14.6*	26.4*	14.5*	30.5*
	700°C	14.5	10.8	14.4	11.7	9.0	7.2
	800°C	24.0	5.6	8.3	6.3	4.2	2.8
	1000°C	60.0	5.9	-	5.9	-	-
99.998%	600 - 800°C	9 - 47	4.5	4.8	4.1	3.4	9.5

* Single Specimen Tested

For 99.9% cobalt, the scatter in results is large, but the trends in ductility are more pronounced. Except for very small grained material, which has over 20% ductility at all temperatures, the ductility decreases as the test temperature increases. The ductility also drops rapidly with increasing grain size, decreasing from over 20% for 6.5 micron material to less than 6% for 60 micron material.

The results show that the small grained 99.9% material behaves similarly to the 99.7% cobalt, but as the grain size increases the former exhibits less ductility. For example, 17.5 micron cobalt of 99.7% purity yields approximately 20% elongation whereas 14.5 micron 99.9% cobalt fails after 11% strain.

After testing several specimens of 99.998% cobalt, and noting the low ductility values, the material was examined to determine if any physical defects were present. Upon careful polishing and washing (no etching) a few small elongated pores became visible. They were less than 1 micron in cross-section perpendicular to the tensile axis and were a maximum of several microns in length parallel to the tensile axis. They did not appear to be contaminated and probably arose during a zone-refining procedure. The cold work introduced during production did not close all the pores. Problems attendant to obtaining a further supply of 99.998% material made it imperative that the material available be used. Attempts were made to swage and draw the material to close the pores. The low ductility, paired

with contamination problems occuring at the temperatures required for working, thwarted every effort to eliminate the pores. Thus, the material was annealed and tested with the porosity present. While parting the high purity cobalt rods into lengths convenient for machining further tensile specimens, 50 random sections were taken. These sections were examined on planes perpendicular and parallel to the tensile axis for porosity. No defects were observed in 80% of the sections.

The porosity, as a fraction of cross-sectional area is negligible and should not affect the yield strength or the work hardening rate, but the pores may influence the ductility by acting as nuclei for fracture processes.

The ductility of 99.998% material below 0.33 T_m (350°C) is low for all annealing procedures. As with the other grades of cobalt, there is a trend to lower ductility as the test temperature and grain size increase. Above 0.33 T_m, the ductility of 99.998% material increases rapidly, reaching 10% by 400°C.

In this very high purity material, 350°C may be sufficient for the onset of the high ductility region observed by other authors surrounding the transformation temperature[81,82,109]. They attribute the high elongation values observed to the transformation proceeding during deformation and relieving stress concentrations.

The behaviour of 99.7% and 99.9% cobalt as a function of grain size is in agreement with data presented recently by Müller[83]. The smallest grain size examined in his work was 35 microns. Although the majority of the results available from the present study are for grain sizes smaller than this, in the areas where comparisons can be made there is general agreement. Ductility decreases up to a certain grain size, beyond this, the ductility remains constant at 4 to 6%. This behaviour also parallels the amount of retained fcc phase as a function of grain size.

Although a detailed study of the fracture processes in cobalt was not attempted, metallographic evidence regarding the fracture surfaces was compiled. Figure 36 shows a fracture surface for 99.9% cobalt having a grain size of 6.5 microns. The specimen failed at approximately 20% strain. The failure is definitely ductile, as evidenced by the ductile cusps visible throughout the fracture surface.

Figure 37 is a large grained (47 micron) specimen of 99.998% cobalt that failed at less than 5% strain. Although the surface does not exhibit the same intensity of ductile cusps as the preceeding replica it may still be considered a ductile fracture. In both figures, there is some evidence of shear failure in selected areas.

The specimens shown in Figures 36 and 37 were tested at room temperature. Replicas were taken from fracture surfaces obtained after tests at -196°C, 20°C, and 250°C.

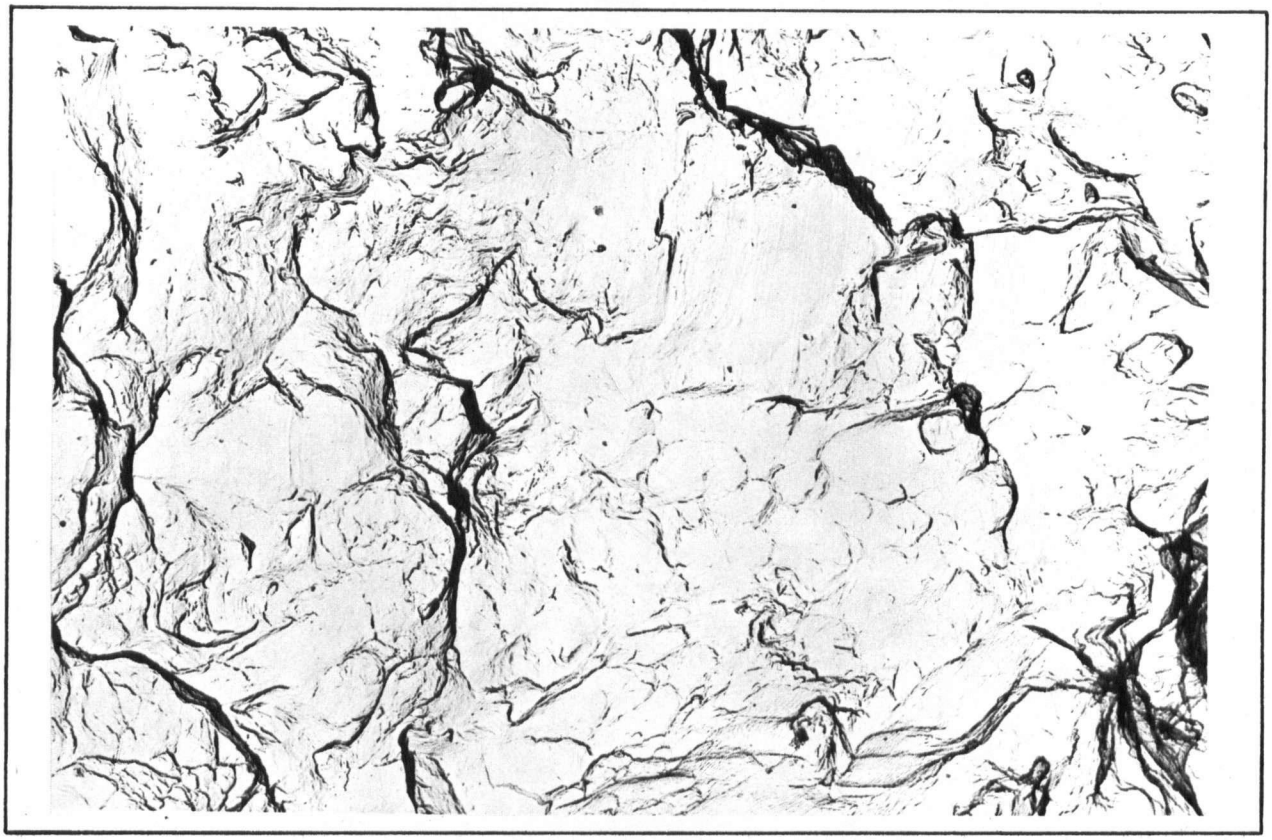

Fig. 36 Fracture surface, 99.9% cobalt tested at 20°C.
6.5 micron grain size. 7500X

Fig. 37 Fracture surface, 99.998% cobalt tested at 20°C.
47 micron grain size. 5000X

No change in the general features of the fracture surface were uncovered. Replicas of the fracture surfaces at 400°C were not obtainable due to the testing environement (salt) and the oxide layer that formed on the specimens following failure.

3.2.1.4 Work Hardening Behaviour

Before discussing the temperature dependence of the work hardening rate, a description of the change in work hardening behaviour with strain is necessary. The anomalous work hardening behaviour in the initial portion of the tensile curves was noted previously. A plot of the work hardening parameter; Θ (the slope of the true stress - true strain curve) is presented for various test temperatures in Figure 38. The data are taken from the test results shown in Figure 22 for 6.5 micron, 99.9% cobalt. The small grain size was chosen because the anomalous behaviour is more pronounced for this type of material. In Figure 38, the effect of the martensitic transformation is quite clear. Instead of a smooth drop in Θ as strain increases beyond yield, cobalt exhibits a region where Θ remains essentially constant before continuing to drop in a normal fashion. For tests carried out above -196°C, the work hardening rate actually increases following this anomalous region before continuing to drop in value. A second observation is that the anomalous behaviour persists for a larger portion of the

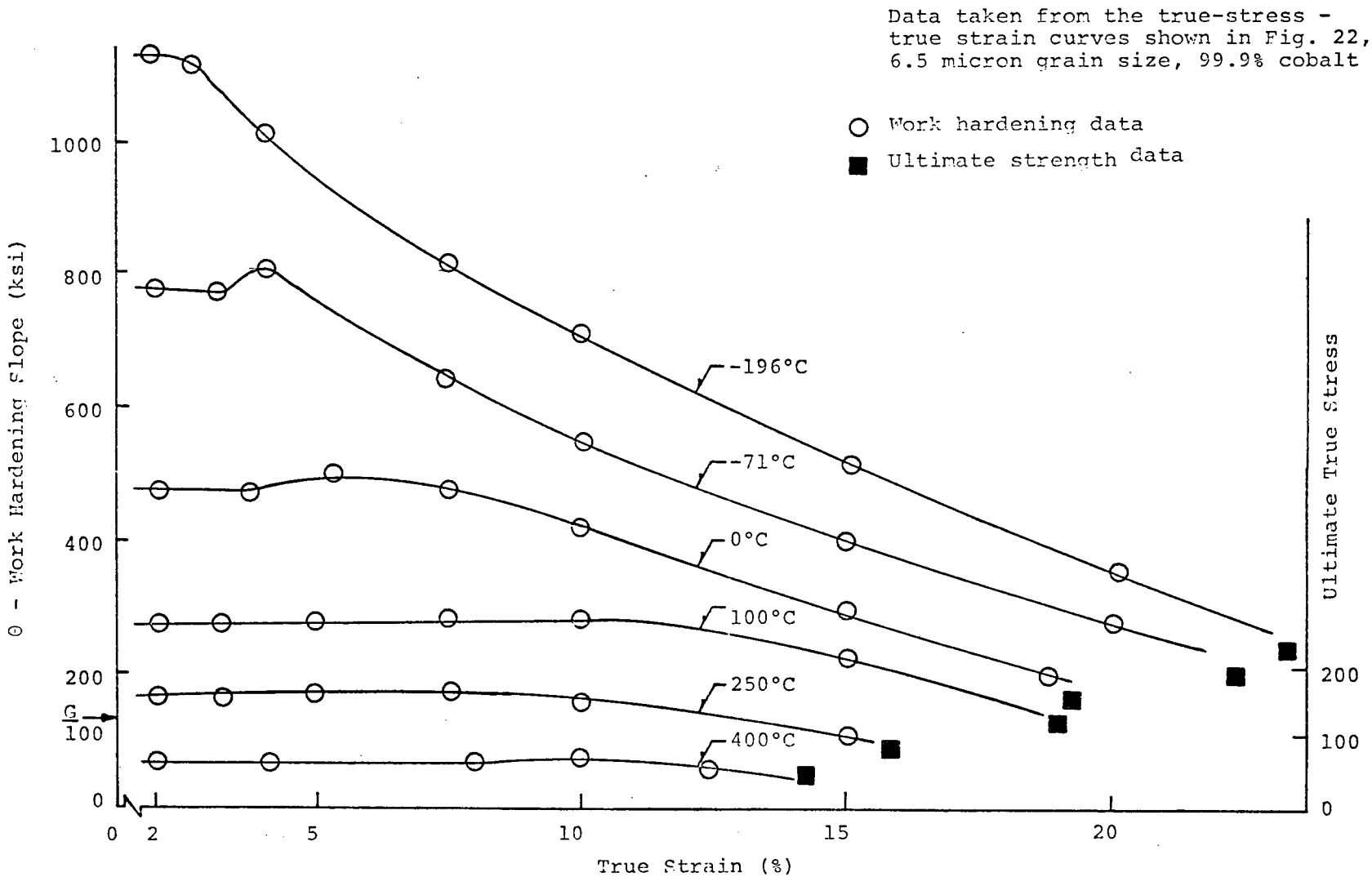

Fig. 38 Variation of work hardening rate with strain for 99.9% cobalt.

tensile curve as the test temperature increases. At -196°C, the region of constant work hardening rate disappears at 3% strain, at 0°C it disappears at about 5% strain, at 400°C a constant value is maintained to over 8% strain.

Both observations are due to the martensitic transformation. It will be shown in the section dealing with deformation and the transformation that the regions where the anomalous work hardening rates exist correspond to strain values where the retained fcc lattice is transforming to hcp at a high rate.

For polycrystalline aggregates that fail in a ductile manner, the elongation at which necking begins in a tensile test is related to the work hardening rate. Plastic instability occurs when the slope of the true stress - true strain curve (Θ) becomes equal to the value of true stress. This result is known as Considères' Criterion. The derivation of this result is available in most standard texts[34]. The veracity of this result for cobalt is shown in Figure 38. Data points representing the maximum stress and elongation at failure for the specimens giving rise to the work hardening curves in Figure 38 are included for comparison. Clearly the specimens neck and fail in accordance with the criterion outlined above. Similar curves were produced for all grain sizes investigated.

For 99.7% and 99.9% cobalt, results similar to those in Figure 38 were uncovered. The results clearly show that the increased ductility observed for 99.7% and 99.9% polycrystal cobalt at low temperatures is a reflection of Considère's Criterion.

The results for 99.998% cobalt do not obey Considère's Criterion. Specimens of this material fail while Θ is still an order of magnitude higher than the true stress, and little or no necking is observed. These results substantiate the proposal that the porosity present in this high purity material promotes fracture at low strain values.

The rate at which polycrystal cobalt work hardens as a function of temperature is shown in Figure 39. Curves of similar shape and magnitude are also observed for all other materials tested. Two general observations are clear: The work hardening rate is not a strong function of grain size or purity. On the other hand, the work hardening behaviour changes sharply with temperature, dropping very steeply from -196°C (0.04 T_m) to approximately 0.25 T_m and decreasing at a lower rate above this temperature.

This observed change in behaviour is recorded for work hardening rates taken at 2% strain. At 10% strain, the effect is not as clear. The temperature at which this break in behaviour occurs is approximately the same fraction of the melting point at which the two stage behaviour of the yield stress and flow stress is observed. Figure 40 traces the change in work hardening behaviour versus temperature at various values of strain to outline how the two stage behaviour of the work hardening rate disappears as strain increases. For low strain values, the anomalous effect shown in Figure 38 is also reflected in Figure 40. The work hardening data in Figure 40 is for 99.9% cobalt having a 6.5 micron grain size. The work hardening curves for this material lose the

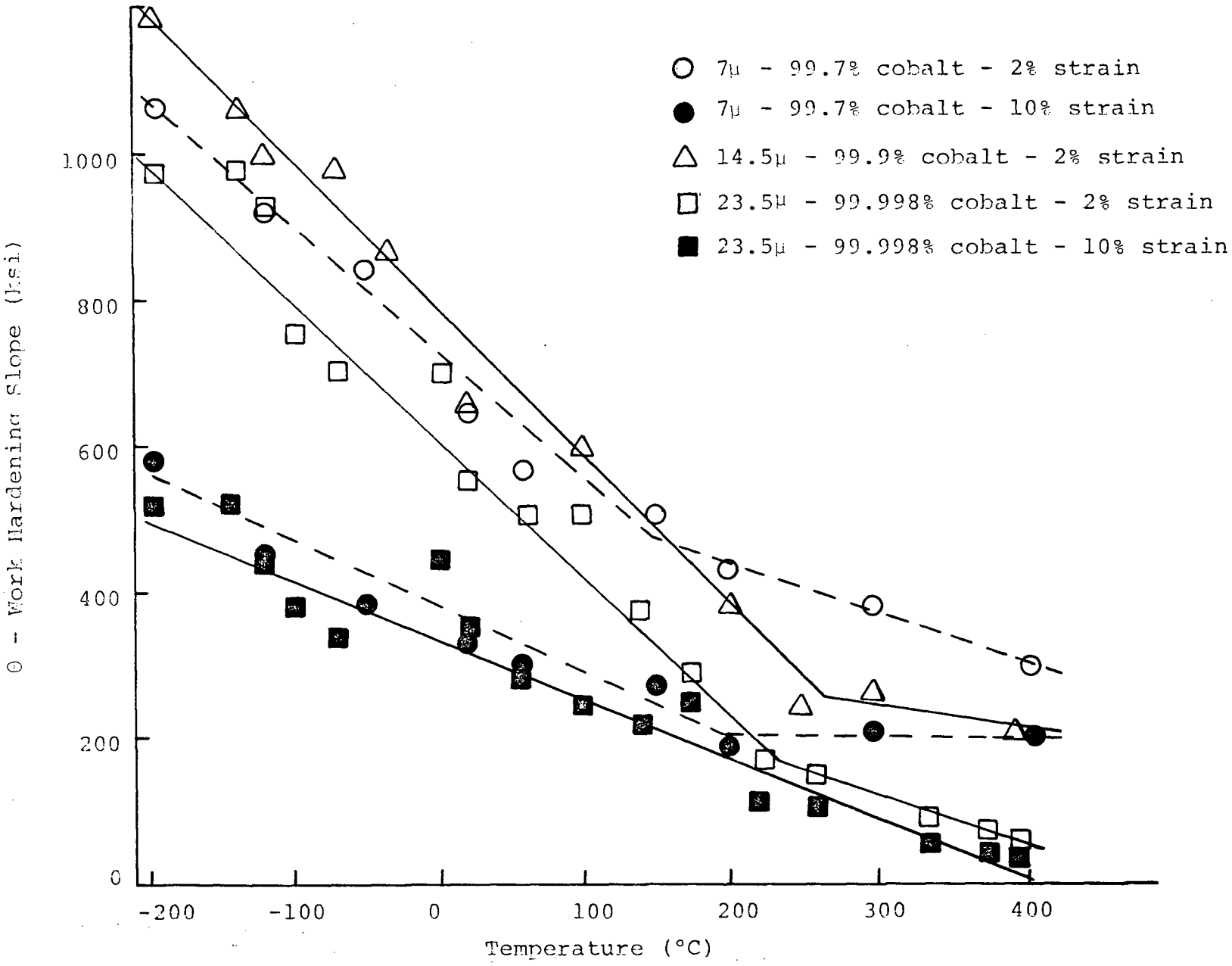

Fig. 39 The work hardening behaviour of cobalt as a function of temperature.

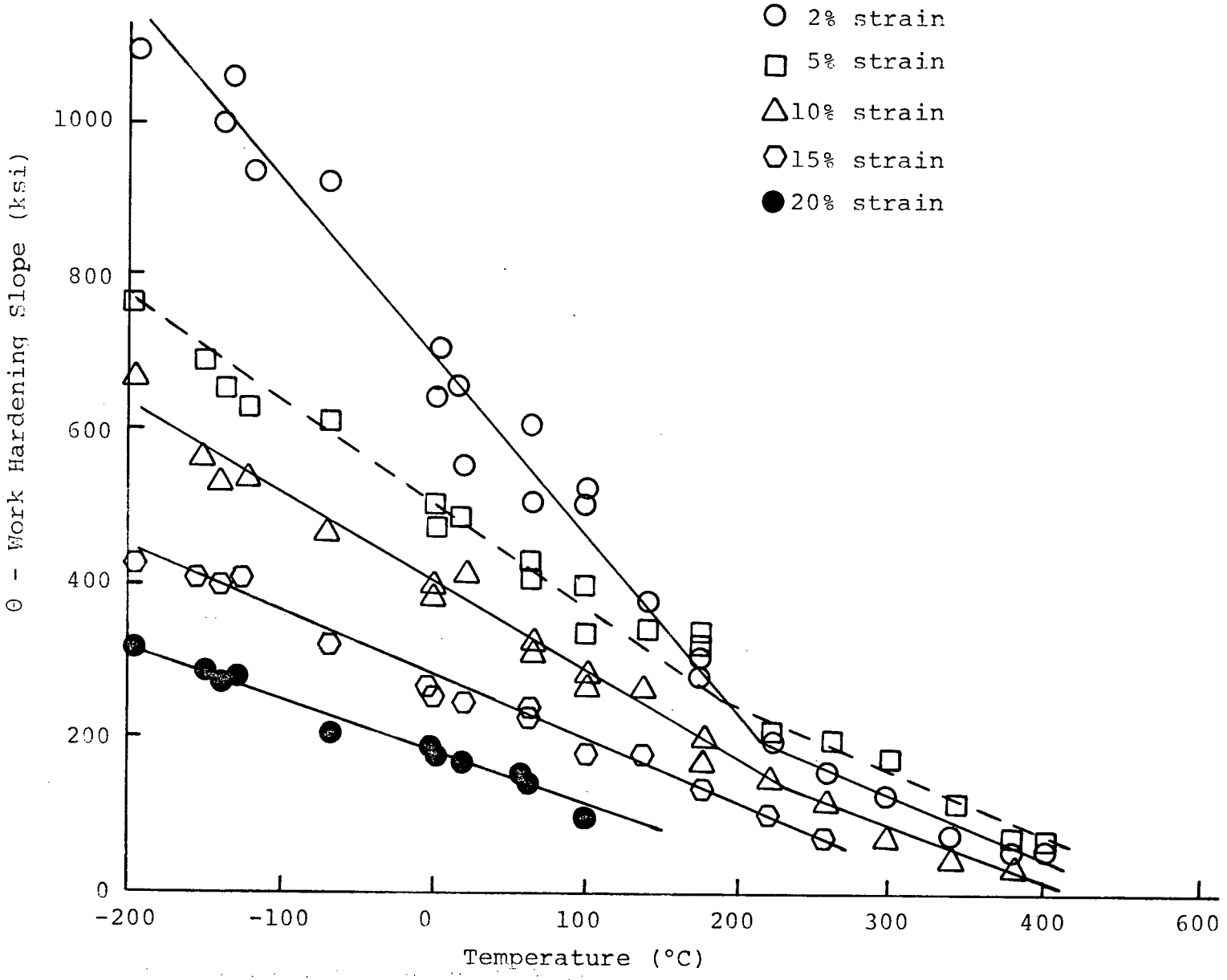

Fig. 40 Variation in work hardening behaviour with increasing strain. 99.9% cobalt, 6.5 micron grain size.

two stage characteristic between 10% and 15% strain. Upon referring to Table VIII it may be seen that the two stage characteristic of the flow stress is no longer evident at 10% strain. The strain above which the two slopes on the work hardening curves merge for various grain sizes is shown in Table XII. The range of temperature at which the slope change is observed is also listed. Similar information relating to the flow stress is included for comparison.

3.2.1.5 Discussion and Summary

At this juncture, it is clear that the tensile behaviour of cobalt is different above and below 0.25 T_m. Pronounced differences in the temperature dependence of yield stress, flow stress, and work hardening rate have been uncovered. The distinction between behaviour above and below 0.25 T_m disappears as strain increases, and disappears at lower values of strain as the grain size increases. The yield stress and flow stress exhibit a less intense temperature dependence below 0.25 T_m than above. On the other hand, the work hardening rate shows a steeper temperature dependence below 0.25 T_m than above.

As a further approach to clarify the differences in behaviour above and below 0.25 T_m, a number of step-pull tests were carried out. Specimens were yielded at a given temperature and strained a small amount. The test temperature was then changed and a further increment of strain was introduced. This procedure was continued,

TABLE XII The Two Stage Behaviour of Flow Stress and Work Hardening Rate as a Function of Temperature

Grain Size (Microns)	Purity (%)	Strain (%) and Temperature (T/T_m) Above Which the Two Stage Characteristic of the Work Hardening Rate is not Observed		Strain (%) and Temperature (T/T_m) Above Which the Two Stage Characteristic of the Flow Stress is not Observed	
		True Strain (%)	T/T_m	True Strain (%)	T/T_m
6.5	99.9	10	0.28 - 0.29	5	0.25 - 0.28
7.0	99.7	10	0.23 - 0.26	10	0.22 - 0.26
9.0	99.998	2	0.24 - 0.25	2	0.25
10.3	99.7	5	0.22 - 0.27	5	0.27 - 0.28
14.5	99.9	5	0.27 - 0.28	5	0.28 - 0.29
17.5	99.7	2	0.26	2	0.27
23.5	99.998	2	0.25	2	0.25
24.0	99.9	2	0.30	2	0.27
47.0	99.998	2	0.28	2	0.32

Note: Curves Plotted For 2, 5, 10, 15, 20% Strain Only.

alternating temperature between two values, until failure occured. The results were then plotted for the step-pull specimens. Data from identical specimens that had undergone all deformation at the individual temperatures being studied were also plotted.

Figures 41 and 42 present the data from a series of step-pull tests as well as stress-strain curves for specimens tested in the normal fashion. The data has been corrected to remove the affect of change in shear modulus with temperature.

Three types of tests are shown:

i) Tests involving a temperature change between -196°C/20°C where both temperatures were below 0.25 T_m.

ii) Tests with both temperatures above 0.25 T_m, 250°C/385°C.

iii) Tests where the low temperature 20°C (0.17 T_m) was below the break in the curves, the high temperature 250°C (0.30 T_m) above.

From Figure 41 the results imply that the structures formed at -196°C and 20°C are very similar. The agreement between the step-pull curves and the individual stress strain curves is very close. The segments of the step-pull test, determined by the intersect technique outlined in Appendix 2, exhibit work hardening slopes that agree closely with the individual tests. At strain values approaching failure some variance occurs.

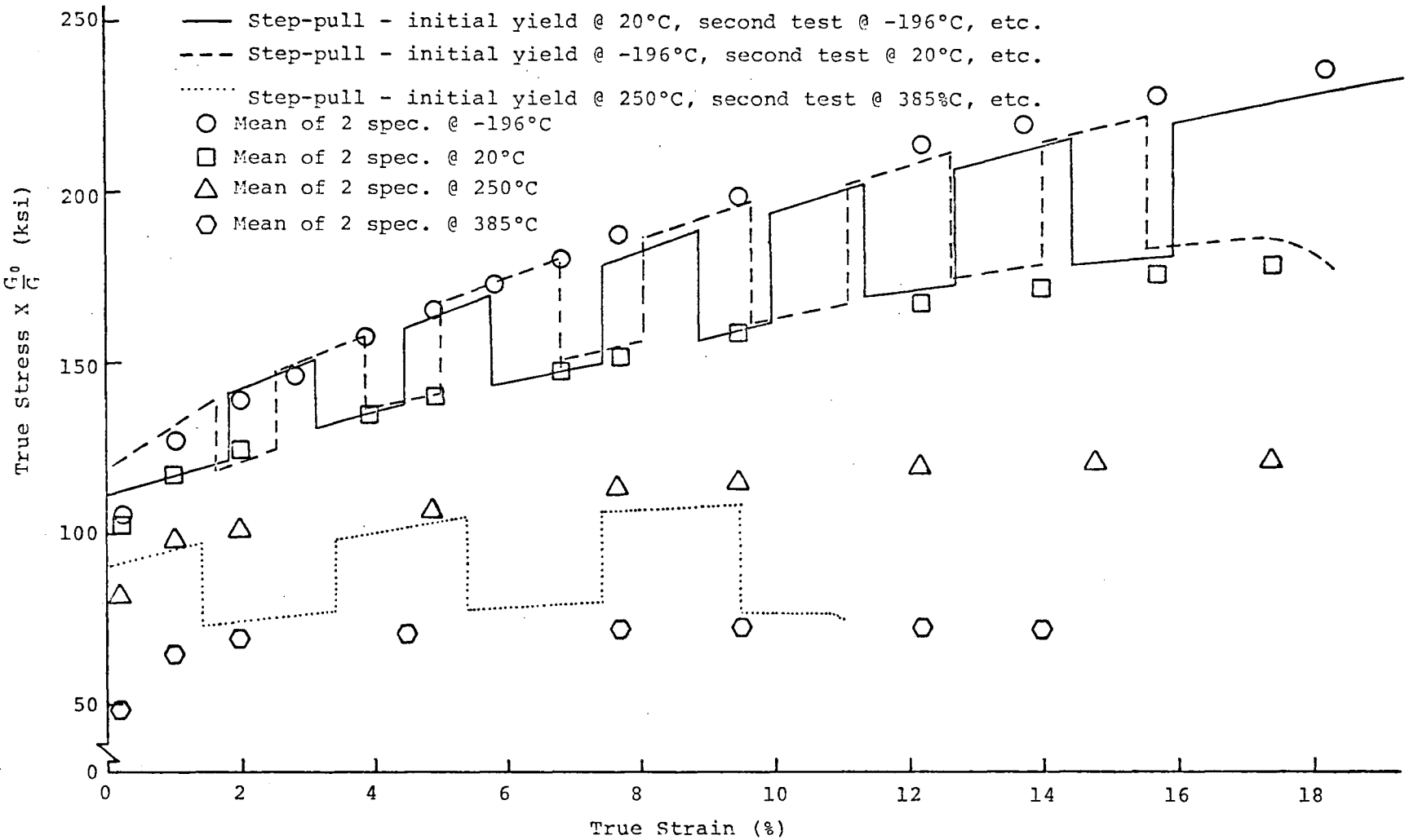

Fig. 41 Temperature change tests, 99.9% cobalt - 6.5 micron grain size.

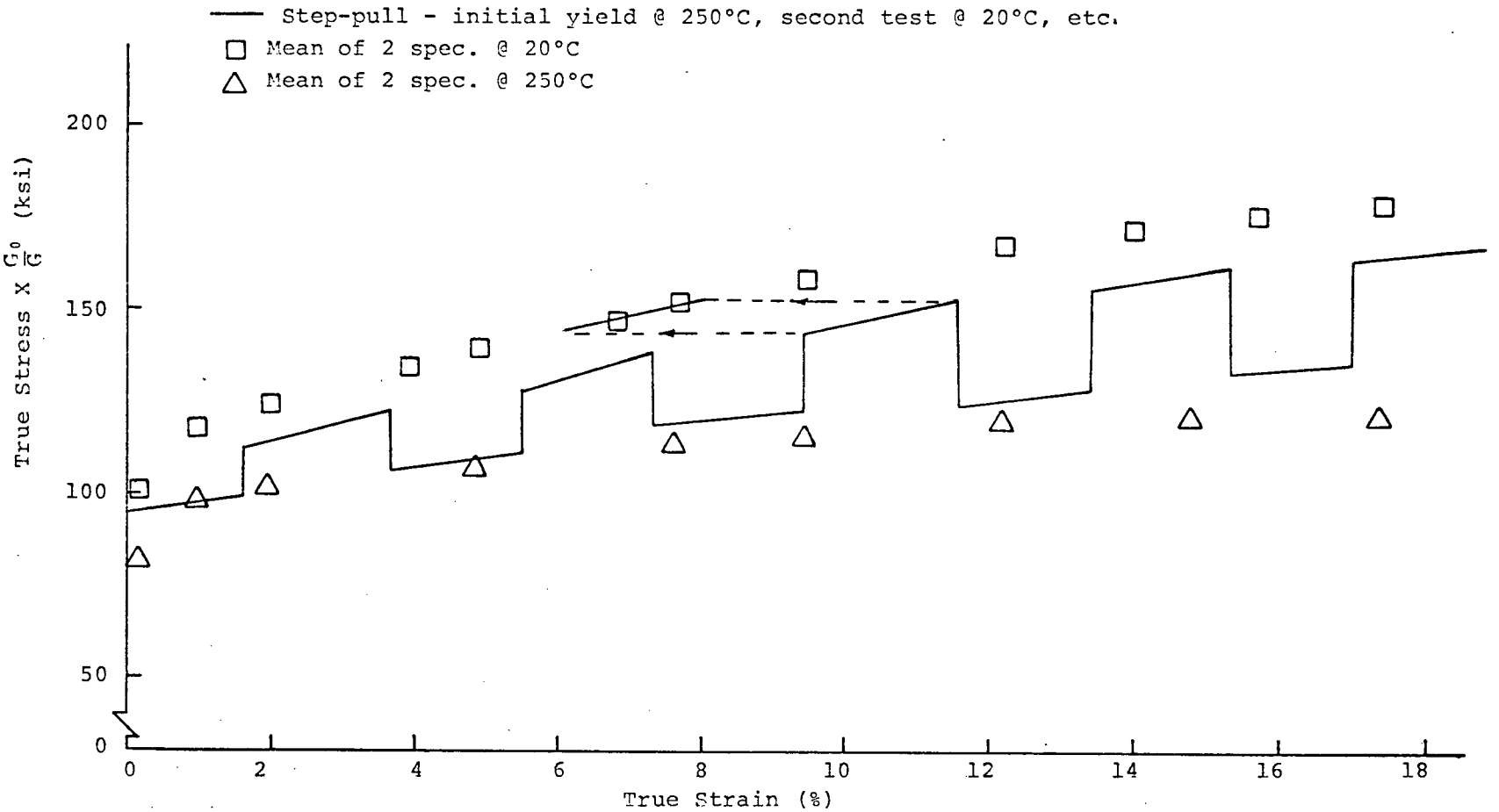

Fig. 42 Temperature change test, 99.9% cobalt - 6.5 micron grain size.

The results at 250°C/385°C do not superimpose as accurately as those for -196°C/20°C. The 250°C segments of the step pull curve fall slightly below the mean data for specimens pulled at 250°C, whereas the 385°C segments fall above corresponding data for individual tests. Thus, it is proposed that the structures giving rise to strain hardening at 385°C must be less restrictive to further dislocation motion than the structures formed at 250°C. A small amount of recovery is also occuring at these high temperatures, but the change in stress level from this avenue is very small (See Section 3.1.2).

The tests for temperatures straddling 0.25 T_m, (20°C/250°C) show a large variance with the individual stress strain curves (Figure 42). The room temperature segments of the curve fall much below the corresponding data for individual specimens. The 250°C segments of the curve fall above the corresponding individual data. The work hardening slopes shown by the individual step pull segments are also in disagreement with the data from the normal tensile tests.

It appears, that the barriers to dislocation motion forming at 250°C are far less restrictive than those occuring at 20°C. After undergoing a small amount of strain at 250°C and then further straining the specimen at 20°C, the work hardening slope for the room temperature segment is higher than would occur for a specimen having had all strain introduced at 20°C, but the stress level is lower. The work hardening slope is equivalent to the slope for a 20°C tensile

test at a lower value of strain. The stress levels required to continue deformation at 250°C following some strain hardening at 20°C reflect the more restrictive structure introduced at 20°C. The stress levels are higher than those observed for a standard test at 250°C and become less representative of a 250°C test as more strain is introduced at 20°C.

This set of tests appear to substantiate several observations made earlier. The fact that the results of the step-pull tests with both temperatures below 0.25 T_m, superimpose very accurately with individual stress strain curves throughout the major portion of the stress-strain curves implies that similar barriers to dislocation motion are controlling the flow stress at both temperatures. The temperature dependence of the flow stress reflects the degree to which the barriers become transparent to dislocations as temperature increases. The observation that the work hardening rates are also coincident with those for a normal stress strain curve, suggest that the rate at which barriers to dislocation motion are forming, are similar at both temperatures. If either result is incorrect a different set of results would occur, unless some very complex thermal behaviour is postulated for the controlling mechanism.

For example: If the rate at which obstacles are formed with increasing strain is higher at -196°C than at 20°C, the segment of strain at 20°C following a segment at -196°C would necessarily exhibit a stress higher than that obtained at similar strain for a normal tensile test. On this basis, it is reasonable to assume that the mechanisms controlling the major portion of the stress strain curves are the same at both temperatures.

Any postulated combination of processes must be capable of producing strong barriers to deformation to justify the high stress levels measured and one component process must be temperature dependent, as it is clear that the barriers to dislocation motion are more easily overcome as temperature increases.

For the tests where one temperature is above 0.25 T_m and the other below, the results reflect a difference in behaviour at the two temperatures. To yield the behaviour observed regarding flow stress levels, two possibilities exist. Either more or different barriers are forming at 20°C than at 250°C, or the obstacles formed at 20°C are more easily overcome at 250°C.

The higher work hardening rate observed for a segment of the step pull tests at 20°C, following a segment at 250°C, implies that the strain introduced at 250°C forms a structure that could be formed by far less strain at 20°C. For example: If the 20°C segments of the step pull tests in Figure 42 are transposed back onto the curve for the normal tensile test, maintaining the measured stress levels,

coincidence of the curves is observed.

This latter observation regarding the work hardening behaviour, reinforces the proposal that similar barriers to dislocation motion are forming at both temperatures, but that the total number of barriers produced is lower at 250°C.

To obtain equal amounts of strain at both temperatures there must be equivalent amounts of dislocation motion. If equivalent amounts of dislocation motion take place, but fewer barriers form, this implies that some mechanism has come into prominence at this higher temperature, allowing similar amounts of dislocation motion as at low temperatures, without forming the same density of barriers.

The results for the tests where both temperatures are above 0.25 T_m reflect similar behaviour to that discussed above. As the temperature increases, the number of obstacles that form for a given input of strain, continues to decrease. The decrease in stress levels required to continue deformation is due to a second mechanism that provides stress relief above 0.25 T_m.

As would be expected from the data presented for other aspects of the tensile deformation of cobalt, the measured work hardening rates are high, approaching G/10 at 2% strain for tests at -196°C. Two important factors that may give rise to the high work hardening values are the low stacking fault energy and the martensitic transformation.

Both factors are important individually and are additive. The low stacking fault energy ensures that the majority of dislocations present in cobalt are dissociated. Continued movement of extended dislocations after intersection is difficult and gives rise to work hardening. As the martensitic transformation proceeds on different (111) planes, the martensitic lamallae formed intersect and growth of the lamallae is inhibited. Dislocations within the lamallae must cross a boundary, similar to a twin boundary, to move out of the martensite, or intiate slip across the boundary. Similarily, other dislocations outside the lamallae must move through these boundaries or initiate slip across them to allow continuing deformation.

Another way of viewing the multivariant transformation, as related to work hardening, is to accept the formation of the various martensite lamallae as formation of new boundaries in the crystal lattice. This boundary formation is similar to a continuing grain refinement. If the transformation is viewed in this manner, it would be expected that the strong effects that grain boundaries impose upon polycrystalline material during the initial portion of the stress strain curve, may continue to be evident as long as the transformation proceeds.

The difficulty arising when dislocations encounter obstacles of the type arising from martensitic transformations has been observed by several authors[36,37,105,106]. Marcincowski[105,106] observed that widely dissociated

dislocations on different (111) planes lock each other very effectively when they intersect. He also observed that martensitic lamallae form formidable barriers to dislocation motion. He proposes that dislocation generation must occur to allow continued deformation.

Barrett[78] working with copper-germanium postulated similar strong obstacles to deformation in this system where a similar martensitic transformation occurs. The transmission studies carried out by Votava[36,37] infer that similar hardening mechanisms are responsible for the high work hardening rates in cobalt.

3.2.2 Deformation and the Allotropic Transformation

Many of the results outlined to this point, may be explained in terms of the martensitic transformation. As described earlier all test specimens utilized for this study contained a large fraction of fcc phase. The initial retained fcc phase for all annealing treatments was summarized in Table V.

A number of step-pull tests were carried out to trace the progress of the transformation towards completion. The data are presented as a function of strain to allow direct comparison to the stress-strain curves. (Figures 43, 44). The progress of the transformation as a function of stress did not yield data that could be readily analysed. The retained fcc phase is also plotted against a logarithmic scale for strain to allow observation of the progress of the transformation at low strain values. (Figures 45-47). The data yields linear relationships when plotted in this manner. This result implies that the relationship between strain and the fcc phase may be represented by an equation of the form:

$$\log \varepsilon = \log A + m(\% \text{ fcc}) \qquad \ldots.6)$$

or equivalently

$$\varepsilon = A\ (10)^{m(\%\text{fcc})} \qquad \ldots.7)$$

Where: ε = true strain
A = strain value where % fcc = 0
% fcc = $(\% \text{ fcc})_{\text{initial}} - (\% \text{ fcc})_{\text{transformed}}$

Certain limits must be placed on the equations. The volume % fcc phase may only vary between the amount present before testing and the amount present at failure. For

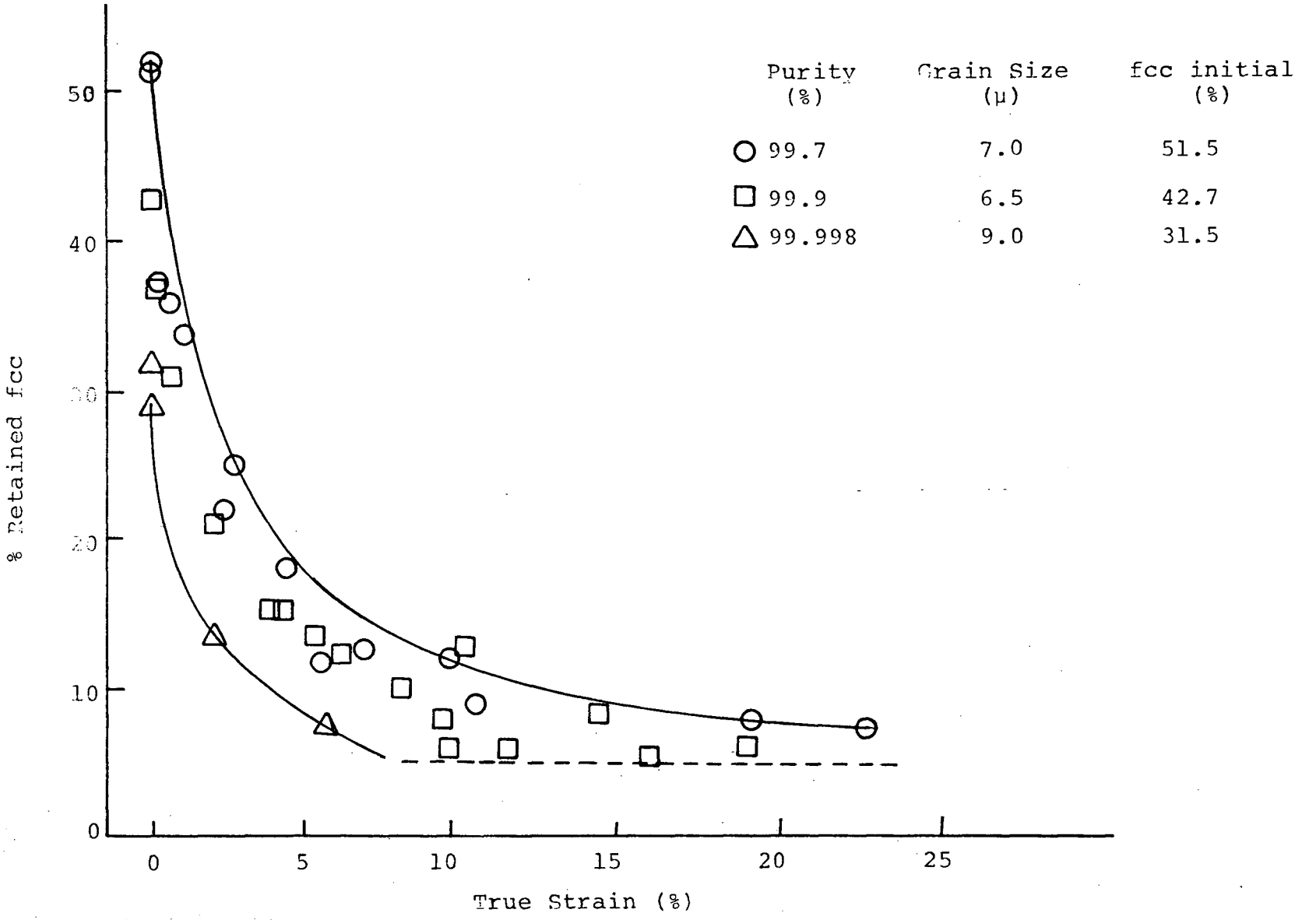

Fig. 43 Tensile strain induced transformation of cobalt at room temperature.

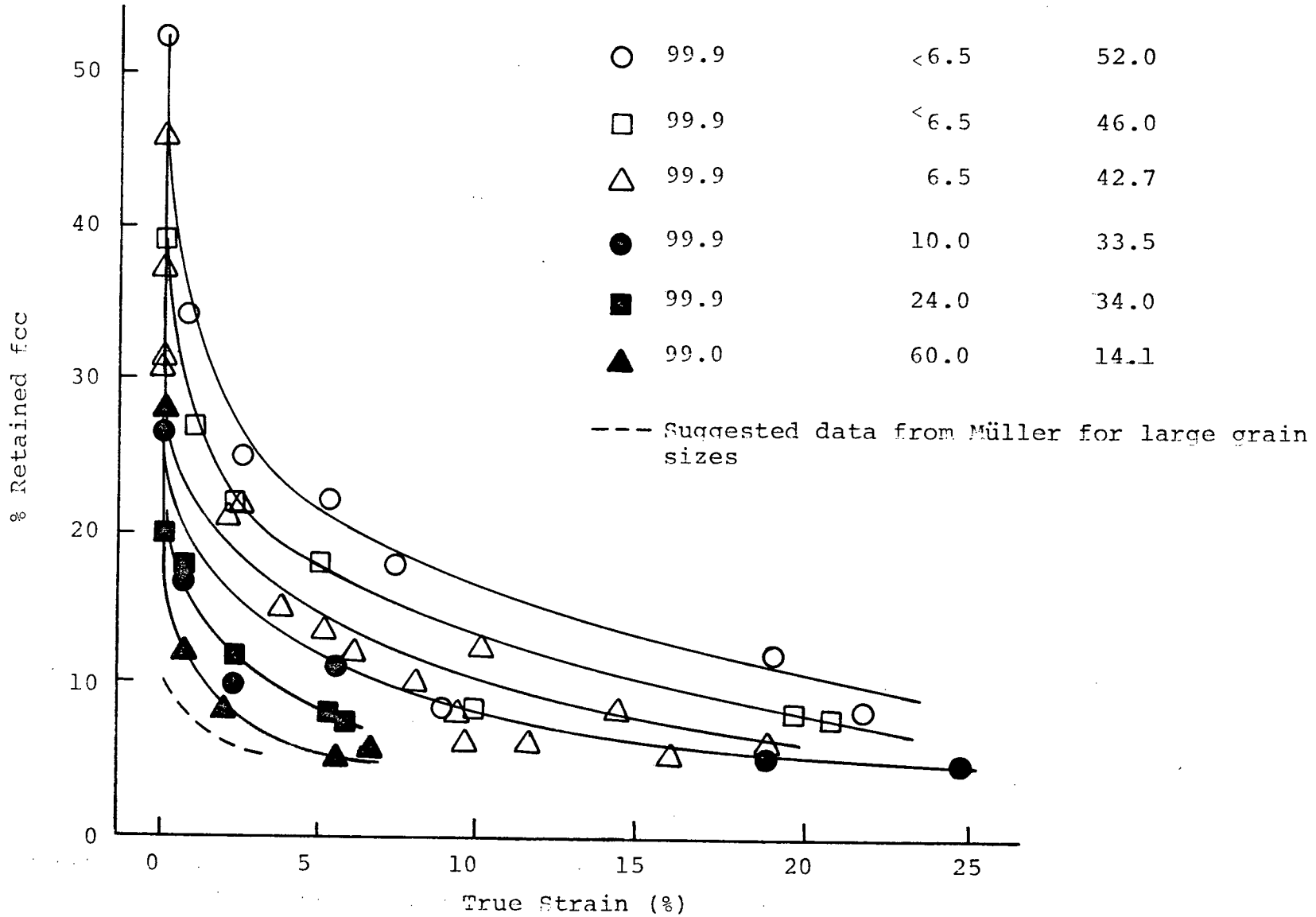

Fig. 44 Room temperature tensile strain induced transformation for cobalt of various grain sizes.

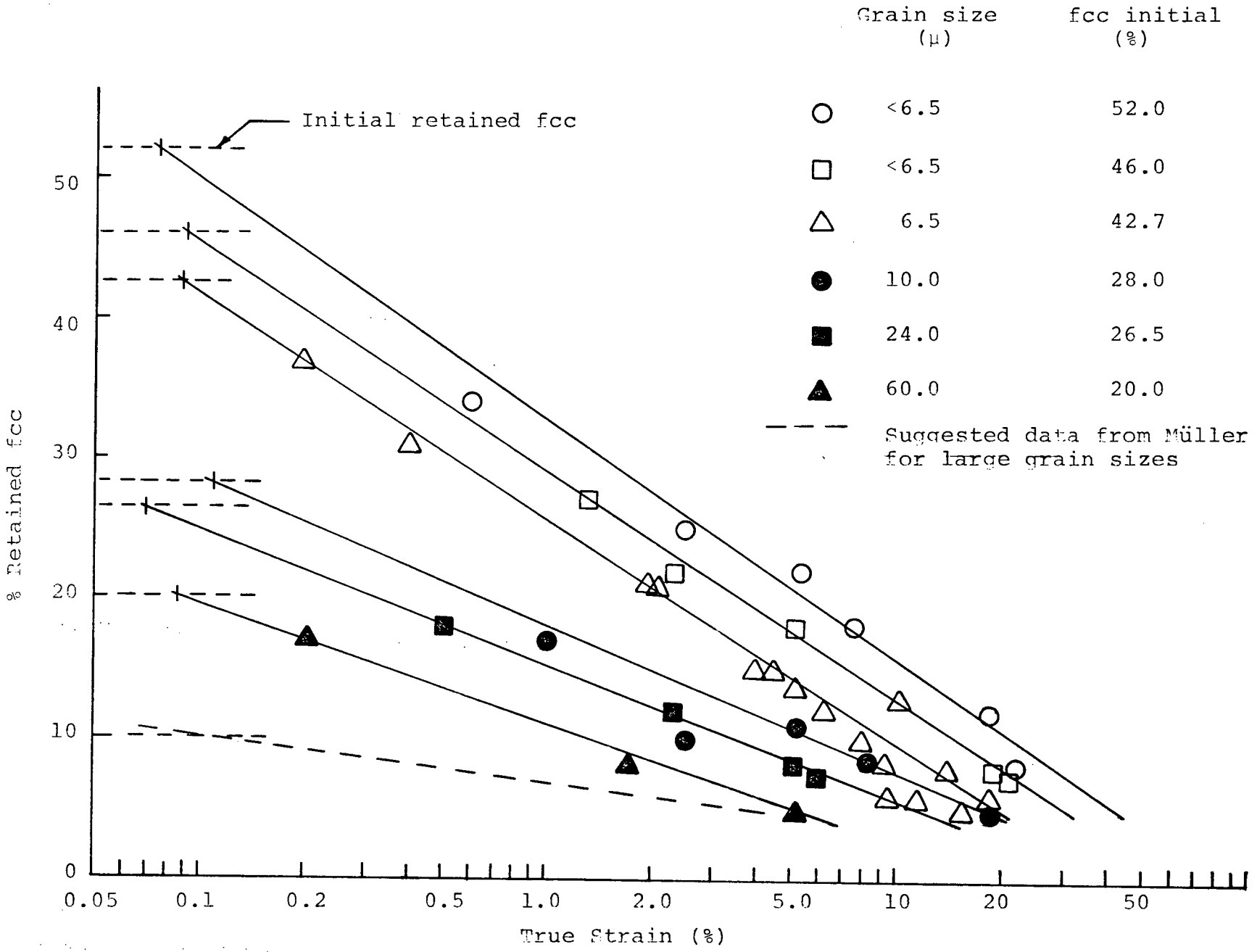

Fig. 45 Room temperature tensile strain induced transformation for cobalt of various grain sizes (semilog).

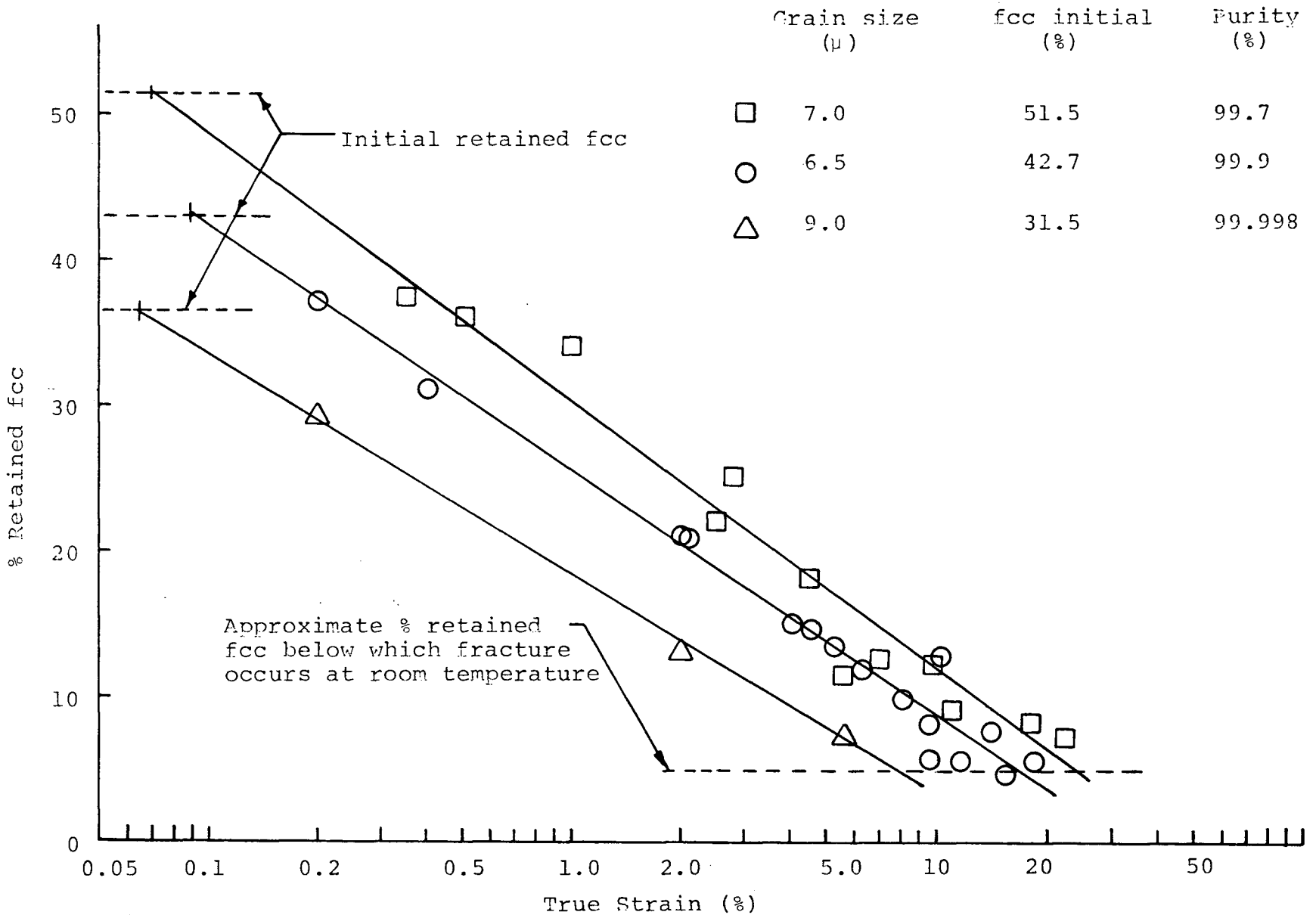

Fig.46 Tensile strain induced transformation of cobalt at room temperature (semilog).

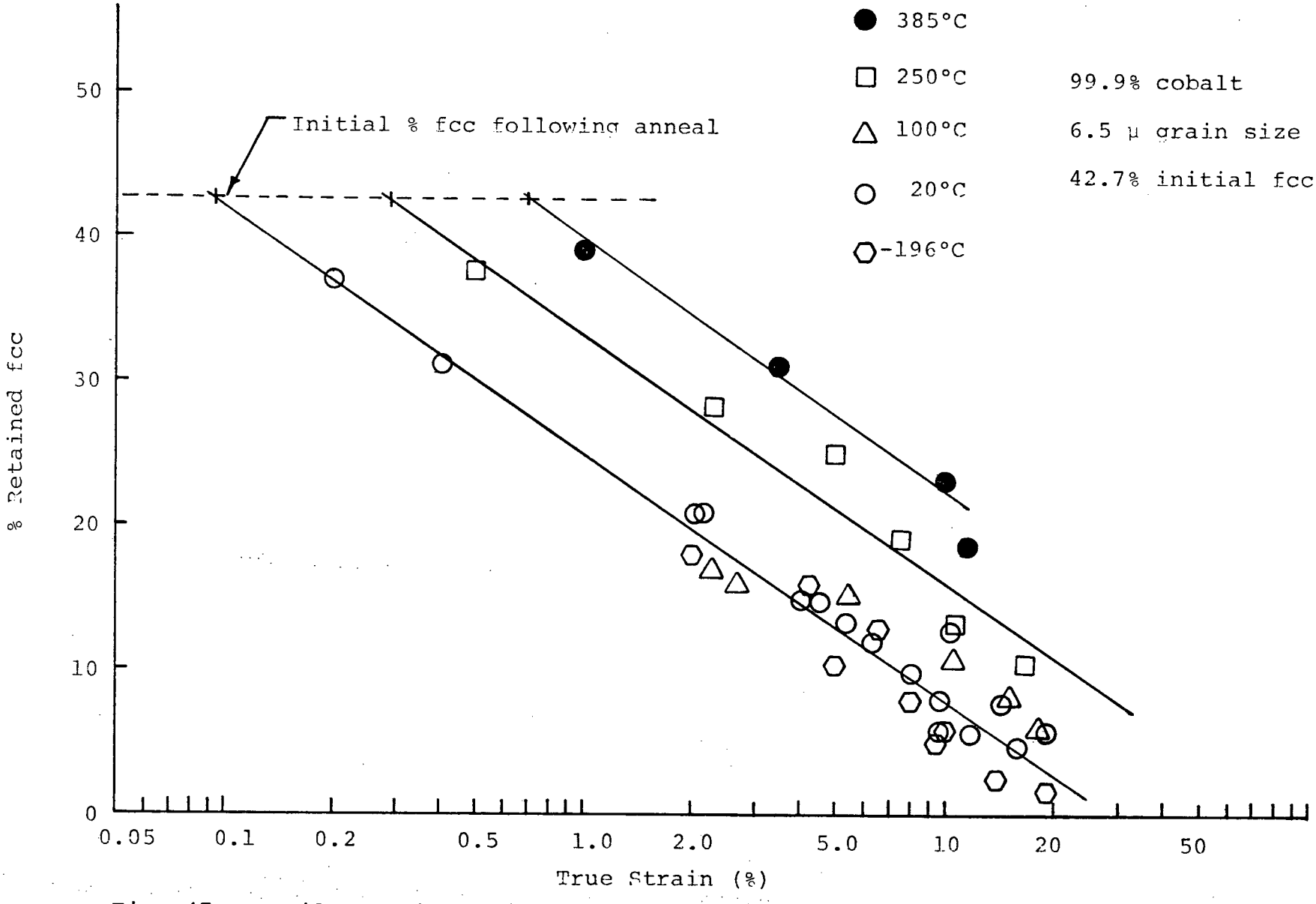

Fig. 47 Tensile strain induced transformation for cobalt at various temperatures. (semilog).

polycrystal cobalt the maximum fcc phase that may be retained following a normal annealing treatment is approximately 60%. The amount present at failure varies from around 2% at -196°C to over 10% at temperatures above 0.25 T_m. Table XIII presents the solutions to the above equation for the curves shown in Figures 45 - 47. A linear relationship has been assumed for tests above 0.25 T_m as well, although this may not be justified.

The general results of this series of tests are as follows. As stress increases, very little transformation takes place before macroscopic yield occurs. This result is shown in Figure 45 for 99.9% cobalt tested at room temperature. The curves have been extrapolated to the strain value where the amount of retained fcc present prior to testing occurs. For the variety of grain sizes shown, the strain at which transformation begins is between 0.07% and 0.11% strain. Similar results are obtained for all material tested below 0.25 T_m. At 0.2% strain, a noticable amount of transformation has taken place at all temperatures below 0.25 T_m. Above 0.25 T_m the situation is not as clear although the data implies that the strain induced transformation begins at higher strain values. The rate at which the transformation proceeds slows as strain increases. At fracture the transformation remains incomplete.

3.2.2.1 Purity

To isolate any differences in behaviour due to impurity levels, small grained specimens of 99.7%, 99.9% and 99.998%

TABLE XIII Behaviour of the Strain Induced Transformation in Cobalt Expressed as an Equation of the Form: $\varepsilon = A(10)^{m(\%fcc)}$. ε = true strain, %fcc = Volume %fcc

Grain Size (μ)	Purity (%)	A	m	Test Temp. °C	ε at which Transformation begins (%)	Volume % transformed at 0.2% ε	ε_{tx}
7.0	99.7	44.8	-0.055	20	0.07	8.0	12.3
6.5	99.9	33.5	-0.060	20	0.09	6.0	8.1
9.0	99.998	16.7	-0.066	20	0.07	7.5	9.4
<6.5	99.9	85.0	-0.059	20	0.08	7.5	10.0
<6.5	99.9	64.5	-0.063	20	0.09	5.5	8.5
6.5	99.9	33.5	-0.060	20	0.09	6.0	8.1
10.0	99.9	51.3	-0.098	20	0.11	2.5	6.6
24.0	99.9	38.8	-0.104	20	0.07	4.5	6.5
60.0	99.9	21.8	-0.120	20	0.09	3.0	No Sol'n
6.5	99.9	33.5	-0.06	-196	0.09	6.0	8.1
6.5	99.9	33.5	-0.06	20	0.09	6.0	8.1
6.5	99.9	33.5	-0.06	100	0.09	6.0	8.1
6.5	99.9	87.0	-0.06	250	0.29	0	No Sol'n
6.5	99.9	195.0	-0.06	385	0.71	0	No Sol'n

cobalt were step-pulled to failure. The results are shown in Figures 43 and 46.

Three observations may be drawn from the data. From Figure 43, it is clear that all grades of material fail prior to complete transformation. Fracture occurs when the volume of retained fcc phase reaches a value between 5 and 7 volume % at room temperature. In Figure 47, it may be seen that a somewhat lower limit applies at -196°C and a higher limit at 250°C and 385°c.

Secondly, the transformation begins between 0.06% and 0.09% strain and is independent of purity (Figure 46, Table XIII.

A final observation is that the progress of the strain induced transformation with respect to strain does not vary appreciably between the various purity grades. This result is in contrast to the earlier observation that purity was found to affect the amount of retained fcc phase in a strong manner. As the purity of cobalt increases, the transformation proceeds further towards completion following an annealing treatment. As there is less retained fcc available in higher purity material, a smaller input of strain is required to bring this material to approximately 5 volume % fcc, where fracture occurs. The equations describing the transformation show this result very clearly. If 5 volume % retained fcc is accepted as the limit for continuing deformation at room temperature, substitution of this value in the appropriate equations in Table XIII.

should yield the measured elongation. Upon substitution, the results are 7.7% for 99.998% material, 17.9% for 99.9% material, and 23.9% for 99.7% cobalt. If these values are compared to the ductility values for the fine grained material presented in Table XI reasonable correspondence is observed.

The fact that the progress of the strain induced transformation does not vary significantly with purity is not unexpected. The driving force tending to complete the transformation upon cooling is very small. It has been estimated that it would be equivalent to an applied stress of several hundred psi[28-31]. At these stress levels it would be expected that small differences in the lattice would yield measurable differences in behaviour. In fact, it has been observed that increasing purity does allow the transformation to proceed further towards completion upon cooling. The stress levels present during strain induced transformation are an order of magnitude larger and therefore any differences in the manner in which the strain induced transformation proceeds due to impurity content should not be significant.

3.2.2.2 Grain Size

The progress of the transformation with strain for various grain sizes is shown in Figures 44 and 45. The initial fcc phase available prior to testing decreases markedly as the grain size increases. The only important

difference between this set of curves and those dealing with purity is that the rate at which the strain induced transformation proceeds decreases as grain size increases. Although the strain values at which transformation begins and the fcc phase remaining at failure are similar, the slopes of the curves change as grain size increases. The difference in slopes means that a larger imput of strain is required to yield an equivalent amount of strain induced transformation for material having a larger grain size. This reduction in the rate of strain induced transformation is not sufficient to overcome the decrease in available fcc phase. Thus, the measured elongation to failure decreases as the grain size increases because the amount of retained fcc reaches the value where failure occurs with less strain imput.

A dotted line has been included in Figure 44 and 45 to represent the data for large grained material tested by Müller[83]. He quotes an initial fcc content of approximately 10% and measured 4 to 6% elongation for material ranging from 300 to 30,000 microns. This line may be assumed to represent a limit on the variation of behaviour with grain size.

3.2.2.3 Temperature

Step-pull tests were performed above and below 0.25 T_m, to ascertain the differences in transformation behaviour that occur. Typical x-ray results for 99.7% and 99.9% cobalt

are shown in Figures 48 and 49. The results are plotted in Figure 47.

Cobalt tested at -196°C, 20°C, and 100°C exhibit similar behaviour. In Table XIII a single equation is presented for behaviour at all three temperatures. The results differ for material tested at 250°C (0.3 T_m) and 385°C (0.37 T_m). Although the slopes of the curves are similar at all temperatures, a much larger amount of fcc phase is retained at any value of strain for tests above 0.25 T_m.

At failure, the transformation is 98% complete for material tested at -196°C, approximately 95% complete for material tested at room temperature and 100°C, and only 80 to 90% complete for material tested above 0.25 T_m. This variation reflects the stress levels attained at the different temperatures. At lower temperatures the stress levels are much higher which is equivalent to applying a larger driving force for transformation.

This final set of results, provides further information that may be compared to the variation in tensile properties with temperature. The volume fraction of strain induced martensite that forms in the initial 0.2% strain during a tensile test is listed in Table XIII. Clearly, the behaviour below 0.25 T_m differs from that above. To obtain macroscopic yield below 0.25 T_m, strain induced transformation must occur. Above 0.25 T_m, this bulk transformation does not appear necessary.

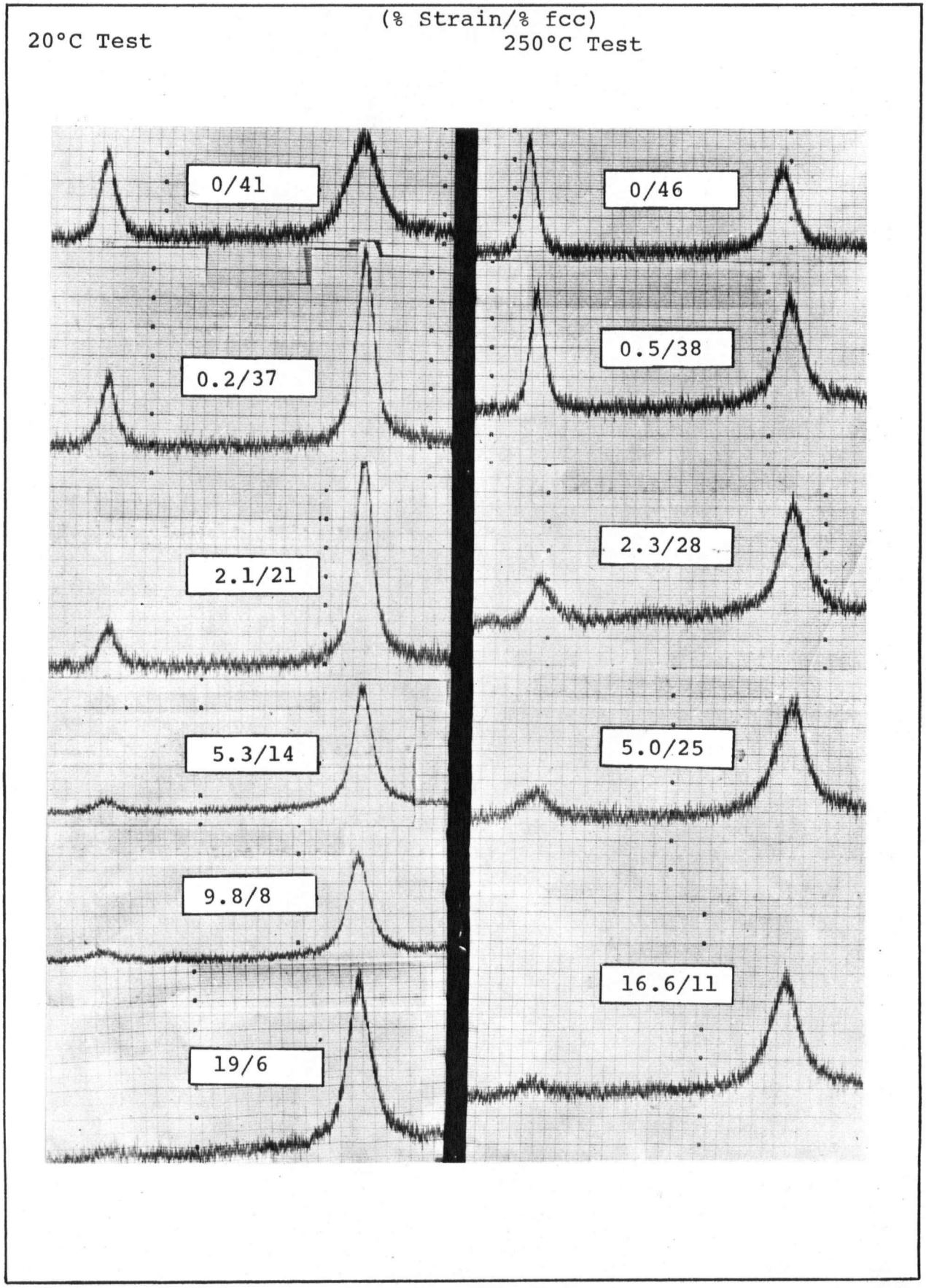

Fig. 48 X-ray data for 99.9% cobalt, step-pulled at 20°C and 250°C 6.5 micron grain size.

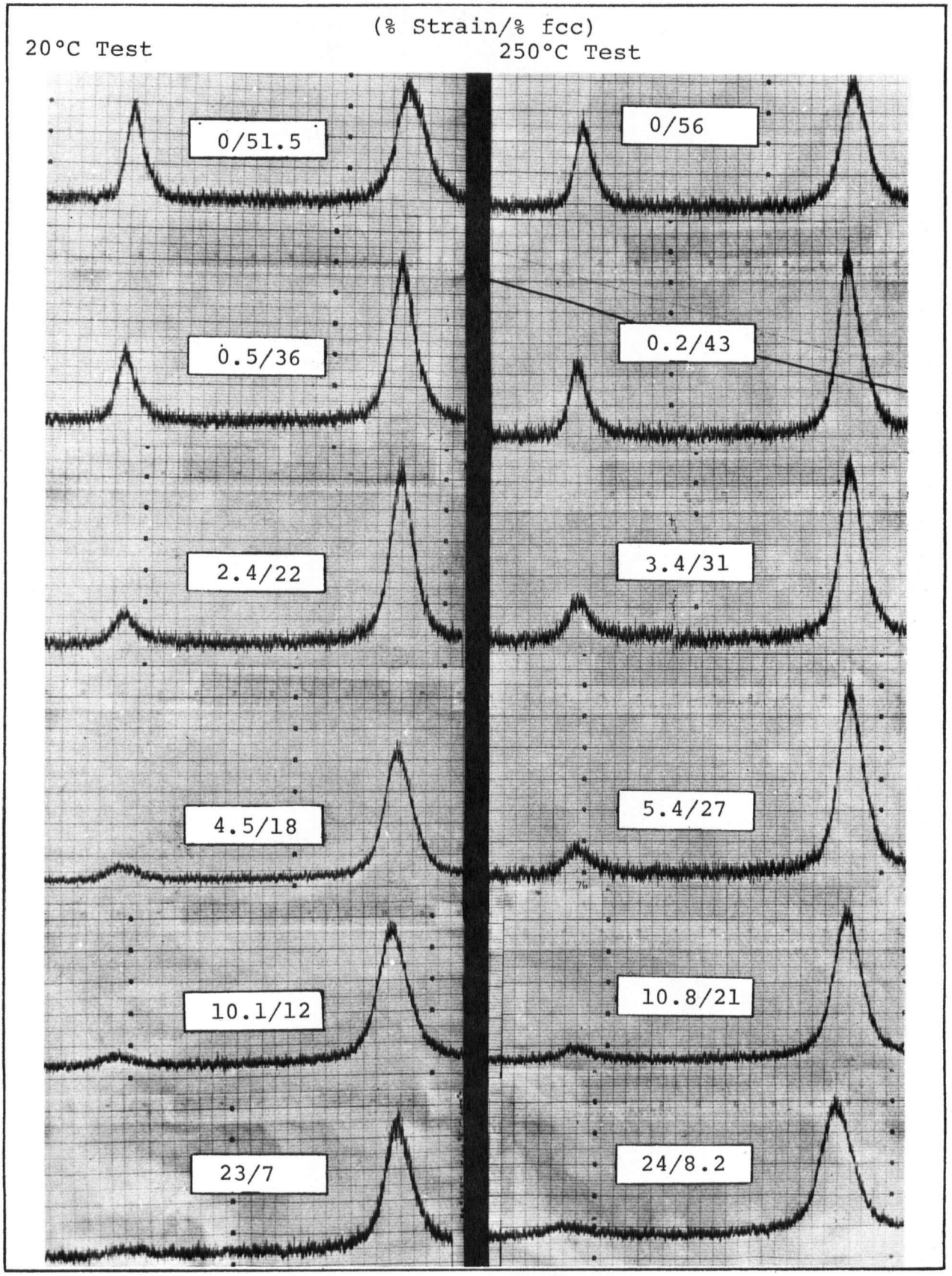

Fig. 49 X-ray data for 99.7% cobalt, step-pulled at 20°C and 250°C 7 micron grain size.

The amount of strain induced martensite formed as a function of strain is plotted in Figure 50 for various test temperatures. The amount of transformation that has taken place at any value of strain, is similar for tests at -196°C, 20°C, and 100°C. It can be seen that the volume fraction of strain induced martensite is much smaller, at any value of strain, for material tested above 0.25 T_m.

The salient features of the strain induced transformation in polycrystal cobalt have been presented. The relationship between strain and retained fcc phase may be represented by an equation of the form $\varepsilon = A(10)^{m\ (\%fcc)}$. "m" varies little with purity or test temperature, but changes rapidly with grain size. "A" represents the strain that could be introduced into polycrystal cobalt if fracture coincided with completion of the martensitic transformation. The initial fcc phase present following an annealing procedure and the strain value at which the strain induced transformation begins determine "A". "A" varies with purity, grain size, and test temperatures above 0.25 T_m.

Before comparing these observations to the results obtained from the tensile tests, a thorough discussion of the martensitic transformation as related to deformation of polycrystal cobalt is required.

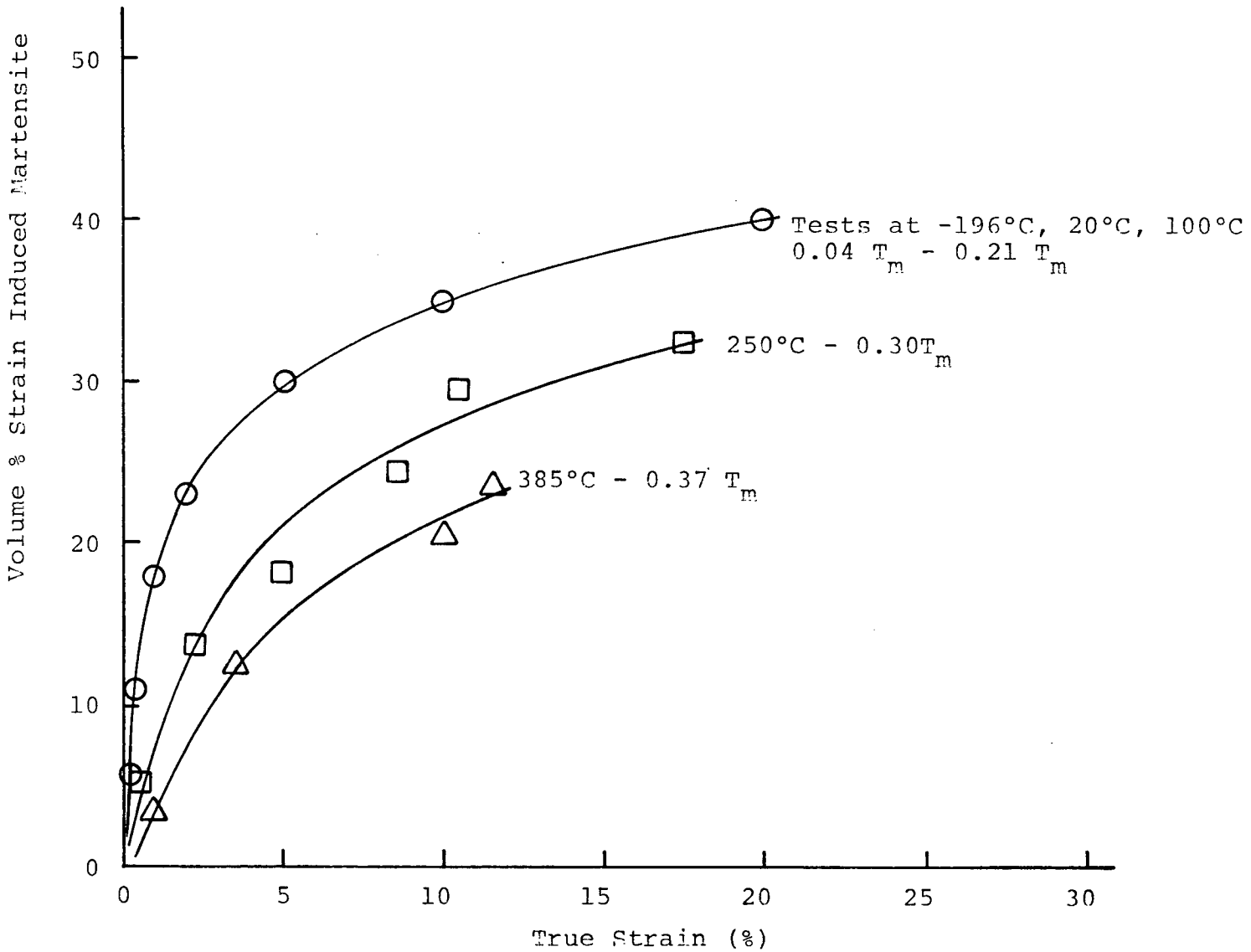

Fig. 50 Volume % strain induced martensite present in 99.9% cobalt as a function of strain.

3.2.2.4 Von Mises Criterion

According to Von Mises Criterion, a polycrystal requires 5 independent shear systems to undergo homogeneous strain without change in volume. Polycrystal cobalt undergoes a slight volume change during deformation and thus in a strict sense, Von Mises Criterion should not be applied.

The change in volume accompanying deformation of cobalt is very small, about 1/3 of 1% for complete transformation. For material used in this study only about 25% to 40% of the bulk transforms during deformation equivalent to a reduction in volume of 0.10% to 0.13%. This facet of the transformation cannot yield a major contribution to the shape change of individual grains.

Basal slip is the major slip mode observed in cobalt. This system provides no extension parallel to the c axis and provides only two independent shear systems. The volume change upon transformation from fcc to hcp provides a small contraction perpendicular to the c axis and a small expansion parallel to the c axis. (Figure 13). The combination of basal slip and the volume change does not satisfy Von Mises Criterion.

If it is accepted that non basal slip is extremely difficult in hcp cobalt[4], the satisfaction of Von Mises Criterion must arise from other sources.

As outlined in the review by Partridge[7], other deformation modes have been observed to satisfy Von Mises Criterion where insufficient slip systems are available. Kink Boundary formation, grain boundary sliding, as well as contributions from twinning shear are all recognized as processes that may supply the needed degrees of freedom to allow deformation of a polycrystalline aggregate. According to Kocks[7], cross slip may also reduce the required number of independent slip systems.

Over the temperature range investigated, grain boundary sliding should not be an important source of strain in cobalt. Due to the very low stacking fault energy of cobalt, cross slip may also be discounted as a major route to an independent shear system. If these processes are discarded as unfavourable, further independent shear systems may arise from twinning and kink boundary formation.

Twinning elements yielding both contraction and expansion perpendicular to the basal plane have been observed in cobalt; $\{10\bar{1}2\}$, $\{10\bar{1}1\}$, and $\{11\bar{2}n\}$twins have all been observed during single crystal deformation. A large shear value for $\{11\bar{2}n\}$ type twins has been postulated[7]. Thus, a large twinned volume may enhance the ductility of cobalt considerably.

Reed-Hill[9] postulates that the amount of strain that may be accommodated by twinning is arrived at as follows:

$$\varepsilon = 1/\sqrt{2}\ (V)\ (S) \qquad \ldots.8)$$

Where: ε = strain
$1/\sqrt{2}$ = average Schmid factor for polycrystals
V = volume fraction twinned
S = shear value for twinning mode considered

as an example. Reed-Hill substitutes values for $\{10\bar{1}2\}$ twinning in zirconium.

S = .17
V = .50

Therefore:

$$\varepsilon = (0.707)\ (0.50)\ (0.17) = 0.06$$

Thus $\{10\bar{1}2\}$ twinning may account for up to 6% strain in zirconium. A similar equation for cobalt would be:

$$\varepsilon = 1/\sqrt{2}\ (V)_{\{10\bar{1}2\}}\ (S)_{\{10\bar{1}2\}} + 1/\sqrt{2}\ (V)_{\{10\bar{1}1\}}\ (S)_{\{10\bar{1}1\}} + \text{etc.} \quad \text{.....9)}$$

In cobalt, the volume fraction twinned would have to be very large as occurs in zirconium to yield more than a few percent strain.

The retained fcc phase that is distributed throughout the grains of the low temperature phase may aid grain shape change. The retained areas of fcc have no lack of slip systems available, but slip and transformation are closely related. Deformation of the fcc phase is probably synonomous with continuation of the transformation. If deformation is possible in the fcc phase without transformation, non basal slip traces should be observed. If slip occurs on a given {111} plane in the fcc phase, transformation on a different {111} variant becomes difficult[4].

The manner in which the disappearance of the fcc phase may provide strain in cobalt may be stated in two ways. The ongoing transformation may be viewed as slip on various {111} planes, thus yielding a number of independent shear systems. The continuing transformation may also be viewed as a type of twin formation. The similarity between twinning and martensitic formation is very close in cobalt because the fcc to hcp transformation is a low energy transformation requiring only a simple shear, with no additional complex shuffles in the plane of shear. (Table VI). The formula used by Reed-Hill to account for the manner in which twinning, in addition to slip processes, may satisfy Von Mises Criterion should be applicable to the martensitic transformation in cobalt. Transformation occurs on many {111} planes in a given fcc grain; thus we have a deformation process that yields contraction and expansion in various directions in the parent grain.

The theoretical shear value for the transformation is $S = 0.353$ and shear up to 35% was observed by Altstetter[28-31] for applied stresses of several thousand psi in single crystals. For the high stresses involved during polycrystal deformation, the transformation may clearly provide large amounts of shear.

If the formation of martensitic plates in cobalt is considered equivalent to the formation of twins the maximum strain available from this source may be determined as for twinning:

$$\varepsilon = 1/\sqrt{2}\ (S)\ (V) \qquad .....8)$$

$$\varepsilon = 1/\sqrt{2}\ (S)_{Tx}\ (V)_{Tx} \qquad .....10)$$

Where: $S_{Tx} = 0.353$
$V_{Tx} = 0.25$ to 0.40

Therefore:

$$\varepsilon = 0.25\ (V)_{Tx} \qquad .....11)$$

For every 4% of the fcc phase transformed a strain of 1.0% could theoretically be obtained from transformation alone. In all material produced for the present study, between 30% and 60% fcc phase was retained in the annealed material. As the transformation is forced near completion during deformation, anywhere from 7 1/2% to 15% strain could theoretically be accomplished through operation of the martensitic transformation. In fact, if the transformation does yield the theoretical maximum shear, $\varepsilon = 0.25\ (V_{tx})$, it is possible for the transformation to provide all the shear necessary in the initial portion of the tensile curve for example:

$$\varepsilon = A(10)^{m(\%fcc)} \qquad .....7)$$

and $\varepsilon = 0.25\ (V_{tx})$ .....11)

but $(\%fcc)_{initial} - (\%fcc) = V_{tx}$

therefore $(\%fcc) = (\%fcc)_{initial} - V_{tx}$

and $(\%fcc) = (\%fcc)_{initial} - 4\varepsilon$

Substitute in equation #7

$$\varepsilon = A(10)^{m(\%fcc\ initial\ -\ 4\varepsilon)} \qquad .....12)$$

Solve for

$$\log \varepsilon + 4m\varepsilon - [\log A + m(\%\ fcc)_{initial}] = 0 \qquad ....13)$$

If the equation is solvable for ε, the value found will correspond to the strain value at which the transformation can no longer provide all the shear required. The progress of the transformation for a given strain imput decreases with increasing strain. Thus, the value found is the amount of true strain that may be introduced without requiring some other shear mechanism to operate. If the equation is not solvable for any positive value of ε, then some shear mechanism other than the martensitic transformation must be required at yield and throughout the tensile curve. The final column in Table XIII lists the value obtained from equation 13 above. The column is titled ε_{tx}. From Table XIII it may be seen that there are two situations where no solution exists. The first case is for large grain sizes. This is not unreasonable as the initial retained fcc phase is very low. Secondly, the equations for tests above 0.25 T_m cannot be solved for positive strain values. This latter observation indicates a change in behaviour at higher temperatures.

In the analysis above it has been assumed that all transformation taking place would contribute to the tensile strain. This is clearly not the case and the basal slip mode is undoubtedly operative throughout the stress-strain curve.

Kink boundary formation has been observed by Theiringer[24,25]. in cobalt at all temperatures with the amount of kink formation increasing with temperature. The observation that this

deformation mode is more common at high temperatures is usually explained as follows: Although the stress required to nucleate and propogate twins is not well understood, it is generally accepted that the nucleation process requires higher stress levels than does growth. At higher temperatures, it is proposed that stress levels are not sufficient to nucleate certain twins (i.e. $\{11\bar{2}n\}$) and the formation of kink boundaries takes place as an adjunct to continuing deformation.

Finally, it should be recalled that in addition to a variety of twinning modes, corrugated $\{11\bar{2}2\}$ $\langle 11\bar{2}3\rangle$ slip has been observed in single crystal cobalt by Seeger[14].

The avenues whereby coherency at grain boundaries may be maintained in polycrystal cobalt are manifold. A summary of the probable deformation modes is presented below:

i) Basal slip

ii) Twinning Modes, $\{10\bar{1}2\}$, Lenticular Twins
$\{10\bar{1}1\}$, $\{11\bar{2}n\}$, Thin Twins
$\{11\bar{2}1\}$, Zig-Zag Twins

iii) Volume Transformation of retained fcc regions yielding shear on various {111} planes.

iv) Corrugated Slip, $\{11\bar{2}2\}$, $\langle 11\bar{2}3\rangle$, Second Order Pyramidal

v) Duplex Slip in retained fcc phase.

3.2.2.5 Metallographic Observations

Presentation of the metallographic observations made during the deformation of polycrystal cobalt has been deferred to this point as the prior information presented is required to explain the surface features that arise. Figure 51 is presented to show the macroscopic shear that may occur during transformation. Gross amounts of transformation tend to obscure all other surface relief as strain increases.

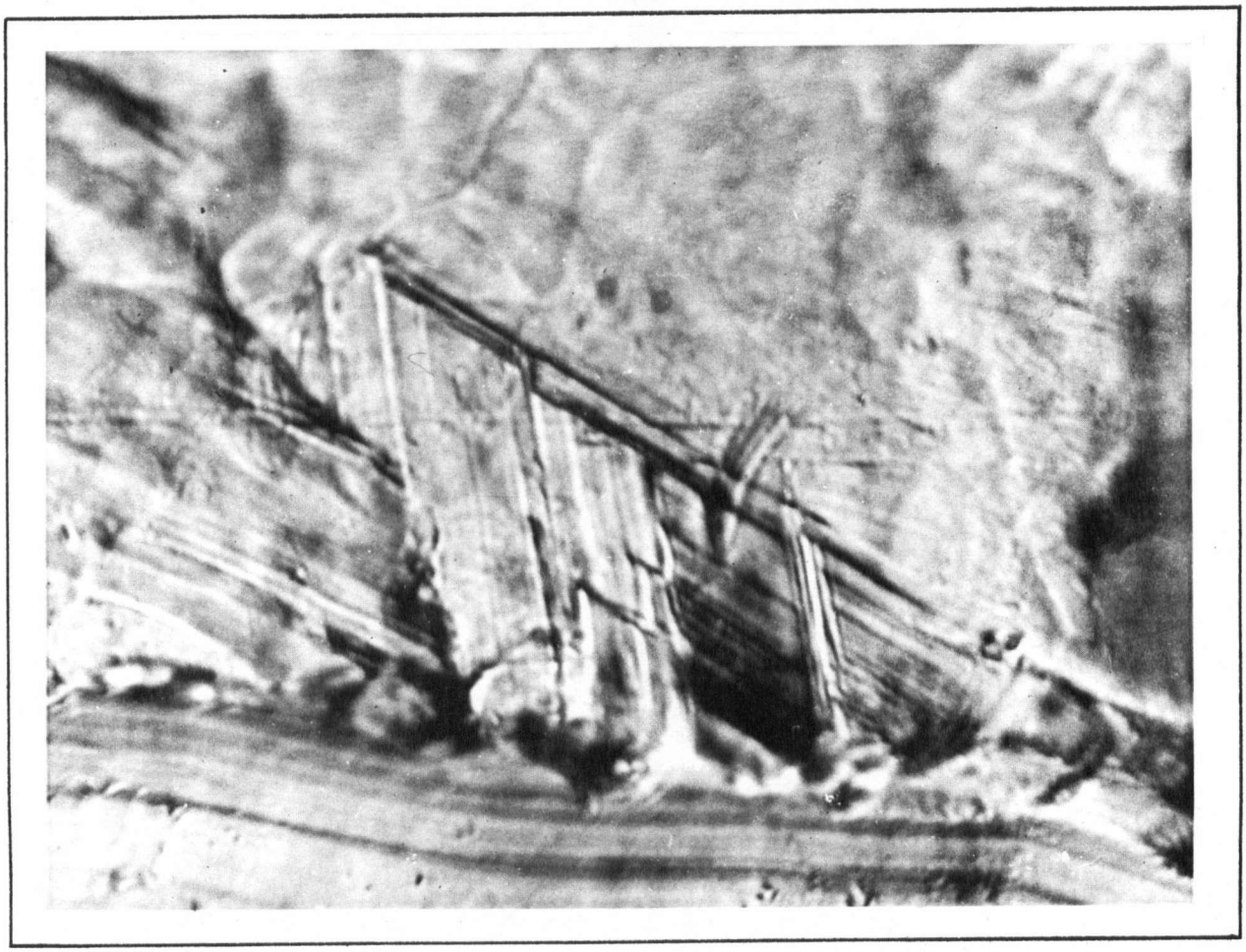

Fig. 51 Martensite shear markings introduced by a surface scratch in 99.9% cobalt. 1900X

The structures produced during deformation of polycrystal cobalt are not documented in the literature. Annealed structures are shown in a few cases[81,82] and the affects of transformation on very large grains has been outlined by Bebring and Sebileau[71]. The structures associated with hardness indentations have been photographed by Lozinsky[108], and Wilcox[89]. Jagged, shear type, fracture zones have also been photographed by Lozinsky. Aucoutuirer and Lacombe[112] delineated the high temperature fcc grains by an auto-radiography technique and compared the observed fcc boundaries with the structure determined by electropolishing the same areas.

Three major objectives were pursued during the experimental work: Attempts were made to follow a defined surface area throughout the tensile curve while varying purity, grain size, and test temperature. A variety of specimens were step-pulled to obtain the required data. After a specimen was strained several percent it was removed from the Instron machine, x-rayed, examined microscopically and then replicated. The specimen was then retested and the procedures continued until failure occured. Tests were carried out at -196°C, room temperature, 100°C, 250°C, and 380°C.

The objectives were not fully realized as it was found impracticable to obtain replicas from the same area after each segment of a step-pull test.

The two methods of examination are complimentary. The replicas show much more detail than the optical observations, but as strain increases the replicas become so complex that the overall situation becomes obscure. The optical work clarifies this gross picture while deleting the fine structure.

3.2.2.5.1 Purity and Grain Size

The effects of differing purity on the surface features of polycrystal cobalt are minimal. The only noticable difference is that the intensity of surface rumpling at failure is lower for an increase in purity. This difference reflects the lower amount of transformation that occurs prior to failure.

Similarly, any differences observed between specimens of different grain size were differences in scale and intensity only. As grain size increases, the amount of strain induced transformation, and the elongation prior to failure decrease yielding less severe microstructures.

Based on these initial findings, further work was concentrated on the variation in observed deformation with strain and temperature.

3.2.2.5.2 Optical Metallography

Figure 52 traces the progress of a large grained specimen from yield to failure at 250°C.

At yield, the largest grain exhibits only one set of obvious shear markings (1), a second set (2) are barely visible. A rumpled band traverses the large grain completely. This band is probably an fcc annealing twin which has been reoriented during the cooling transformation.

At 2.3% strain the situation has changed radically. A large amount of shear on two systems (1 and 2) is shown clearly. A twin is also forming in the central grain. The increasing constraint in the system has also caused the small grain in the upper left to twin. The surface is rumpled so severely that some small grains are tilted out of focus.

At failure, the twin forming at 2.3% strain has propogated and reflected from two boundaries to take up a zig-zag configuration. The twin has not taken on a lenticular shape during growth, inferring a high shear value. Twins of this zig-zag type have been observed in single crystal cobalt by Davis[11] and polycrystal titanium by Rosi[15]. Both investigators determined that the twins had a $\{11\bar{2}1\}$ habit plane.

Figure 53 presents a different area in the same specimen at failure. Three important shear planes have been operative in a single grain.

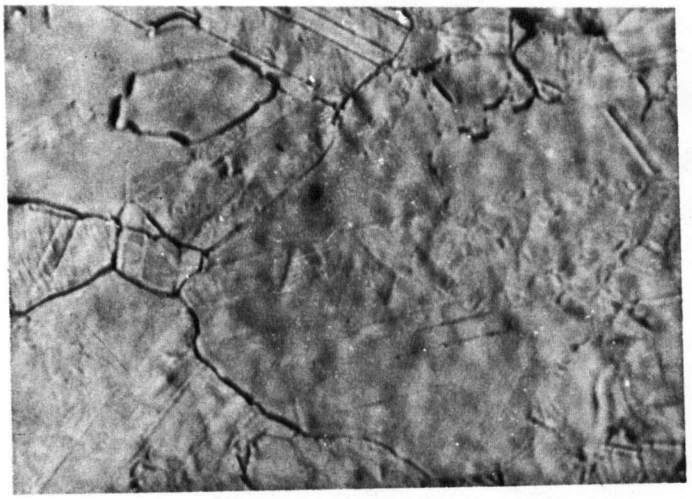

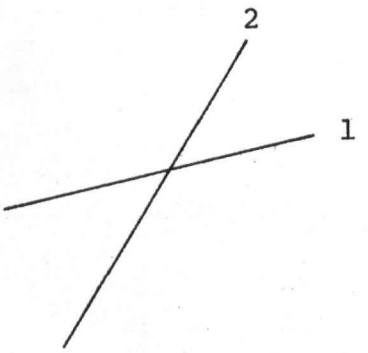

Fig. 52(a) 0.2% strain

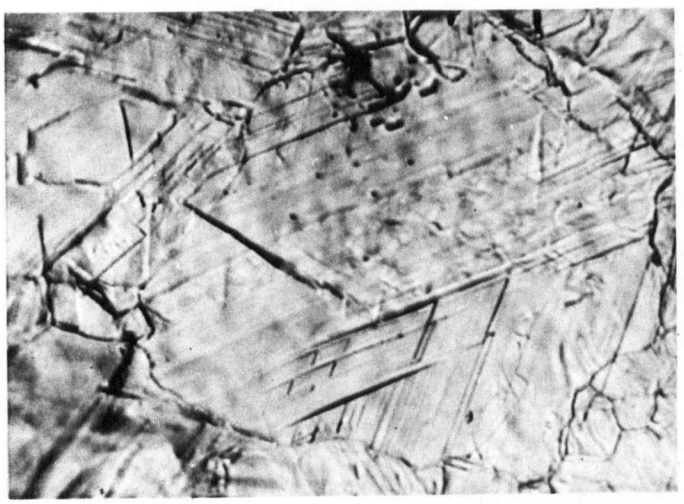

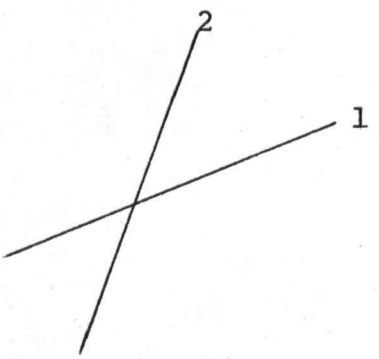

Fig. 52(b) 2.3% strain

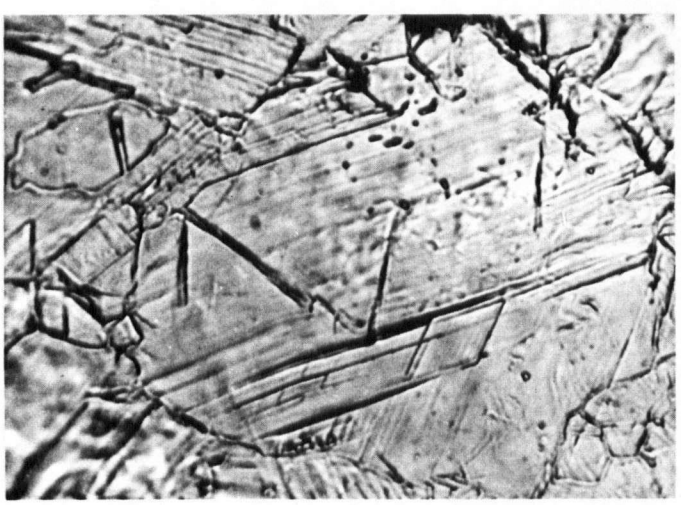

Fig. 52(c) failure

Fig. 52 Deformation of 99.998% cobalt, 850X

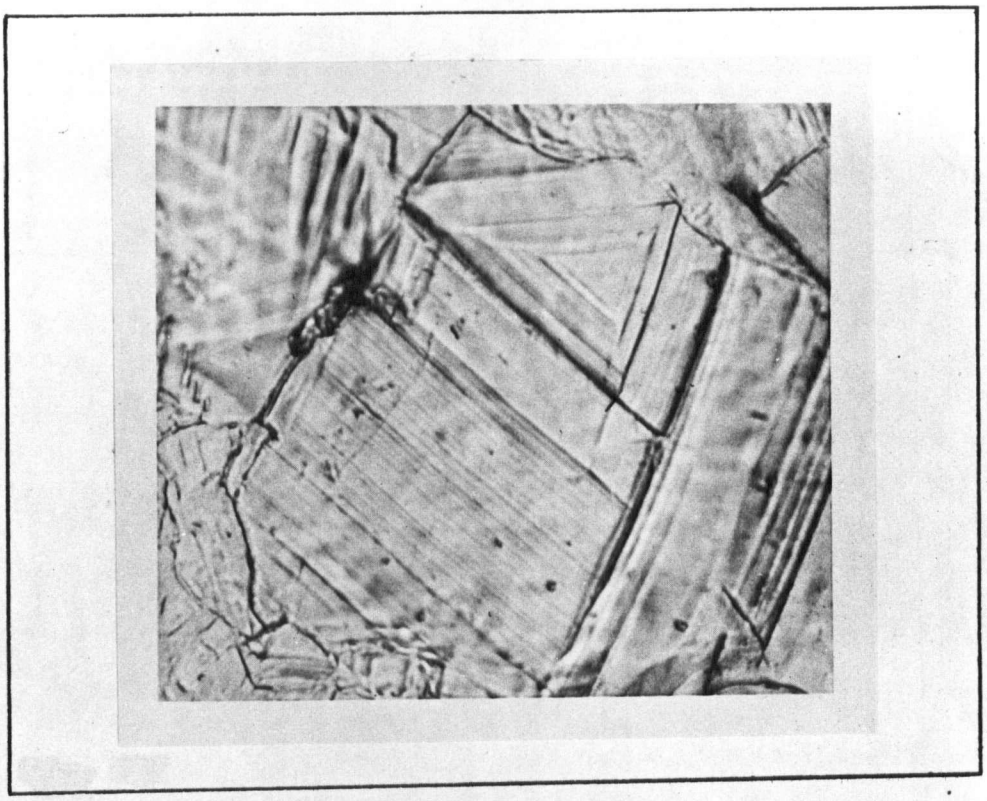

Fig. 53 Deformation markings in 99.998% cobalt at failure. 1000X

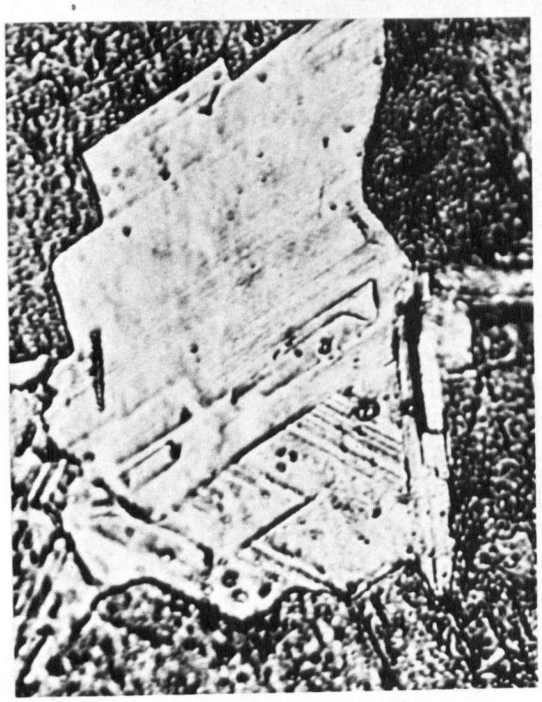

Fig. 54(a) 1.9% strain

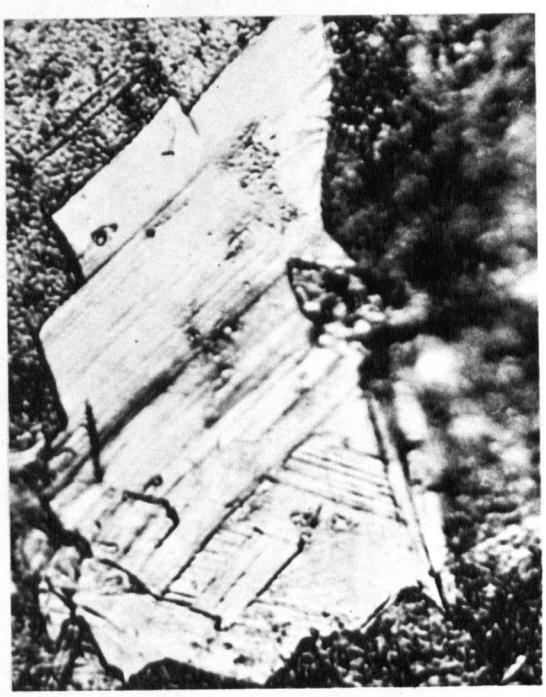

Fig. 54(b) 6.6% strain

Fig. 54 Grain shape change in 99.9% cobalt. 1000X

Figures 52 and 53 show cobalt having the largest grain size, lowest ductility, and least strain induced transformation of any material used in the present study. All other materials show very similar behaviour, although the rumpling and shear increase in intensity.

Figure 54 shows the amount of grain shape change that may occur with little increase in tensile strain. The tensile axis is shown and the dislocation activity appears to be limited to a single slip system in a majority of this grain.

Although optical metallography was found to be of limited use in determining the presence or absence of non-basal slip, Figures 55 and 56 show the complexity of twinning that occurs in polycrystal cobalt. Very few twins are observed at low strain values. At fracture all specimens exhibit a very complex twinned structure. Purity, grain size, and test temperature have little affect on this facet of the deformation. Figure 55 shows the twinning present following a test at -196°C, Figure 56 after a test at 350°C. Figure 56 shows a single grain after testing at 350°C. Several twins have taken on a lenticular configuration and are probably $\{10\bar{1}2\}$ twins, whereas the thin straight twins probably represent $\{10\bar{1}1\}$ and $\{11\bar{2}n\}$ habit planes. Over a dozen habit planes are represented in this single grain. The appearance of the thin twins at high temperature infers that high internal stress concentrations were available to nucleate them.

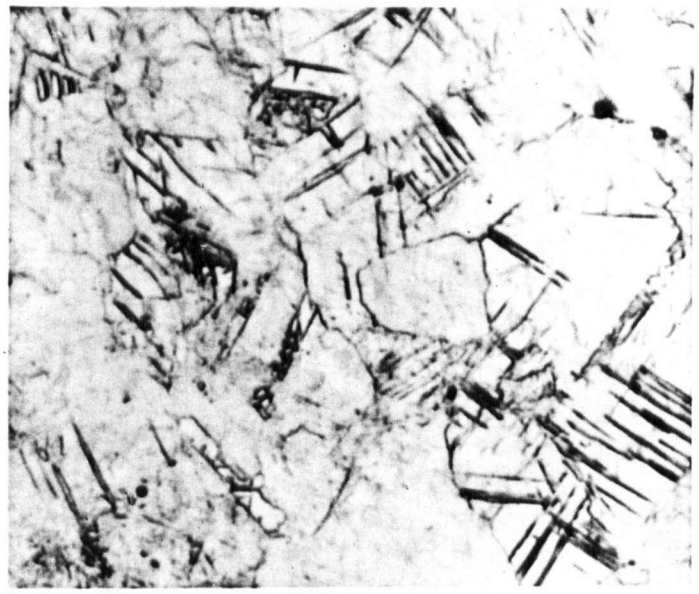

Fig. 55 Twinning in cobalt at -196°C. 850X

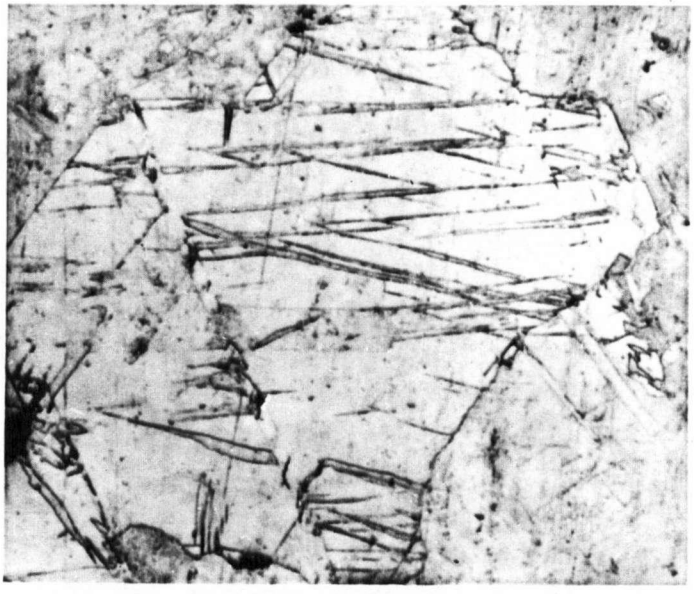

Fig. 56 Twinning in cobalt at 350°C. 850X

The information gained by optical metallography may be summarized as follows:

i) Purity and grain size do not affect the observed deformation modes. A reduction in purity or grain size simply increases the intensity of the structures observed.

ii) Little difference was noted between deformation above and below 0.25 T_m. Surface rumpling was somewhat less severe at high temperature which simply reflects the smaller volumes of strain induced martensite formed at these temperatures.

iii) Deformation is very heterogeneous. Some grains exhibit gross amounts of deformation at low strain values while neighbouring grains appear undeformed.

iv) Macroscopic shear occurs on two or more planes within the regions delineated by an fcc grain boundary. The amount of shear that may occur on any plane is very large.

v) Twins are observed in cobalt specimens tested at all temperatures between -196°C and 380°C. The amount of twinning observed at yield is negligible but increases with strain. Zig-zag twinning, assumed to occur in the $\{11\bar{2}1\}$ habit plane, is a common observation at all temperatures. Lenticular $\{10\bar{1}2\}$ twins as well as straight thin twins of probable habit planes $\{10\bar{1}1\}$ and $\{11\bar{2}n\}$ are also observed. Although a multiplicity of twinning modes are observed, the twinning volume remains small.

3.2.2.5.3 Replica Observations

The features observed by replica techniques are difficult to correlate with those delineated optically. As shown in Figure 57 for a small grained specimen of 99.7% cobalt, the effect of strain on the surface topography is very pronounced. To allow comparison to the optical observations replicas taken after limited amounts of strain are presented. In Figure 58, the majority of shear has taken place on two slip systems approximately at right angles. Where one region abutts the other, twins have been initiated to relieve stress. Although evidence of twinning does exist in this case, a total lack of visible stress relief is more common. In Figure 59, shear has taken place on three distinct systems. The amount of shear is large in all cases, yet no evidence of twinning at points of intersection is observed. The observed pattern shown in Figure 59 involving two or three shear systems is the most commonly observed surface feature in polycrystal cobalt. The topography is clearly a result of the multivariant martensitic transformation. The large step heights reflect the passage of many dislocations over a single slip plane. Therefore, it may be inferred that the stress system producing transformation on some planes is cabable of continuing dislocation production on these planes.

Fig. 57(a) 0.1% strain

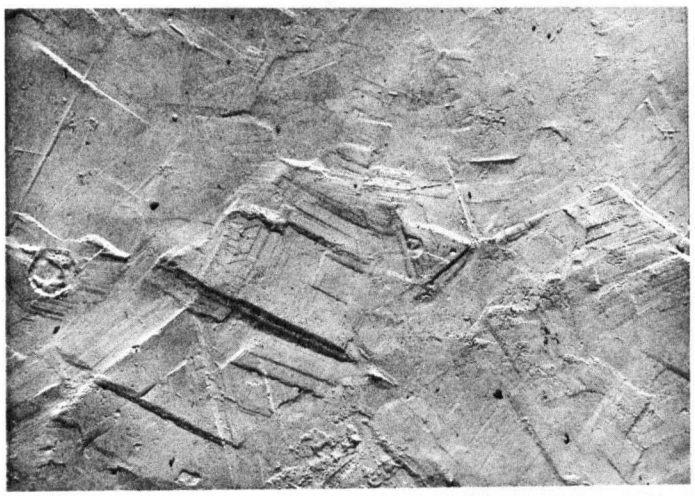

Fig. 57(b) 5.3% strain

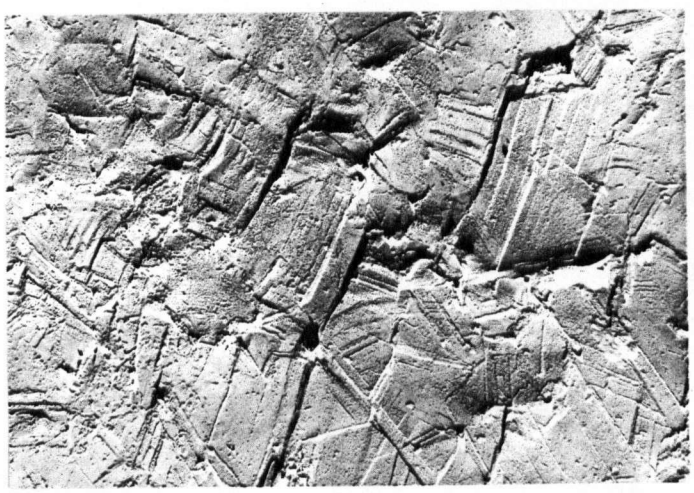

Fig. 57(c) 10.8% strain

Fig. 57 Deformation of 99.7% cobalt at 250°C. 3000X

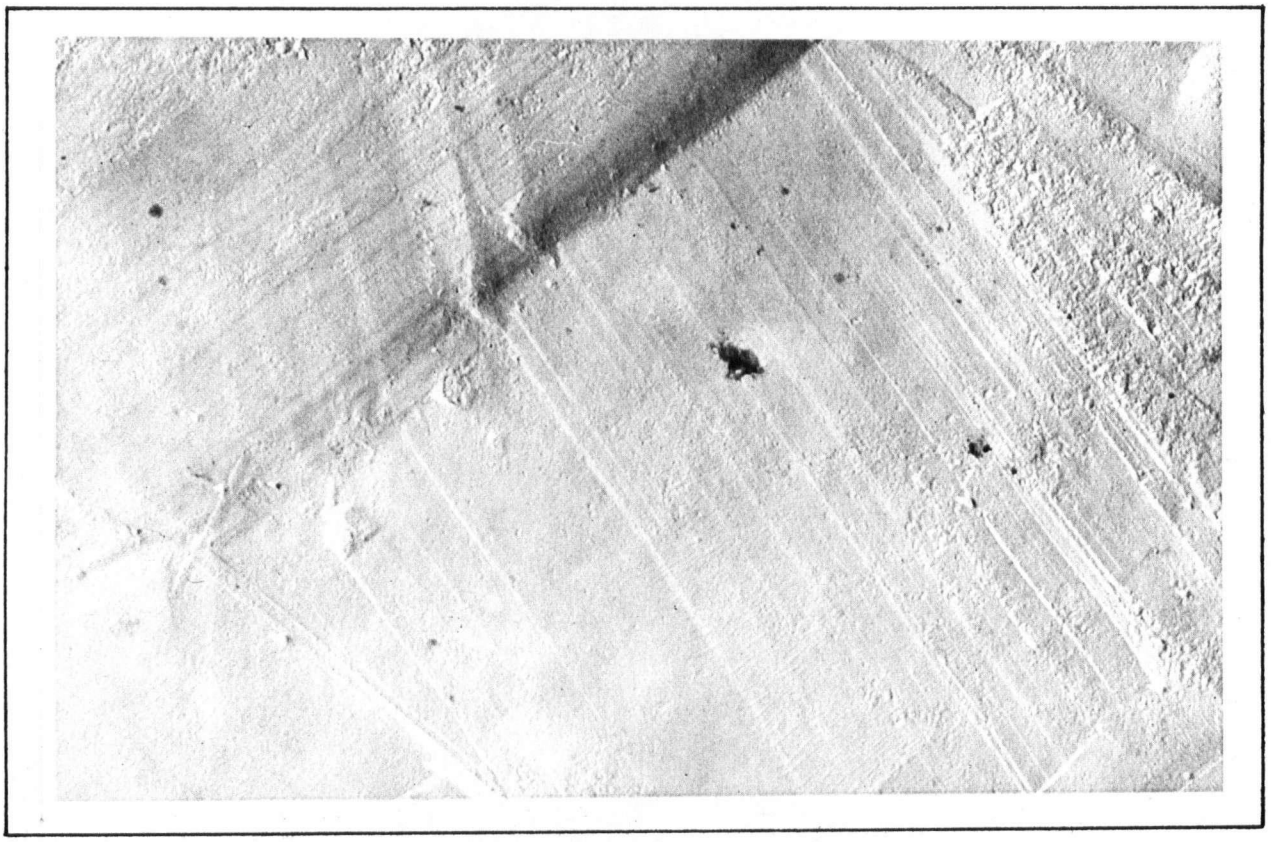

Fig. 58 Stress relief at a boundary between two regions where shear has taken place on different systems. 6500X

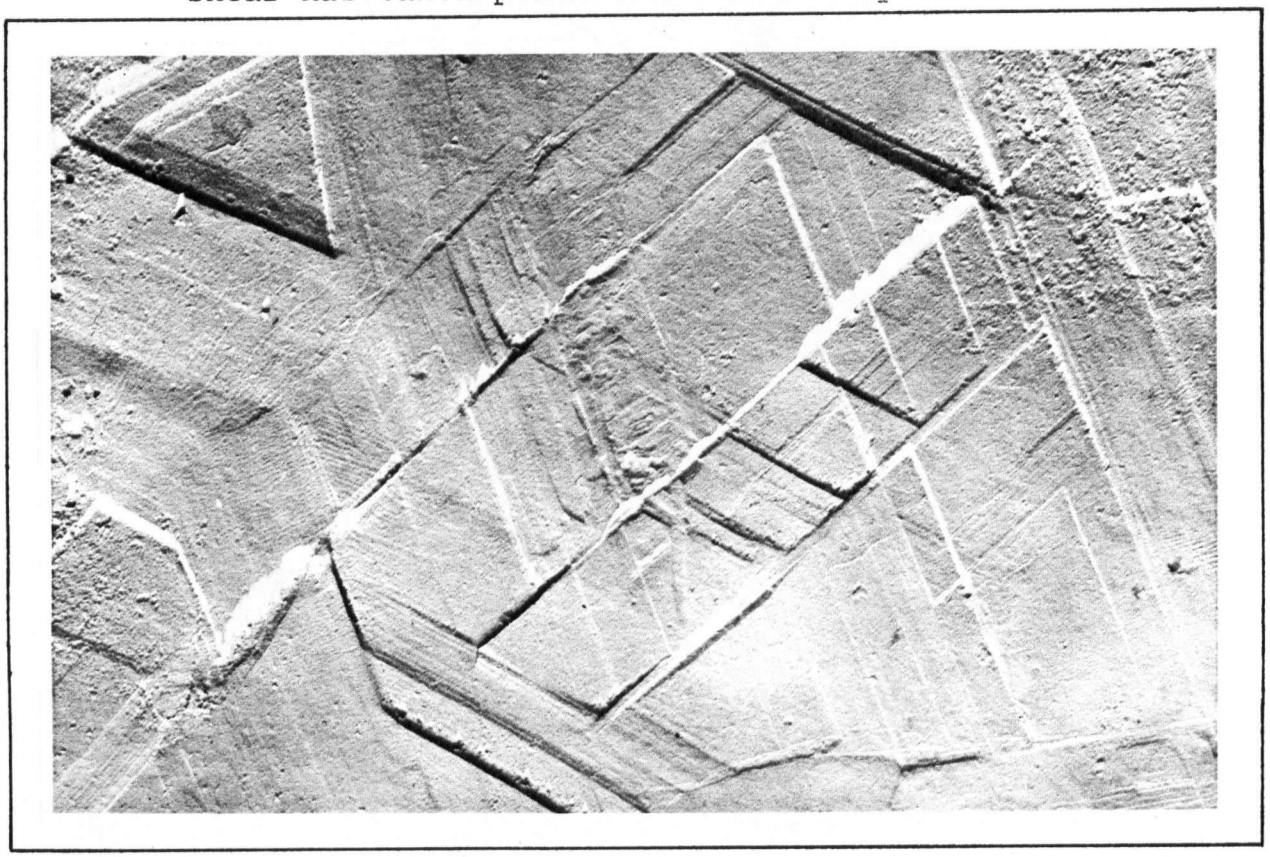

Fig. 59 Typical surface shear markings in cobalt. -196°C Test. 6500X

In contrast to the markings shown in Figure 59 are the twins shown in Figures 60 and 61. Slip on martensitic transformation planes is characterized by noticable shear on many parallel planes with gross amounts on occasional planes. The twins, on the other hand, are characterized by a single volume of sheared lattice. In Figure 61, a large lenticular twin appears in the center of the grain and another twin has formed in zig-zag fashion between the lenticular twin and a grain boundary.

The replica work was undertaken to ascertain if non-basal slip occured in polycrystal cobalt. A second goal was to determine whether the fine details of deformation differ above and below 0.25 T_m.

Non-basal slip was observed during tests at 250°C (0.30 T_m) but no similar observations were made at -196°C, 20°C, or 100°C. Figure 62 shows slip markings on a second system. The non-basal traces are assumed to occur on the $\{11\bar{2}2\}$ $\langle 11\bar{2}3\rangle$ system, as this is the only non-basal slip system that has been observed in single crystal cobalt[14]. The appearance of non-basal slip is not observed in all grains. This is to be expected in view of the heterogeneity of deformation.

One further observation may be drawn from the surface features above and below 0.25 T_m. Below 0.25 T_m all shear markings were very straight, and remained so until failure occured. Although large amounts of shear occured on some planes they exhibited very little bending or waviness. Figure 63 demonstrates this situation. At temperatures

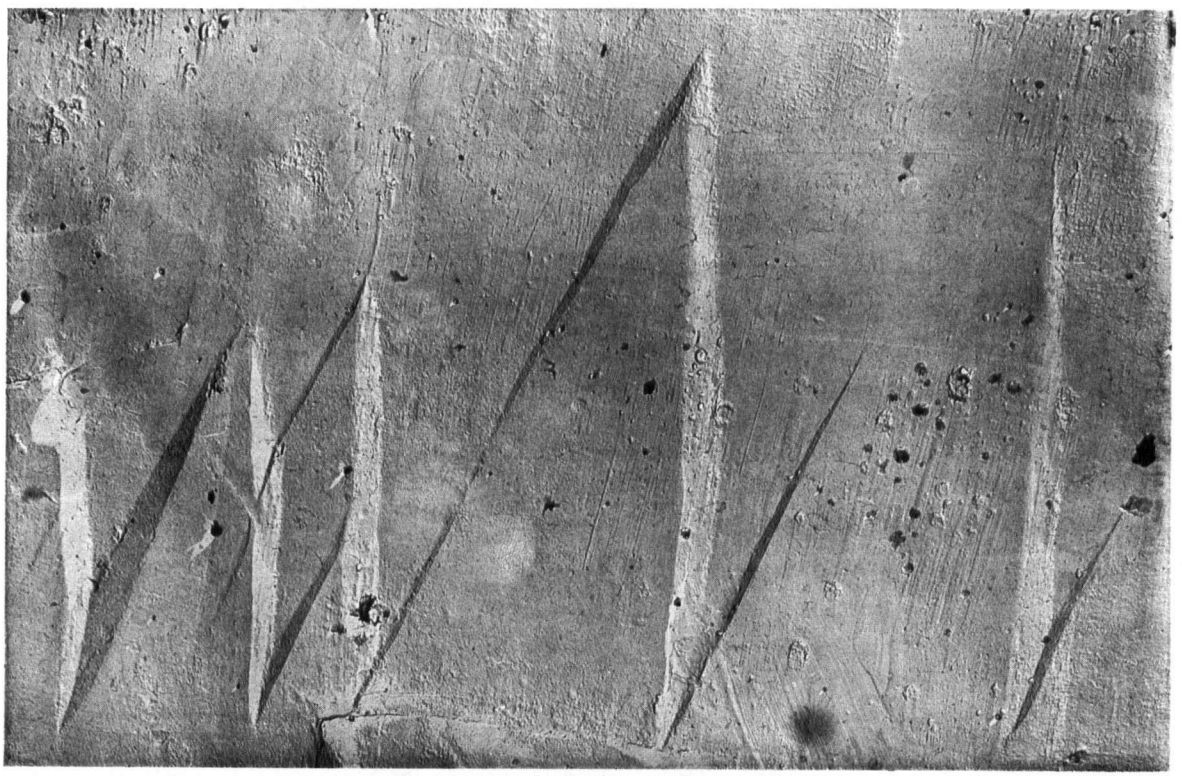

Fig. 60 Twinning in cobalt at -196°C. 3700X

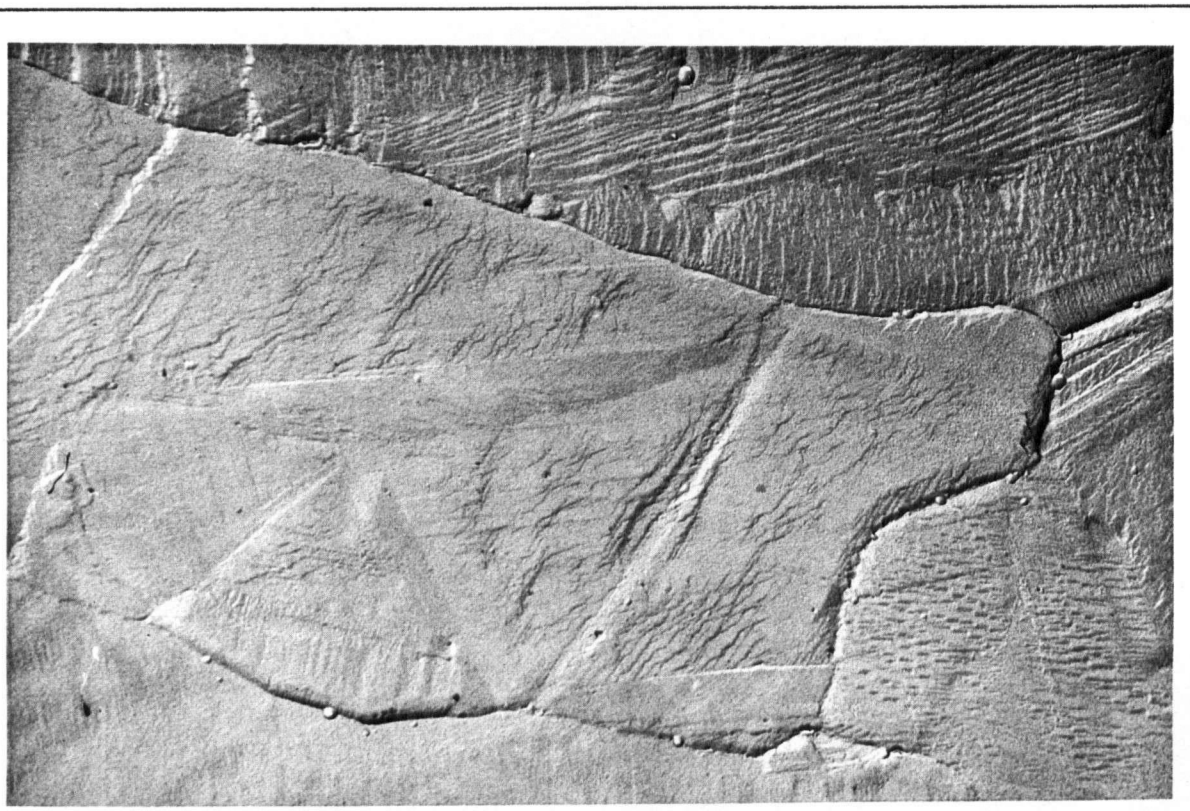

Fig. 61 Twinning in cobalt at 250°C. 3700X

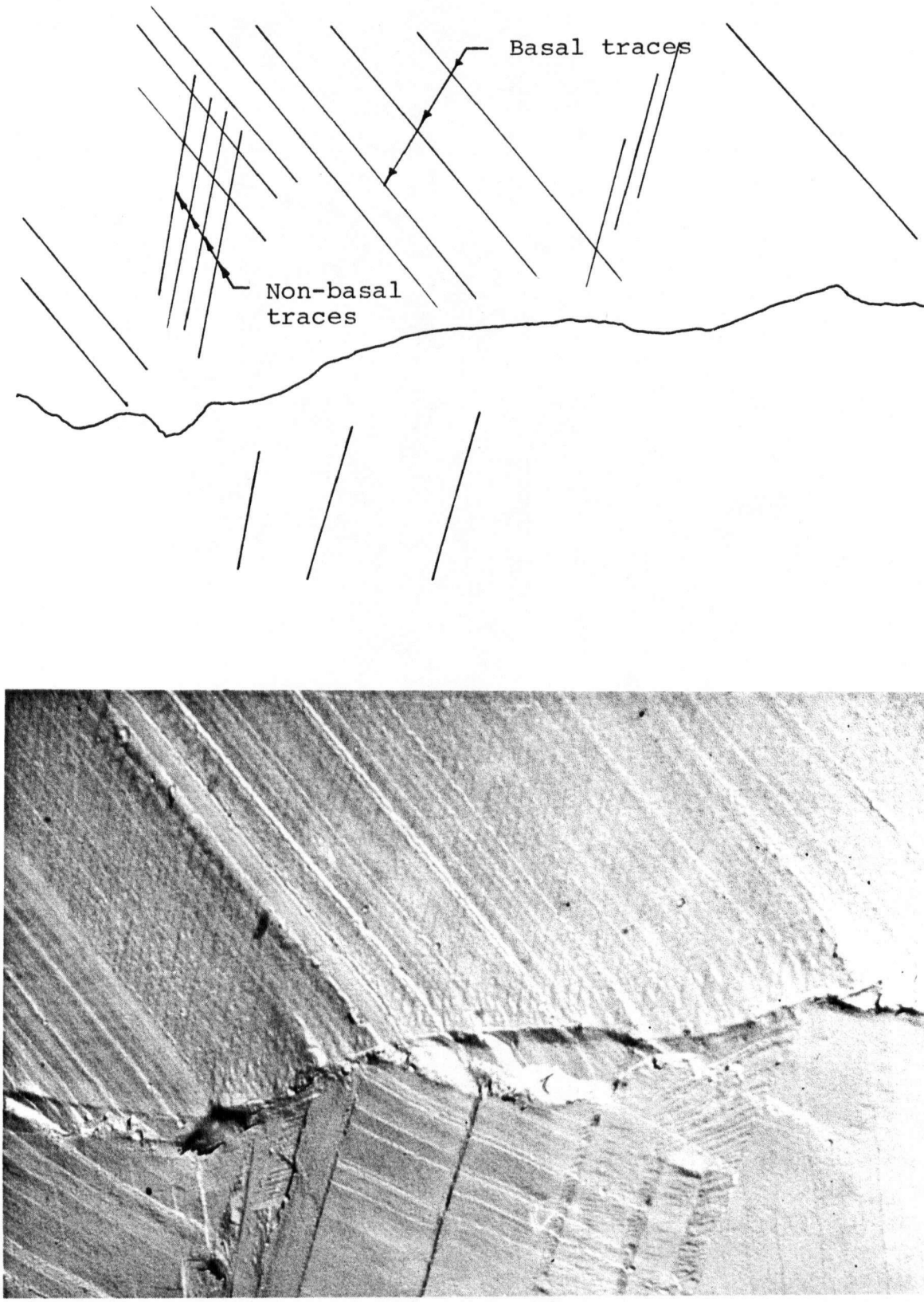

Fig. 62 Non-basal slip in polycrystal cobalt tested at 250°C, 7500X

above 0.25 T_m the situation differed. In areas, where large amounts of shear were visible on several systems, one set of shear markings often took up a curved or wavy orientation. Figure 64.

This non linearity of the slip bands may arise from an increase in the amount of glide polygonization occuring, allowing visible changes in slip band orientation.

3.2.2.5.4 Summary

The metallographic evidence presented for polycrystal cobalt agrees with the behaviour postulated earlier and with observations made in single crystal material[4,14].

Purity and grain size had little affect on the observed deformation mechanisms. As grain size and purity increased the surface topography became less intense due to less strain induced transformation occuring.

The majority of the surface structure is related to the allotropic transformation. The multivariance within fcc grains provides several basal orientations within an fcc grain boundary. Shear is commonly observed on more than one basal system and is extremely heterogeneous.

A variety of twinning modes occured at all temperatures The number of twins increased with strain; lenticular and zig-zag twins as well as many straight thin twins were observed. The lenticular twins were $\{10\bar{1}2\}$ twins common to hcp metals. The twins taking up a zig-zag configuration were

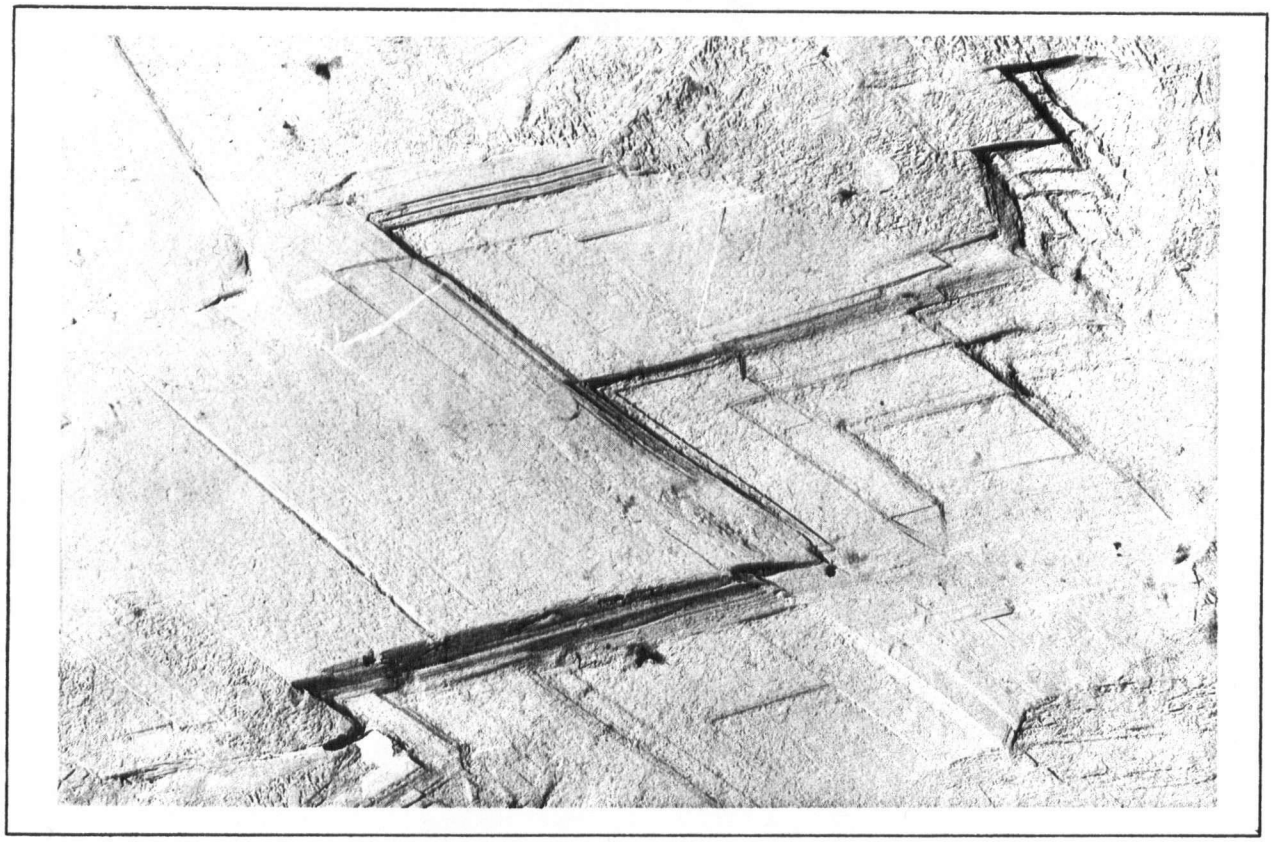

Fig. 63 Shear Markings in 99.9% cobalt tested at 20°C. 7500X

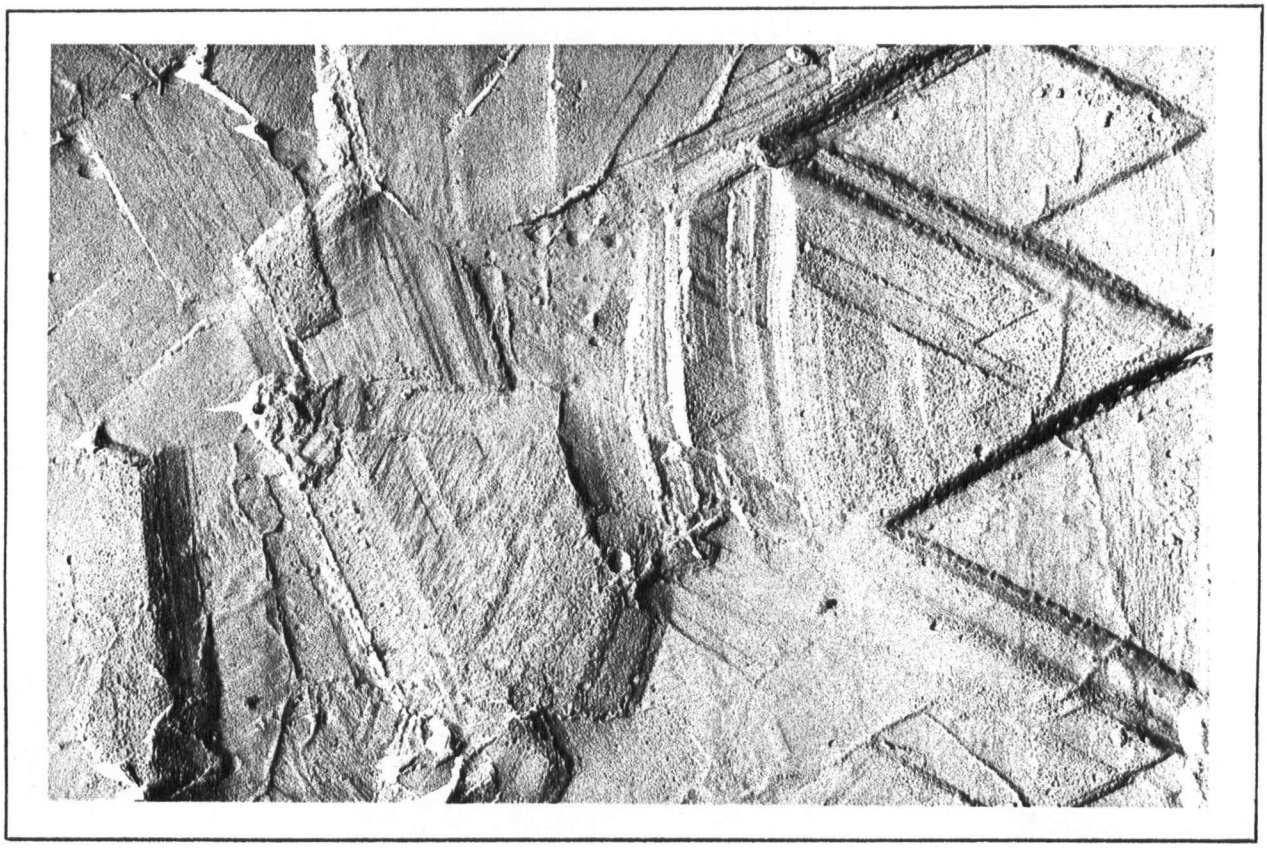

Fig. 64 Shear markings in 99.9% cobalt tested at 250°C. 7500X

assumed to belong to the $\{11\bar{2}1\}$ twinning plane, as twins of similar configuration were identified in single crystal cobalt by Davis[11]. The thin straight twins probably belong to the $\{10\bar{1}1\}$, $\{11\bar{2}2\}$, or $\{11\bar{2}4\}$ twin systems as all three have been observed in cobalt single crystals[4,14].

Non-basal slip was observed above 0.25 T_m but not below. It is postulated that the slip occurs on the $\{11\bar{2}2\}$ $<11\bar{2}3>$ system, as corrugated slip has been observed in single crystal cobalt[14].

A further observation outlining a difference in behaviour above and below 0.25 T_m is the non linearity of basal slip traces. The observed bending and waviness may reflect concentrations of dislocations of similar sign on parallel slip planes.

3.2.2.6 Discussion and Summary

It remains to compare the data regarding the strain induced transformation to that determined from tensile procedures. The easiest way to avoid confusion while discussing the numerous observations made in this study is to deal with various measured parameters in a tabular form.

A summary of the experimental results is presented in Table XIV. A series of footnotes are included for those observations that do not lend themselves to the tabular format.

3.2.2.6.1 The Yield Stress

A great deal of information has been gathered regarding the yield stress. The most important observation is the difference in behaviour above and below 0.25 T_m. (Table XIV.) This result is mirrored in the results for the strain induced transformation. Below 0.25 T_m, the initiation of the strain induced transformation occurs at 0.05% to 0.10% strain and is well underway at the 0.2% offset yield stress. On the other hand, as the temperature is increased above 0.25 T_m, the initiation of the transformation is delayed to higher values of strain. At 0.2% strain, little if any transformation has occured in specimens tested at 0.30 or 0.37 T_m. This combination of results leads to the conclusion that the essentially athermal yield behaviour observed below 0.25 T_m, is due to the onset of bulk transformation of fcc cobalt.

TABLE XIV Summary of Experimental Results

	As Purity Increases	As Grain Size Increases	At Test Temperatures $<0.25\ T_m$	At Test Temperatures $>0.25\ T_m$
% retained fcc	decreases rapidly	decreases rapidly	N/A	N/A
0.2% yield stress	decreases slightly	decreases rapidly	∿constant	decreases rapidly
Elongation to Failure	decreases	decreases rapidly	decreases	decreases
Work Hardening Rates	little effect	little effect	decreases rapidly	decreases slowly
Total Work Hardening	decreases	decreases	decreases	decreases
Ultimate Strength	decreases	decreases	decreases	decreases
Strain at which Tx. Begins	little effect	little effect	constant	increases
Volume Tx. at 0.2% strain	little effect	little effect	large	nil
Volume Tx. at Failure	decreases	decreases	decreases	decreases
Rate of Strain Induced Tx.	little effect	decreases	little effect	little effect
Volume Tx. at any Strain	little effect	little effect	constant	decreases rapidly

- Fracture surfaces exhibit ductile failure at all temperatures.
- High values are observed for σ_i and K in a Hall-Petch relationship and both parameters decrease rapidly above $0.25\ T_m$.
- The relationship between percentage fcc and strain may be represented by an equation of the form $\varepsilon = A(10)^{m\%\,fcc}$.

The behaviour is athermal because the driving force for transformation arising from thermodynamic considerations is very small when compared to the stress levels involved.

Above 0.25 T_m, it is postulated that initiation of dislocation activity on the corrugated slip plane can occur at stress levels below those required for martensitic transformation. Thus, slip on the second order pyramidal system controls yield above 0.25 T_m. The sharp decrease in yield strength measured is due to the temperature dependence of the Peierls stress on the corrugated slip plane.

This result was outlined during discussion of the effect of grain size on the yield strength. The results presented in Section 3.2.2.4 on the strain induced transformation are consistent with the postulated behaviour, but do not dismiss the possibility that some other strongly temperature dependent mechanism may be responsible for the behaviour.

The large increase in yield stress as grain size decreases was discussed earlier. A change in grain size has little affect on the manner in which the strain induced transformation proceeds in the region of yield.

It was noted during discussion of the tensile results that the temperature at which the yield stress changes behaviour increased as the grain size increased. This result is also consistent with the behaviour postulated above. The change in temperature dependence occurs at higher temperatures as the grain size increases because the stress levels accomplished during deformation differ radically.

In Figure 65, two lines have been drawn to represent corrugated slip and bulk transformation at yield. As the applied stress increases yield will occur when Von Mises Criterion can be satisfied. At low temperatures, yield occurs when transformation begins. Above 0.25 T_m, it is postulated that yield occurs when the stress level is sufficient to initiate dislocation motion on the corrugated slip plane. If material of a different grain size is tested, a different set of curves apply.

As outlined earlier, the yield stress may be considered as arising from a combination of factors; σ_i, the lattice friction and K, a factor representing the difficulty with which slip may be initiated across a boundary. It was determined that both σ_i and K decrease more rapidly above 0.25 T_m. As grain size increases, the yield stress drops rapidly reflecting the large value of K. At temperatures greater than 0.25 T_m, the value of K is decreasing rapidly and therefore a less severe drop in yield stress is observed.

A second set of lines representing the behaviour of 24 micron, 99.9% cobalt are shown in Figure 65. These lines are consistent with the tensile observations and the postulated behaviour.

Purity has little effect on the strain induced transformation. This parallels the results for the 0.20% yield stress, where purity was not found to be an important parameter.

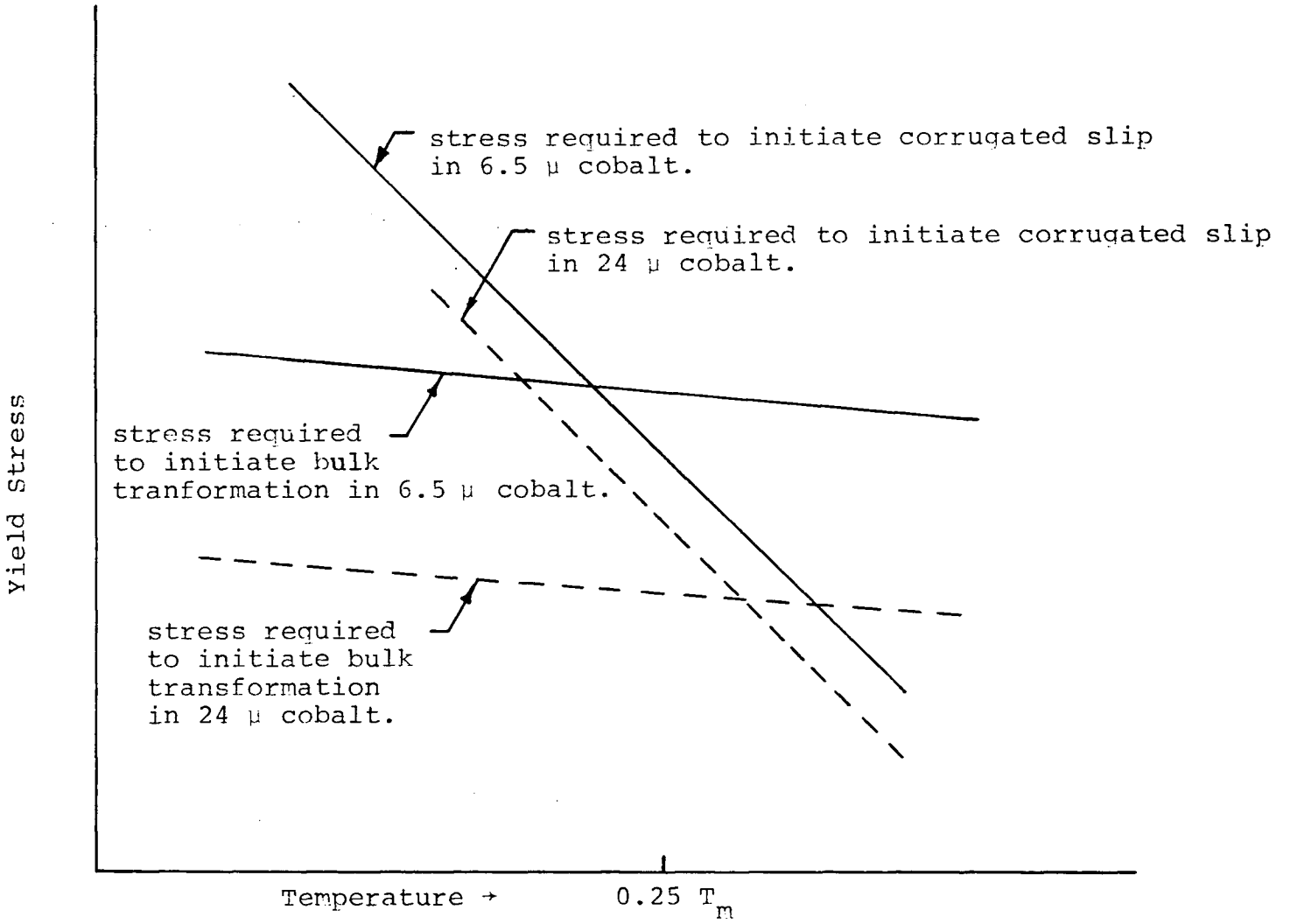

Fig. 65 Mechanisms controlling yield in polycrystal cobalt

3.2.2.6.2 Flow Stress

The observed tensile characteristics of the flow stress are directly related to the strain induced transformation. The two stage temperature dependence of flow stress disappears as strain increases, paralleling the observation that as strain increases the amount of transformation taking place during any strain increment is also dropping. As less transformation is occuring at higher strains, the athermal behaviour attributed to the strain induced transformation also disappears, and the flow stress becomes more representative of the other controlling deformation mechanisms. The anomalous behaviour noted in the initial portion of the stress-strain curve is simply a further manifestation of the high rate of transformation at low strain values.

3.2.3.6.3 Elongation to Failure

Based on the observations made in this study, it is not surprising that the ductility of polycrystal cobalt quoted elsewhere forms no recognizable pattern.

Elongation varies via a complex inter-relationship between purity, grain size, and test temperature. The reasons behind the behaviour only become clear when the amount of fcc phase present, and the manner in which this fcc phase disappears with strain, is understood.

Polycrystal cobalt fractures when either of two criteria are satisfied. First, polycrystal cobalt will fail when the volume percent of fcc phase is reduced to a critical value. If the stress level is very high, as in tests at -196°C, the transformation may come within 2% of completion before failure occurs. At room temperature, the critical value is about 5% retained fcc phase.

The second limit is due to Considère's Criterion; When the work hardening rate becomes equal to the applied true stress, instability occurs and failure becomes imminent.

The measurable parameter that determines the ductility of polycrystal cobalt is the amount of fcc phase present in the material following an annealing procedure. The rate at which the fcc phase disappears with strain does not vary with purity, or test temperature. Thus, the lower ductility measured for high purity material simply reflects the reduced amount of fcc phase available following heat treatment. The observed decrease in ductility as test temperature increases arises from Considère's Criterion.

The rate at which the strain induced transformation proceeds decreases as the grain size increases, also the retained fcc phase present prior to testing decreases as the grain size increases. The latter factor is larger and thus, the measured elongation for polycrystal cobalt decreases as grain size increases.

3.2.2.6.4 Work Hardening Behaviour

Earlier, work hardening behaviour in polycrystal cobalt was compared to that for metals undergoing a similar martensitic transformation. The essentially constant work hardening rate observed at low strain was attributed to the transformation taking place at a high rate. The monitored progress of the transformation verifies that the majority of strain induced martensite forms during the initial portion of the tensile curve.

The two stage temperature dependence of the work hardening rate was also attributed to the martensitic transformation, as was the disappearance of the two stage behaviour as strain increased. These results parallel the observed behaviour of the flow stress and may be explained in like manner.

At low temperatures and low strain values, the rate at which martensite plates are forming is very high, thus, the structure through which dislocations must move is increasing in intensity very quickly. As strain increases, the rate at which the transformation proceeds drops off rapidly. Simultaneously, the stress level is increasing, initiating other deformation mechanisms to relieve stress concentrations. Eventually, there is insufficient fcc phase available to allow further deformation or the work hardening rate becomes equal to the stress level and failure occurs.

Above 0.25 T_m, the onset of bulk transformation occurs at some point following yield while corrugated slip is postulated as occuring throughout the stress strain curve. Transformation does take place, but at any value of strain far less strain induced martensite has formed than at temperatures below 0.25 T_m. The structure formed during deformation above 0.25 T_m is probably less intensive than that formed below. Less lattice debris and fewer martensite boundaries due to transformation are produced. In addition, slip may be more easily initiated across boundaries due to the reduction in Peierls stress on the corrugated slip plane. Therefore the measured work hardening rates are lower above 0.25 T_m.

Although little variation in work hardening rates were recorded for changes in purity or grain size, the total work hardening between yield and fracture (and the ultimate strength) decreases with an increase in either parameter. This result reflects the reduction in ductility that accompanies increasing purity or grain size.

4 Conclusions

i) Although the hcp allotrope is the stable form for cobalt below 417°C, polycrystal hcp cobalt is only a theoretical possibility. Cobalt exists as a two phase mixture of fcc and hcp crystal lattices following normal heat treating procedures.

ii) The amount of fcc phase retained in cobalt following an annealing treatment decreases with increasing purity and increasing grain size. The maximum amount of metastable fcc phase that may be retained is approximately 60%, the minimum 10%.

iii) The retained fcc phase present in polycrystal cobalt transforms martensitically to the hcp modification as deformation is introduced yielding tensile properties that may be compared to other metals that undergo a similar transformation. The relationship between strain and the retained fcc phase may be described by an equation of the form $\varepsilon = A(10)^{m\%fcc}$. The transformation interferes with comparisons between cobalt and other common hcp metals.

iv) The yield stress of cobalt, below the transformation temperature, has two distinct regions of temperature dependence. Below 0.25 T_m the yield stress is essentially temperature independent and is determined by the stress necessary to initiate bulk transformation of retained fcc phase. Above 0.25 T_m it is postulated that the strong temperature dependence observed is due to the decreasing value of the Peierls stress on the corrugated $\{11\bar{2}2\}$ slip planes.

v) The strengthening effect of grain boundaries in cobalt is large, as is the case for other hcp metals which do not exhibit a multiplicity of slip systems at room temperature.

vi) The ductility of cobalt is related to the amount of retained fcc phase present in the polycrystal aggregate. A larger initial proportion of fcc phase yields higher ductility. The observed decrease in ductility as test temperature is increased is due to Considere's Criterion.

vii) The work hardening rates measured for polycrystal cobalt are high and may be compared to the behaviour of other materials that transform martensitically during deformation. A two stage temperature dependence of the work hardening rate is observed at low strain values.

viii) The commonest surface feature in deformed cobalt is the heterogeneous shear that occurs on basal planes of more than one orientation within an fcc grain-boundary. The intense surface shears arise from transformation from fcc to hcp on these planes combined with continued dislocation production on these planes.

ix) A number of twinning modes are observed in cobalt at all temperatures from 0.04 T_m to 0.38 T_m. Although many twins form the twinned volume is small (several %).

x) Non-basal slip occurs above 0.25 T_m but not below. The secondary slip system is postulated as the $\{11\bar{2}2\}$ $\langle 11\bar{2}3\rangle$ second order pyramidal system.

5 Suggestions for Future Work

The results of the present study open many avenues for further study. The most obvious areas where further work is required are outlined below.

i) If more is to be learned about the deformation modes, studies must be carried out with very large grained specimens. This would allow direct measurement of planes and directions involved in deformation allowing accurate verification of the operative slip and twinning modes in cobalt.

ii) A second area where useful information could be gained is in a study of the strain induced transformation. From what has been found in the present study it should be possible to produce some very ductile, high strength cobalt via a series of ausforming procedures or by variations in annealing procedures. Certain combinations should yield large volumes of retained fcc phase and thus yield high ductility coupled with high strength.

iii) From the high K values and σ_i values found in pure polycrystal cobalt, it is reasonable to assume that judicious additions of alloying elements should yield cobalt alloys with extremely high tensile properties at room temperature. To extend the useful strength to higher temperatures requires alloying additions that would move the allotropic transformation to higher temperatures while maintaining useful proportions of the metastable, high temperature, phase.

Appendix 1

X-Ray Analysis

The following outline for the quantatative analysis of volume fractions of fcc and hcp cobalt is based on work done by Sage and Guillaud[90] and a thorough treatment of the procedure provided by Lanners[84].

The method utilizes diffracting planes that are affected similarly by any preferred orientation present. Anomalies that occur in certain diffracted intensities are discussed and allowed for. The anomalies uncovered by Sage and Guillaud and Lanners are the same and it is assumed that their results apply to the material utilized for the present work.

When the fcc cubic structure transforms to hcp, certain (111) planes become (0002) planes. The number of diffracting atoms is constant but the transformation preserves only two planes out of eight existing in the cubic structure. The position of the diffracted line does not change but it's intensity is reduced by a factor of four.

$$\frac{I_{(0002)}}{I_{(111)}} = \frac{1}{4} \qquad \ldots.1)$$

In a mixture of mx grams of cubic cobalt and m(1-x) grams of hcp cobalt, the common line consists of a fraction due to the cubic phase and a fraction due to the hcp phase.

$$\frac{I_{(111)}}{I_{(0002)}} = \frac{4mx}{m(1-x)} = \frac{4x}{(1-x)} \qquad \ldots.2)$$

The relative intensities of pairs of lines in the hcp or fcc phase have been calculated. For example:

$$\frac{I_{(111)}}{I_{(200)}} = 2.22 \qquad \ldots.3)$$

$$\frac{I_{(0002)}}{I_{(10\bar{1}1)}} = 0.28 \qquad \ldots.4)$$

The calculation giving rise to the ratios above assumes that the intensity of the lines are independent of the diffraction angle. The values for these ratios determined by Sage and Guillaud are 1.85 and 0.27 respectively[90].

Combine equation 2,3,4.

$$\frac{x}{1-x} = \frac{I_{(111)}}{4I_{(0002)}} = \frac{1}{4}\frac{I_{(111)}}{I_{(200)}} \cdot \frac{I_{(10\bar{1}1)}}{I_{(0002)}} \cdot \frac{I_{(200)}}{I_{(10\bar{1}1)}}$$

$$= \frac{1}{4} \cdot \frac{2.22}{0.28} \cdot \frac{I_{(200)}}{I_{(10\bar{1}1)}} = 1.98 \frac{I_{(200)}}{I_{(10\bar{1}1)}} \qquad \ldots.5)$$

$$\frac{x}{1-x} \simeq \frac{2I_{(200)}}{I_{(10\bar{1}1)}} \qquad \ldots.6)$$

Edwards and Lipson[55] carried out their analysis using the lines (200) and $(10\bar{1}0)$. The present work compares (200) and $(10\bar{1}1)$ as did Lanners and Sage and Guillaud. The $(10\bar{1}1)$ line is four times as intense as $(10\bar{1}0)$ and allows for more accurate calculations especially when the amount of hcp phase is small.

Both Lanners[84] and Troiano[54] found anomalous intensities for the (111) and (0002) lines. By electron microscopy they determined that the results were due to a preferred presentation

of these planes to the x-ray beam, that is, a texture existed. This abnormally high presentation of (0002) and (111) implies normal presentation of (200) and (10$\bar{1}$1).

The equation used for quantitative analysis is not affected by these anomalies. Let the enhanced intensities for the (111) and (0002) planes be:

$$I'_{(0002)} = 0.28\ HI_{(10\bar{1}1)} \qquad ....7)$$

$$I'_{(111)} = 2.22\ CI_{(200)} \qquad ....8)$$

$$\frac{I'_{(111)}}{I'_{(0002)}} = \frac{2.22\ CI_{(200)}}{0.28\ HI_{(10\bar{1}1)}} \qquad ....9)$$

from equation 6

$$\frac{I'_{(111)}}{I'_{(0002)}} = 4 \cdot \frac{C}{H} \cdot \frac{x}{(1-x)} \qquad ...10)$$

from equations 9 and 10

$$\frac{x}{(1-x)} = \frac{1}{4} \cdot \frac{H}{C} \cdot \frac{I'_{(111)}}{I'_{(0002)}} = \frac{1}{4} \cdot \frac{H}{C} \cdot \frac{2.22}{0.28} \frac{C}{H} \frac{I_{(200)}}{I_{(10\bar{1}1)}}$$

$$= 2\ \frac{I_{(200)}}{I_{(10\bar{1}1)}} \qquad ....6)$$

The difference between the equations used by Sage and Guillaud and Lanners is as follows:

$$\frac{x}{(1-x)} = 2\ \frac{I_{(200)}}{I_{(10\bar{1}1)}} \qquad \text{used by Lanners}^{84} \qquad ....6)$$

$$\frac{x}{(1-x)} = 1.5\ \frac{I_{(200)}}{I_{(10\bar{1}1)}} \qquad \text{used by Sage and Guillaud}^{90} \qquad ...11)$$

Although a large discrepancy appears obvious, calculation shows that the differences observed are acceptable when considered in light of the normal experimental scatter in results. For example see the chart below.

Measured Ratio $\frac{I_{(200)}}{I_{(10\bar{1}1)}}$	% fcc, eqn. 6	% fcc, eqn. 11
1	66	60
1/2	50	43
1/10	16	13

Equation 6 was chosen for the present work because all the recent investigations have used this formula, i.e. Beckers[82], Müller[83].

Appendix 2

Measurement of Tensile Parameters by an Intersect Method

The following paragraphs outline a method for determining the yield stress versus temperature relationship from data taken from a step-pull test.

Figure 66 shows the step pull results for a specimen initially strained at -196°C and retested after increasing the temperature in 40°C steps. The data is plotted as true stress versus true strain, and is also normalized for the change in G with increasing temperature. Due to the parabolic shape of the curve upon retesting, the proper slope to apply to the individual segments of curve was found from graphical data similar to that shown in Figure 38. From curves of this type, the work hardening rate at any value of strain and temperature can be determined. This slope was then applied to each individual segment of the curve to determine the stress level corresponding to the start of the strain segment under scrutiny. The manner in which the data is determined is shown in Figure 67. The data for the complete test shown in Figure 66 is presented in Table XV.

Because all data is to be normalized to 0.2% strain, this value is tabulated for the initial step pull in Table XV.

At first glance, it would appear that if the summation of $\Delta\sigma$ values due to work hardening was subtracted from the intersect yield strength a plot of yield strength versus temperature would result. Some curve is found if this is done, but it is incorrect, because no work hardening rate

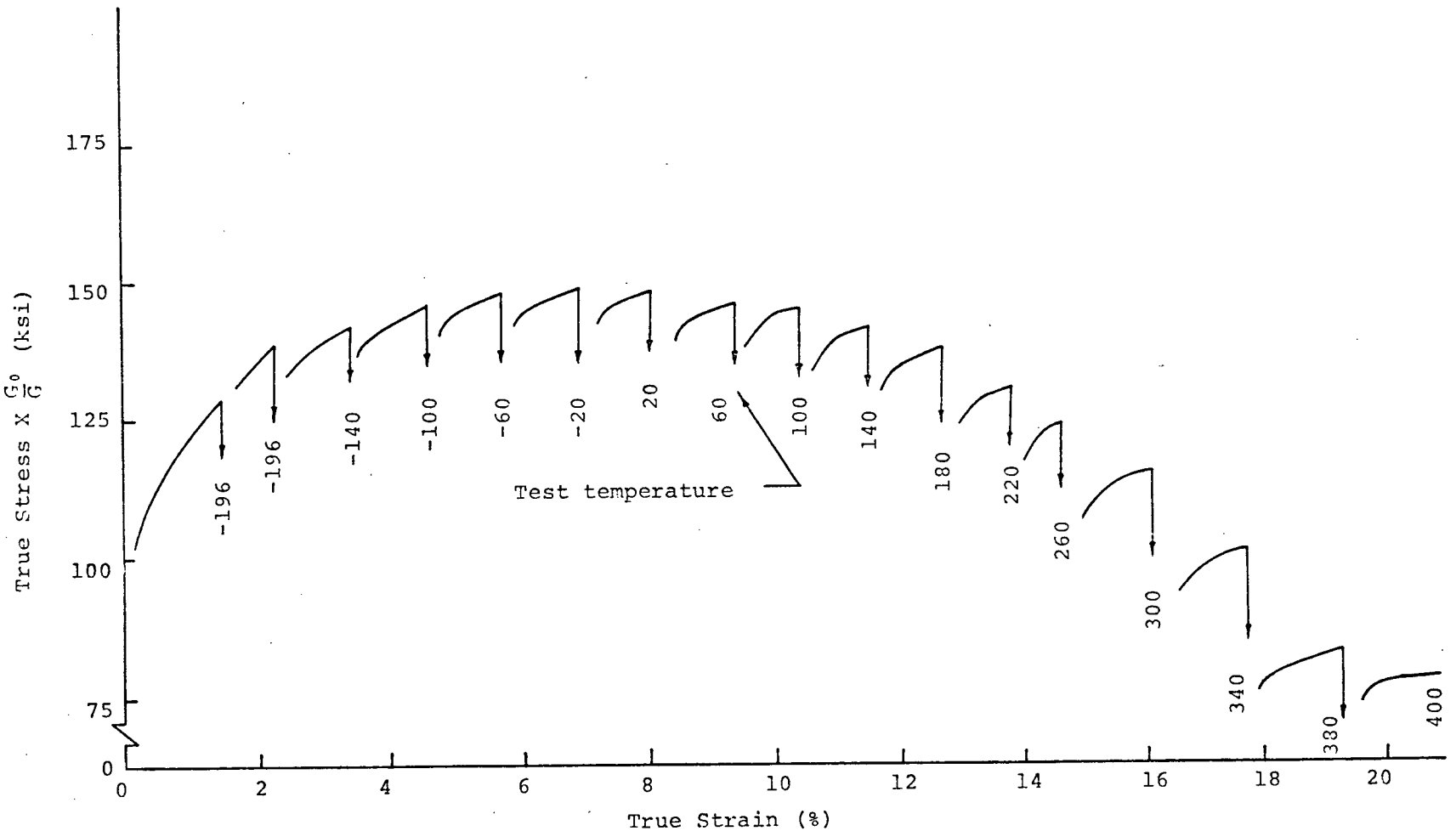

Fig. 66 Step-pull tensile test. 99.9% cobalt, 6.5 micron grain size.

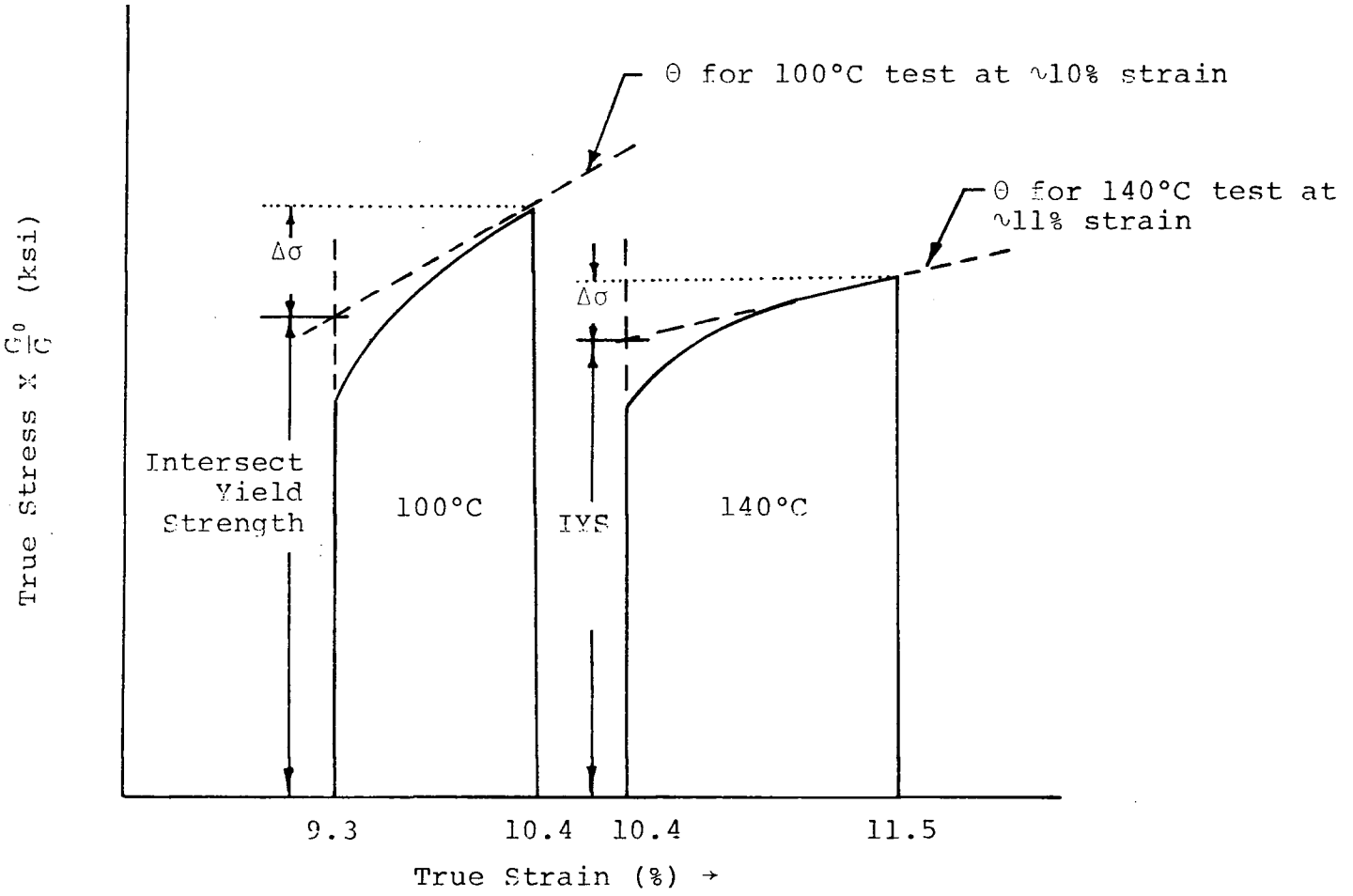

Fig. 67 Determination of the intersect yield strength from step-pull data.

TABLE XV Typical Data From a Step-Pull Tensile Test

Specimen ADJ - 99.9% cobalt annealed 1 hr. at 600°C

Pull (#)	Temp. (°C)	True Strain (%)	Intersect yield stress (ksi)	Maximum stress (ksi)	Δσ	Uncorrected yield stress (ksi)	Corrected for θ and to 0.2% (ksi)
1	-196	0 - 1.5	104.0	123.9	19.9	104.0	102.0
2	-196	1.5 - 2.2	126.9	131.4	4.5	107.0	101.2
3	-140	2.2 - 3.4	125.0	131.1	6.1	100.6	98.4
4	-100	3.4 - 4.6	127.0	131.4	4.4	96.5	97.8
5	- 60	4.6 - 5.7	126.9	129.8	2.9	92.0	96.7
6	- 20	5.7 - 6.9	125.1	127.3	2.2	87.3	96.2
7	20	6.9 - 8.2	122.7	123.9	1.2	82.7	95.1
8	60	8.2 - 9.3	118.8	119.4	0.6	77.6	93.4
9	100	9.3 - 10.4	114.4	115.0	0.6	72.6	92.5
10	140	10.4 - 11.5	108.4	109.7	1.3	66.0	90.2
11	180	11.5 - 12.7	102.1	103.7	1.6	58.4	86.5
12	220	12.7 - 13.8	93.8	95.2	1.4	48.5	81.0
13	260	13.8 - 14.6	84.8	86.2	1.4	38.1	74.6
14	300	14.6 - 16.1	75.6	77.7	2.1	27.5	65.9
15	340	16.1 - 17.7	66.2	67.4	1.2	10.0	59.5
16	380	17.7 - 19.0	52.9	55.5	2.6	1.5	46.9
17	400	19.0 - fail	50.7	50.8	-	-3.3	45.6

corrections have been applied to the $\Delta\sigma$ values. A sample calculation best explains the problem. For example, determine the 0.2% yield stress at -100°C. From Table XV the stress levels measured are 127 X 10^3 psi at 3.4% strain to 131.1 X 10^3 psi at 4.6% strain. To determine the yield stress at -100°C, subtract out the work hardening that occurs for the strain introduced at -140°C and -196°C. Thus,

$$\sigma_{\text{yield (-100°C)}} = \sigma_{\text{iys}} - (\Delta\sigma_{\text{-196°C}} + \Delta\sigma_{\text{-140°C}})$$

Where

σ_{iys} = intersect yield strength

$\Delta\sigma_{\text{-196°C}}$ = work hardening introduced at -196°C. (Similarly for all $\Delta\sigma_{\text{T°C}}$)

From Table XV

$$\sigma_{\text{yield (-100°C)}} = 127.0 - (19.9 + 4.5 + 6.1) = 96.5 \text{ X } 10^3 \text{ psi}$$

This value does not appear out of line; but for the tests at 400°C.

$$\sigma_{\text{yield (400°C)}} = 50.7 - \Sigma\Delta\sigma_{\text{T°C}} < 0$$

and thus an error has been made.

The missing element is that the work hardening rate is a strong function of temperature and strain. Therefore, all work hardening introduced prior to the test under scrutiny must be normalized to the temperature at which the yield stress is desired.

For the yield stress at -100°C, we then have:

$$\sigma_{\text{yield (-100°C)}} = \sigma_{\text{iys}} - \left[\Delta\sigma_{\text{-196°C}} \left(\frac{\Theta_{\text{-100°C @ 1\%}\varepsilon}}{\Theta_{\text{-196°C @ 1\%}\varepsilon}}\right) + \Delta\sigma_{\text{-140°C}} \left(\frac{\Theta_{\text{-100°C @ 2\%}\varepsilon}}{\Theta_{\text{-140°C @ 2\%}\varepsilon}}\right)\right]$$

Where

$\Theta_{-100°C\ @\ 1\%\varepsilon}$ is the work hardening rate for material tested at -100°C at 1% strain. (Similarly for other $\Theta_{T°C\ @\ \%\varepsilon}$)

$$\sigma_{yield\ (-100°C)} = 127.0 - 20.2 = 97.8$$

If calculations of this type are carried out for each segment, reasonable agreement is found between the results of the step-pull tests and the results from many individual tests. The advantage of the step-pull test is that it allows a more accurate determination of the temperature at which the 0.2% yield stress changes temperature dependence.

Clearly, this normalizing procedure is only approximate. Nevertheless, the manipulation of data in this manner allows a second approach to the problem. The agreement between the curves shown in Figure 29 implies that the major corrections have been included.

References

1. B. Chalmers, 'Physical Metallurgy', John Wiley and Sons, N. Y., 1959.

2. Cobalt, Monograph-Cobalt Information Centre, Brussels, 1960.

3. J. B. Hess and C. S. Barrett, J. Metals, N. Y. 4 (1952) 645.

4. R. T. Holt, Ph. D. Thesis, U.B.C. (1968).

5. O. Boser, Z. Metallkunde, 58 (1967) 404.

6. I. S. Bolgov, Yu. N. Smirnov, and V. A. Finkel, Phys. Met. Metall., 17 (1964) 76.

7. P. G. Partridge, Met. Rev., 12 (1967) 169.

8. Metals Handbook, Vol. 1, A.S.M., Metals Park Ohio, 1961.

9. R. E. Reed-Hill, J. P. Hirth and H. Cordon Breach, 'Deformation Twinning', Science Publisher, N. Y., 1963.

10. M. H. Yoo and C. T. Wei, J. Ap. Phys., 38 (1967) 4317.

11. K. G. Davis and E. Teghtsoonian, Acta. Met., 10 (1962) 1189.

12. K. G. Davis and E. Teghtsoonian, TMS-AIME, 227 (1963) 762.

13. K. G. Davis and E. Teghtsoonian, Cobalt, 22 (1964) 31.

14. A. Seeger, H. Kronmueller, O. Boser, and M. Rapp, Phys. Stat. Sol., 3 (1963) 1107.

15. F. D. Rosi, C. A. Dube, and B. H. Alexander, J. Metals, 5 (1953) 257.

16. N. R. Risebrough, Ph. D. Thesis, U.B.C. (1965).

17. A. G. Crocker, Phil. Mag., 7 (1962) 1901.

18. R. A. Jeffery and E. Smith, Phil. Mag., 13 (1966) 1163.

19. T. Ericsson, Acta Met. 14 (1966) 853.

20. N. E. Noskova and V. A. Pavlov, Phys. Met. Metall. 14, 6 (1962) 86.

21. R. D. Heidenreich and W. Shockley, Report on Conference on Strength of Solids, London (1948) 57.

22. W. Bollman, Acta. Met. 9 (1961) 972.

23. J. M. Drapier, E. Votava and L. Habraken, Journées Internationalles des Applications du Cobalt, Bruxelles (1964) 58.

24. H. M. Thieringer, Z. Metallkunde, 59 (1968) 400.

25. H. M. Thieringer, Z. Metallkunde, 59 (1968) 476.

26. S. Mader, A. Seeger, and H. M. Thieringer, J. Ap. Phys., 34 (1963) 3376.

27. P. Gaunt and J. W. Christian, Acta. Met., 7 (1959) 529.

28. J. Nelson and C. J. Altstetter, TAIME., 230 (1964) 1577.

29. M. A. Gedwell, C. J. Altstetter, and C. M. Wayman, TAIME., 230 (1964) 453.

30. R. Adams and C. Altstetter, TAIME., 242 (1968) 139.

31. E. deLamotte and C. Altstetter, TAIME., 245 (1969) 651.

32. A. Akhtar, Ph. D. Thesis, U.B.C. (1968).

33. D. McLean, 'Mechanical Properties of Metals', John Wiley and Sons, N. Y., 1962.

34. G. E. Dieter, Jr., 'Mechanical Metallurgy', McGraw-Hill, N. Y., 1961.

35. R. E. Reed-Hill, 'Physical Metallurgy Principles', D. Van Nostrand, Princeton, N. J., 1964.

36. E. Votava, Acta. Met., 8 (1960) 901.

37. E. Votava, J. Inst. Met., 90 (1961) 129.

38. A. W. Hull, Phys. Rev., 17 (1921) 571.

39. S. Umino, Sci. Rep. Tohoku Imp. Univ., 16 (1927) 593.

40. H. Masumoto, Trans. Am. Soc. Steel Treat., 10 (1926) 489.

41. S. Sekito, Sci. Rep. Tohoku Imp. Univ., 16 (1927) 545.

42. A. Schulze, Z. Techn. Physik, 8 (1927) 368.

43. F. Wever and U. Haschimoto, Mitt. Kaiser-Wilhelm Inst. Eicenforsch., 11 (1929) 293.

44. F. L. Uffelmann, Phil. Mag., 10 (1930) 633.

45. A. Schulze, Z. Metallkunde., 22 (1930) 308.

46. S. B. Hendricks, M. E. Jefferson, and J. E. Schultz, Z. Krist., 73 (1930) 376.

47. A. B. Cardwell, Phys. Rev., 38 (1931) 2033.

48. G. Wassermann, Metallwirtschaft, 11 (1932) 61.

49. W. P. Sykes, Trans. Am. Soc. Steel Treat., 21 (1933) 385.

50. W. P. Sykes and H. F. Graff, Trans. ASM., 23 (1935) 50.

51. A. V. Seybolt and C. H. Mathewson, AIME., 117 (1935) 156.

52. H. Von Steinwehr and A. Schulze, Z. Metallkunde, 27 (1935) 90.

53. L. Marick, Phys. Rev., 49 (1936) 831.

54. W. F. Meyer, Z. Krist., 97 (1937) 145.

55. O. S. Edwards and H. Lipson, J. Inst. Met., 69 (1943) 177.

56. A. R. Troiano and J. L. Tokich, TAIME., 175 (1948) 728.

57. E. A. Owen and D. M. Jones, Proc. Phys. Soc. (London), 67 (1954) 456.

58. H. H. Cottrell and B. A. Bilby, Phil. Mag., 42 (1951) 573.

59. J. W. Christian, Proc. Royal Soc. (London), A206 (1951) 51.

60. A. Seeger, Z. Metallkunde, 47 (1956) 653.

61. A. Seeger, Z. Metallkunde, 45 (1954) 247.

62. M. J. Bibby, A. G. McMullen, and J. G. Parr, Cobalt, 19 (1963) 69.

63. M. J. Bibby and J. G. Parr, Cobalt, 20 (1963) 111.

64. J. Nemeth, R. T. Hamilton, and J. G. Parr, Cobalt 45 (1969) 177.

65. H. Bibring and F. Sebileau, Compt. Rendu., 239 (1954) 54.

66. H. Bibring and F. Sebilleau, Compt. Rendu., 238 (1954) 1026.

67. H. Bibring, C. Lenoir, and F. Sebilleau, Rev. Met., 52 (1955) 609.

68. H. Bibring and F. Sebilleau, Rev. Met., 52 (1955) 569.

69. H. Bibring and F. Sebilleau, Rev. Met., 56 (1959) 279.

70. H. Bibring and F. Sebilleau, Compt. Rendu., 245 (1957) 2269.

71. F. Sebilleau, C. Bibring, and C. Buckle, J. Inst. Met., 87 (1958/59) 71.

72. J. Venables, Phil. Mag., 7 (1962) 35.

73. J. B. Cohen and J. Weertman, Acta. Met., 11 (1963) 996.

74. M. B. Kasen, R. Taggart, and D. H. Polonis, A.S.M. Trans. Quart., 60 (1967) 144.

75. K. Sumino, Acta. Met., 14 (1966) 1607.

76. C. R. Houska, B. L. Averbach, and M. Cohen, Acta. Met., 8 (1960) 81.

77. T. R. Anantharaman and J. W. Christian, Phil. Mag., 43 (1952) 1338.

78. C. S. Barrett, TAIME., 188 (1950) 123.

79. P. S. Kotval and R. W. K. Honeycombe, Acta. Met., 16 (1968) 597.

80. Yu. I. Petrov, Soviet Phys. Cryst., 11, 6 (1967) 788.

81. R. W. Fraser, D. J. Evans, and V. Mackiw, Cobalt, 23 (1964) 72.

82. H. Beckers, L. Fontainas, B. Togarinoff, and L. Habraken, Cobalt, 25 (1964) 171.

83. D. Müller, Neue Hutte, 13, 2 (1968) 110.

84. A. Lanners, Thèse de doctorat, Universite Catholique de Louvain, (1954).

85. V. F. Yegolayev, L. S. Malinov, L. D. Chumakova, and R. Sh. Shklyar, Phys. Met. Metall., 23 (1967) 77.

86. I. N. Bogachev, V. F. Yegolayev, L. D. Chumakova, and R. Sh. Shklyar, Phys. Met. Metall., 26 (1969) 91.

87. F. R. Morral, J. of Metals, 10 (1958) 662.

88. H. Winterhager and J. Kruger, Cobalt, 29 (1965) 185, and 30 (1966) 27.

89. R. C. Wilcox, Ph. D. Thesis, University of Missouri, (1962).

90. M. Sage and Ch. Guillaud, Rev. Met., 47 (1950) 139.

91. A. F. Giamei and E. J. Freise, TAIME, 239 (1967) 1676.

92. H. G. Feller, Z. Metallkunde, 54 (1963) 560.

93. K. H. Klitzing and A. Pietzcker, Z. Metallkunde, 54 (1963) 359.

94. D. S. Eppelsheimer and R. C. Wilcox, J. Inst. Met., 93 (1964) 229.

95. P. Rama Rao and T. R. Anantharaman, Proc. Indian Academy of Science, (A), 6, 4 (1965) 230.

96. N. C. Halder, Phil. Mag., 86 (1963) 273.

97. L. E. Toth, T. R. Cass, S. F. Ravitz, and J. Washburn, Phil. Mag., 9, 100 (1964) 607.

98. M. H. Loretto, Phil. Mag., 12, 115 (1965) 125.

99. T. R. Anantharaman and J. W. Christian, Acta. Cryst., 9 (1956) 479.

100. H. Bilger and H. Kronmüller, Phys. Stat. Sol., 22 (1967) 683.

101. M. Feller-Kneipmeiser, Z. Metallkunde, 57 (1966) 862.

102. J. V. Sharp, A. Mitchell, and J. W. Christian, Acta. Met., 13 (1965) 965.

103. C. R. Houska, Proc. A.S.M. Metals/Materials Conf., 2 (1964) 111.

104. R. Kamel and K. Halim, Phys. Stat. Sol., 15 (1966) 63.

105. M. J. Marcincowski, A. S. Sastri and D. Koskimaki, Phil. Mag., 18 (1968) 945.

106. K. S. Raghave, A. S. Sastri, and M. J. Marcincowski, TAIME, 245 (1969) 1569.

107. D. S. Eppelsheimer, R. C. Wilcox, Rev. Met., 61 (1964) 149.

108. M. G. Lozinsky, Rev. Met., 57 (1960) 395.

109. O. Rudiger, J. Burbach and A. Hoffmann, Techn. Mitt. Krupp. Forsch.-Ber., 24 (1966) 61.

110. N. R. Risebrough and J. A. Lund, A.S.M. Trans. Quart., 61 (1968) 722.

111. R. C. Cook, M. A. Sc. Thesis, U.B.C. (1968).

112. M. Aucouturier and P. Lacombe, Compt. Rendu., 255 (1962) 1110.